SYNCHROPHASOR MEASUREMENT USING SUBSTATION INTELLIGENT ELECTRONIC DEVICES: ALGORITHMS AND TEST METHODOLOGY

A Dissertation

by

JINFENG REN

Submitted to the Office of Graduate Studies of
Texas A&M University
in partial fulfillment of the requirements for the degree of

DOCTOR OF PHILOSOPHY

December 2011

Major Subject: Electrical Engineering

Synchrophasor Measurement Using Substation Intelligent Electronic Devices:

Algorithms and Test Methodology

SYNCHROPHASOR MEASUREMENT USING SUBSTATION INTELLIGENT ELECTRONIC DEVICES: ALGORITHMS AND TEST METHODOLOGY

A Dissertation

by

JINFENG REN

Submitted to the Office of Graduate Studies of
Texas A&M University
in partial fulfillment of the requirements for the degree of

DOCTOR OF PHILOSOPHY

Approved by:

Chair of Committee,	Mladen Kezunovic
Committee Members,	Garng M. Huang
	Shankar P. Bhattacharyya
	William McCain Lively
Head of Department,	Costas Georghiades

December 2011

Major Subject: Electrical Engineering

ABSTRACT

Synchrophasor Measurement Using Substation Intelligent Electronic Devices:

Algorithms and Test Methodology. (December 2011)

Jinfeng Ren, B.S., Xi'an Jiaotong University, China

Chair of Advisory Committee: Dr. Mladen Kezunovic

This dissertation studies the performance of synchrophasor measurement obtained using substation Intelligent Electronic Devices (IEDs) and proposes new algorithms and test methodology to improve and verify their performance when used in power system applications.

To improve the dynamic performance when exposed to sinusoidal waveform distortions, such as modulation, frequency drift, abrupt change in magnitude, etc, an adaptive approach for accurately estimating phasors while eliminating the effect of various transient disturbances on voltages and currents is proposed. The algorithm pre-analyzes the waveform spanning the window of observation to identify and localize the discontinuities which affect the accuracy of phasor computation. A quadratic polynomial signal model is used to improve the accuracy of phasor estimates during power oscillations. Extensive experimental results demonstrate the advantages. This

algorithm can also be used as reference algorithm for testing the performance of the devices extracting synchronized phasor measurements.

A novel approach for estimating the phasor parameters, namely frequency, magnitude and angle in real time based on a newly constructed recursive wavelet transform is developed. This algorithm is capable of estimating the phasor parameters in a quarter cycle of an input signal. It features fast response and achieves high accuracy over a wide range of frequency deviations. The signal sampling rate and data window size can be selected to meet desirable application requirements, such as fast response, high accuracy and low computational burden. In addition, an approach for eliminating a decaying DC component, which has significant impact on estimating phasors, is proposed using recursive wavelet transform.

This dissertation develops test methodology and tools for evaluating the conformance to standard-define performance for synchrophasor measurements. An interleaving technique applied on output phasors can equivalently increase the reporting rate and can precisely depict the transient behavior of a synchrophasor unit under the step input. A reference phasor estimator is developed and implemented. Various types of Phasor Measurement Units (PMUs) and PMU-enabled IEDs (Intelligent Electronic Devices) and time synchronization options have been tested against the standards using the proposed algorithm. Test results demonstrate the effectiveness and advantages.

DEDICATION

To My Dearly Beloved Wife Yaping Wang, and My Parents for Their Love, Patience and Support.

ACKNOWLEDGEMENTS

I would like to express my sincere gratitude to my advisor, Dr. Mladen Kezunovic, for his support and guidance throughout my studies at Texas A&M University. His knowledge and experience contributed many of the inspiring ideas to this dissertation.

I gratefully thank my committee members, Dr. Garng M. Huang, Dr. Shankar P. Bhattacharyya and Dr. William McCain Lively, for their time, comments and support.

Special thanks to Mr. Gerard N. Stenbakken, formerly with the National Institute of Standards and Technology (NIST), for his great help in my research, particularly during my internship at NIST. Sincere acknowledgements are extended to my colleagues, Mr. Chengzong Pang and other group members, for their collaboration and assistance. It was a most enjoyable experience in my life working with them.

My research was mainly funded by two projects. One is from US DOC, – National Institute of Standards and Technology (NIST): “Standardized Performance Test Protocols and Capabilities for Phasor Measurement Units (PMUs)”; another is from NSF I/UCRC Power System Engineering Research Center (PSERC): “Verifying Interoperability and Application Performance of PMUs and PMU-enabled IEDs at the Device and System Level.” I would like to acknowledge the financial support from all the sponsors.

NOMENCLATURE

DC	Direct Current
DDR	Digital Disturbance Recorder
DFR	Digital Fault Recorder
DFT	Digital Fourier Transform
DPR	Digital Protective Relaying
GPS	Global Positioning System
IED	Intelligent Electronic Device
IRIG-B	Inter Range Instrumentation Group Time Code Format B
NIST	National Institute of Standards and Technology
PDC	Phasor Data Concentrator
PMU	Phasor Measurement Unit
PPS	Pulse per Second
PTP	Precision Time Protocol
TVE	Total Vector Error
UTC	Coordinated Universal Time

TABLE OF CONTENTS

Page

ABSTRACT iii

DEDICATION v

ACKNOWLEDGEMENTS vi

NOMENCLATURE vii

TABLE OF CONTENTS viii

LIST OF FIGURES xii

LIST OF TABLES xvi

1. INTRODUCTION 1

    1.1 Problem Statement 1
        1.1.1 Synchrophasor Measurement under Power System Transients 1
        1.1.2 Conformance to Standard-defined Performance 4
    1.2 Existing Solutions 5
        1.2.1 Algorithms and Techniques 5
        1.2.2 Research Problem 9
        1.2.3 Associated Standards and Guides 11
    1.3 Research Approach 12
    1.4 Organization of the Dissertation 14

2. SYNCHROPHASOR TECHNOLOGY FUNDAMENTALS 16

    2.1 Introduction 16
    2.2 Synchrophasor Measurement Concept 16
    2.3 Devices and Network 21
        2.3.1 Phasor Measurement Units 21
        2.3.2 Time Synchronization Options 23
        2.3.3 Phasor Data Concentrators (PDCs) 27
        2.3.4 Synchrophasor Data Network 30
    2.4 Applications to Power System 31

Page

2.4.1 Real-time Operations 33
2.4.2 Off-line Applications 39
2.4.3 Wide-area Controls 40
2.5 Summary 42

3. ADAPTIVE SYNCHROPHASOR ESTIMATOR 44

3.1 Introduction 44
3.2 Power System Transients 45
3.3 Disturbance Identification and Localization 48
3.3.1 Lipschitz Exponent 49
3.3.2 Wavelet Function and Transform Coefficient 51
3.3.3 Measuring Signal Regularity with Wavelet Transform 52
3.3.4 Modulus Maxima Detection and Localization 54
3.3.5 Step Identification with LE 55
3.3.6 Implementation and Threshold 58
3.4 Adaptive Phasor Estimation Scheme 59
3.4.1 Adaptive Data Window 60
3.4.2 Phasor Estimation Algorithm 61
3.4.3 Study of Model Accuracy 64
3.5 Implementation of Adaptive Estimator 65
3.6 Application Studies 67
3.6.1 Power Swing Followed by Three-phase Fault 67
3.6.2 Out of Step Caused by Loss of Load 70
3.7 Summary 71

4. NEW PHASOR ESTIMATION ALGORITHM 73

4.1 Introduction 73
4.2 Recursive Wavelet Transform 75
4.2.1 Wavelet Transform Background 75
4.2.2 Newly Constructed Recursive Wavelet 78
4.3 Frequency and Phasor Estimation Algorithm 81
4.3.1 RWT Based Frequency and Phasor Estimation 81
4.3.2 Study of Convergence Characteristics 86
4.3.3 Analysis of Computational Burden 89
4.4 Eliminating Decaying DC Component 90
4.5 Performance Evaluation 93
4.5.1 Static Test 94

Page

4.5.2 Noise Test 95
4.5.3 Dynamic Test 96
4.5.4 Transient Test 101
4.6 Summary 102

5. CHARACTERIZING DYNAMIC BEHAVIOR USING STEP SIGNALS 104

5.1 Introduction 104
5.2 Computing Reference Phasors 105
5.2.1 Phasor Estimation Method 105
5.2.2 Increasing Phasor Output Rate 108
5.3 Implementation of Step Test 112
5.3.1 Test Plan 112
5.3.2 Test Procedure 115
5.4 Test Results 116
5.5 Summary 119

6. EVALUATING CONFORMANCE PERFORMANCE 120

6.1 Introduction 120
6.2 Conformance Test References 121
6.3 Synchrophasor Test System 123
6.3.1 Laboratory Setup 123
6.3.2 Reference PMU 129
6.4 Test Results 132
6.5 Summary 134

7. CONCLUSIONS 136

7.1 Summary of Achievements 136
7.2 Research Contribution 139
7.3 Conclusions 140
7.4 Suggestions for Future Work 140

REFERENCES 142

APPENDIX A 159

APPENDIX B 160

Page

APPENDIX C 162

APPENDIX D 167

VITA 169

LIST OF FIGURES

Page

Figure 1 Synchrophasor measurements across North America....2

Figure 2 Phasor representation for a sinusoidal waveform [7] 17

Figure 3 Time synchronization for phasor measurement....18

Figure 4 Phasor measurement at remote locations [7]....19

Figure 5 Errors in phase difference caused by time skews in measurements [7] 20

Figure 6 Hardware modules of an IED [9]....22

Figure 7 A typical PMU installation [6]....23

Figure 8 Time synchronization options....24

Figure 9 Three levels of PDCs [54] 28

Figure 10 A basic synchrophasor network....31

Figure 11 Synchrophasor applications for difference users 32

Figure 12 A screen shot of RTDMS for eastern interconnection....34

Figure 13 Frequency deviations during a large generation outage 36

Figure 14 Moving windows for a waveform with steps in magnitude 46

Figure 15 Evolution of phasor measurements over transient period....46

Figure 16 An oscillation example and estimated phasors by DFT-based algorithm....48

Figure 17 An example of sinusoidal waveform containing various components 50

Page

Figure 18 Singularities and their coefficients of wavelet transform across scales 57

Figure 19 Occurrence of a step change in a data window.....60

Figure 20 Implementation flow chart for the adaptive approach.....66

Figure 21 Voltage waveform under fault and power swing condition.....68

Figure 22 Parameter estimates and errors of three algorithms at t_1 and t_2.....69

Figure 23 Current waveform under out of step condition.....70

Figure 24 Estimated amplitude, phase, frequency and TVE for three algorithms.....71

Figure 25 Time domain waveforms of $\psi(t)$.....77

Figure 26 Frequency domain waveforms of $\Psi(\omega)$.....77

Figure 27 Flow chart of the frequency, magnitude and phase estimation.....85

Figure 28 Convergence analysis results.....87

Figure 29 Estimated frequency error for f_1=65 Hz 88

Figure 30 Estimated TVE for f_1=65 Hz.....88

Figure 31 Static test results using a quarter cycle data window 95

Figure 32 Frequency ramp test results 97

Figure 33 Dynamic response for amplitude step.....98

Figure 34 Dynamic response for phase angle step.....98

Figure 35 Dynamic response for frequency step.....98

Page

Figure 36 Dynamic response for amplitude step with pre-filtering 99

Figure 37 Phase-A current waveform 101

Figure 38 Example of the step point at a time stamp 107

Figure 39 Example of the step point between timestamps 108

Figure 40 *N* sets of output phasors obtained by repeated measurements 109

Figure 41 Interleaving of phasors 110

Figure 42 Output phasors of a PMU before interleaving 111

Figure 43 Output phasors of a PMU after interleaving 111

Figure 44 Illustration of performance indices 114

Figure 45 Framework of step test programs 116

Figure 46 Illustration of performance indices 117

Figure 47 Synchrophasor test and calibration system 124

Figure 48 Synchrophasor test system architecture 125

Figure 49 A screenshot of front panel for test initialization 127

Figure 50 A screenshot of front panel for data transfer 127

Figure 51 A screenshot of front panel for phasor alignment 128

Figure 52 A screenshot of front panel for error analysis 129

Figure 53 Phase compensation for phasor measurements 130

Page

Figure 54 Diagram for performing conformance tests.....131

Figure 55 Results of magnitude test.....162

Figure 56 Results of phase test 163

Figure 57 Results of recovery magnitude test.....164

Figure 58 Results of recovery phase test.....165

LIST OF TABLES

Page

Table 1 Specific functions and their Lipschitz exponents....51

Table 2 Ratios of wavelet transform modulus maxima and LEs....58

Table 3 Results for accuracy studies....65

Table 4 Test results for noise tests....96

Table 5 Test results for modulation tests....100

Table 6 Test results for decaying DC offset....102

Table 7 Feature summary of PMUs being tested....112

Table 8 Description of test types and conditions....113

Table 9 Test signal models for conformance test....121

Table 10 Test scenarios for steady state condition....122

Table 11 Test scenarios for bandwidth condition....122

Table 12 Test scenarios for step change condition....122

Table 13 Test scenarios for frequency ramp condition....123

Table 14 Test signal models for accuracy study....131

Table 15 Results of reference algorithm accuracy study....132

Table 16 Performance indices of magnitude tests....163

Table 17 Performance indices of phase tests....164

Page

Table 18 Performance indices of recovery magnitude tests.....165

Table 19 Performance indices of recovery phase tests.....166

Table 20 Configurations for PMUs and PMU-enabled IEDs.....167

Table 21 Conformance test result: steady state test 168

Table 22 Conformance test result: dynamic state test.....168

1. INTRODUCTION

1.1 Problem Statement

1.1.1 Synchrophasor Measurement under Power System Transients

The synchrophasor measurement technology has exhibited great superiority in enhancing system situational awareness since it was developed and introduced into power system in the early eighties [1]-[3]. Its value was reinforced after the August 14, 2003 blackout [4] where availability of such measurements could have prevented the blackout. In the last few years the effort of deploying and demonstrating variety of applications that can benefit from synchronized measurements, particularly in wide area monitoring, protection and control, has been accelerated through the North American Synchrophasor Initiative (NASPI) and other related industry efforts. Figure 1 shows an example of the synchrohasor measurements available across the North America due to recently installed PMU or PMU-enabled units.

Electric power system is one the most complex systems which suffers various disturbances all the time. Relying on different types of control and protective functions the system can remain stable conditions during such dynamic chnages. Some

---

This dissertation follows the style of *IEEE Transactions on Power Delivery*.

disturbances, for example faults and switching operations, produce discontinuous points such as steps and ramps in voltage and current waveforms due to electromagnetic transients. The effect of these transients also introduces high frequency components in voltage and current signals. Typically a PMU generates phasor measurements at a certain rate, i.e. reporting rate [5], and performs phasor estimation over one cycle of

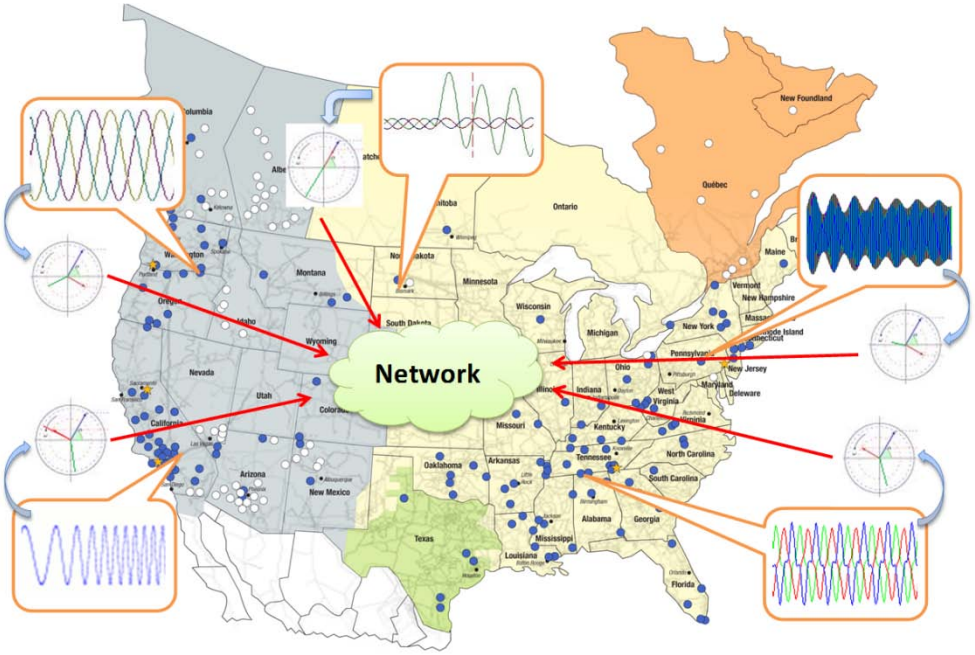

Figure 1 Synchrophasor measurements across North America

nominal power frequency. The discontinuities in waveforms caused by the transient steps may occur within an observed data window. In this case accuracy of the phasor

output estimated over such a data window is affected by discontinuities, and it can represent accurately neither the pre-state before the discontinuous point nor the post-state after that point.

A power swing may occur in a power system when a balance between the power generation and consumption is lost because of a fault, line switching, generation tripping, loss of load or other system disturbances. This phenomenon in a power system can be categorized as an electromechanical transient because it typically involves the rotor movement of large electric machines. During a power swing the amplitude and phase angle of the voltage and current are modulated with a low frequency which corresponds to the deviation of rotating speed among generators. Various examples of power swings observed in practice can be found in a technical report [6]. Fourier filter based phasor estimation algorithms, which have been predominately used in PMUs, have difficulties in processing dynamic sinusoidal waveform distortions, such as modulation, frequency drift, abrupt change in magnitude, and decaying DCs. Thus, the approaches for achieving better performance under transients, accurately estimating phasors while eliminating the effect of various transient disturbances on voltages and currents are highly desired. Such algorithms may help to improve the performance of synchrophasor based applications.

1.1.2 Conformance to Standard-defined Performance

As the deployment of the Smart Grid programs is underway, new applications using synchronized phasor measurements for enhancing the power grid reliability and security become an important part of the overall power system operation [7]. The American Recovery and Reinvestment Act (ARRA) funding and other unrelated infrastructure investment plans in the utility business accelerate the deployment of PMUs (dedicated high precision recording instruments) and PMU-capable IEDs (such as DFRs, DPRs, and DDRs, etc. that have phasor measurement function capability) across the North American power grids.

While the number of PMUs across the USA utility networks is estimated at 250, the number of PMU-enabled IEDs may range in thousands. With the recent investments through the ARRA and other funding sources, the total number of PMUs and PMU-enabled IEDs may increase by an order of magnitude with tens of thousands of such units being installed or enabled in the next 5-10 years. This asset will require costly solutions for substation installation, communications, data integration, and visualization. The total cost of the overall solution may exceed the cost of individual recording devices by several orders of magnitude. With installation of such costly infrastructure the risks of the asset becoming stranded are real and mitigating measures need to be put in place to avoid such an undesirable (disastrous) outcome.

The existing issue of compliance with standards makes the risks of the stranded assets outcome real in the synchrophasor technology implementations that include: a. Multi-vendor PMUs and PMU-enabled IEDs with proprietary features; b. Various Time synchronization options; c. Mixed PDCs and communication networks.

While many efforts have been made to evaluate the static and dynamic performance of PMUs, the responses to a step change in magnitude, which is a typical electromagnetic phenomenon in electric power system caused by faults or switching operations, have not been discussed earlier. A new standard for synchrophasor measurement (37.118.1) being balloted by the Power System Relaying Committee (PSRC) specifies the performance requirements under dynamic conditions. Some dynamic conditions, such as the simultaneous modulations in both amplitude and phase, and frequency ramp, have not been studies as well. A comprehensive test methodology for evaluating the conformance performance of the PMUs and PMU-enabled IEDs against the new standard is in demand. This type of test requires an accurate synchrophasor measurement algorithm to be used as a reference point in evaluations of such measurements found in different products.

1.2 Existing Solutions

1.2.1 Algorithms and Techniques

As defined by Steinmetz [8], a static sinusoidal waveform with known frequency

can be represented by its amplitude and angular position with respect to an arbitrary time reference. The Fourier filter, which is widely used in PMUs, can accurately compute phasors for the signals with constant parameters within an observation interval [9]. In general, power system voltage and current waveforms are not static sinusoids. Instead they contain sustained harmonics and noise. During system disturbances, oscillations, step changes and high frequency interferences in the magnitude and phase angle may occur because of the faults, switching operations and electromechanical transients of machine rotors. The Fourier based phasor estimation algorithms are derived based on the static sinusoidal signal model. As a result, significant algorithm errors are expected when dynamic waveforms containing modulation, abrupt change in magnitude and/or phase angle, and frequency drifts are used as inputs.

The PSRC is updating the synchrophasor standards with specification of dynamic requirements for PMUs. This will accelerate the applications in power system and enhance the interoperability for products from different vendors. In this context, the interoperability means conformance with the standard's requirements. Meanwhile many efforts have been made to improve the accuracy of phasors computation under transient conditions [10]-[14]. A raised cosine filter is proposed in [10]. This filter is able to obtain accurate results during amplitude modulation. An intuitive way to improve the estimates for signal oscillation is to use the polynomial models in magnitude and phase angle,

instead of constant values, and then to approximate the envelope of the changing waveform parameters within an observation span. Based on this idea, paper [11] proposes a second-order Taylor polynomial model to improve the measurements under power system oscillations. If the parameters reflecting the changing characteristics of signals can be estimated, this provides more information to the applications tracking the dynamic progress compared to the traditional static phasor measurement. Papers [12] and [13] define the dynamic phasor computation using multi-parameter models and provide a compensation method for canceling the error in the classical Fourier algorithm that arises under dynamic conditions. Some issues regarding implementation of the algorithm in different IEDs are discussed as well.

In [14] the phasor measurements under transient system conditions are reviewed looking at the basic definition, estimation architecture and power system dynamic characteristics. As discussed in [14], step changes in the magnitude and phase angle because of electromagnetic transients may occur within the computation data window, in which case, the phasor estimate obtained from that window may be invalid. This may postpone the response time of the time critical applications, and in worse case it may cause wrong protective or control decisions. How to properly solve this issue is not addressed in the above efforts.

A variety of techniques for the real time estimation of power system frequency have

been developed and evaluated in past two decades. As an example, DFT has been extensively applied to extract frequency due to its low computation requirement. However, the implicit data window in DFT approach causes errors when frequency deviates from the nominal value [15]. To improve the performance of DFT based approaches, some adaptive methods based on feedback loop by tuning the sampling interval [16], adjusting data window length [17], changing the nominal frequency used in DFT iteratively [15], correcting the gains of orthogonal filters [18] and tuning the weighted factor [19] recursively are proposed. Because of the inherent limitation in DFT, at least one cycle of analyzed signal is required, which hardly meets the demand of high-speed response for protection schemes. A method using three consecutive samples of the instantaneous input signal is discussed in [20]. The noise and zero crossing issue may bring large errors to this method. On the basis of stationary signal model, some non-linear curve fitting techniques, including extended Kalman filter [21] and recursive Least Squares algorithm [22], are adopted to estimate fundamental frequency. The accuracy is only reached in a narrow range around nominal frequency due to the truncation of Taylor series expansions of nonlinear terms. Some artificial intelligence techniques, such as genetic algorithm [23] and neural networks [24] have been used to achieve precise frequency estimation over a wide range with fast response. Although better performance can be achieved by these optimization techniques, the

implementation algorithm is more complex and intensive in computation.

Many techniques have been proposed to eliminate the impact of decaying DC component in phasor estimation. A digital mimic filter based method was proposed in [25]. This filter features high-pass frequency response which results in bringing high frequency noise to the outcome. It performs well when its time constant matches the time constant of the exponentially decaying component. Theoretically, the decaying component can be completely removed from the original waveform once its parameters can be obtained. Based on this idea, [26], [27] utilize additional samples to calculate the parameters of the decaying component. Reference [28] uses the simultaneous equations derived from the harmonics. The effect of dc components by DFT is eliminated by using the outputs of even-sample-set and odd-sample-set [29]. Reference [30] hybridizes the partial sum based method and least squares based method to estimate the dc offsets parameters. A new Fourier algorithm and three simplified algorithms based on Taylor expansion were proposed to eliminate the decaying component in [31]. In [32], author estimates the parameters of the decaying component by using the phase angle difference between voltage and current. This method requires both voltage and current inputs. As a result, it is not applicable to the current-based protection schemes.

1.2.2 Research Problem

With the increasing number of the deployment of PMUs many vendors with their

PMU capable devices are competing in this market. The performance requirements of synchrophasor measurements may differ as per the applications requirements [14]. For example, the power grid monitoring requires phasor measurements with high accuracy while the protection applications require such measurements with fast response. In this case the performance of each individual device potentially becomes an essential aspect that could directly affect the performance of the entire system. The risk of using such elaborate high precision measurement infrastructure requires the substantial support of standards and appropriate testing to ensure compliance and consistency across multiple IED types, as well as future scalability and upgradeability, hence avoiding the costly infrastructure becoming a stranded asset.

Many efforts have been made for evaluating the performance of PMUs. The NIST has established a SynchroMetrology Laboratory [33]. Two systems for PMU testing under steady-state and dynamic conditions respectively have been developed in this laboratory [34]-[36]. The NIST steady-state calibration service tests PMUs for compliance with the parameter requirements in IEEE C37.118-2005. In the dynamic test, modulated signals with varying magnitude and frequency are used to investigate PMU's dynamic performance. These test signals simulate the conditions of various power system dynamic oscillations.

While the test environment and methodology for PMU testing under both

steady-state and dynamic conditions have already been studied [33]-[51], the PMU responses to a step signal, which is a typical signal in dynamic conditions, have not been discussed earlier. Besides, how to verify the performance of PMUs under the simultaneous modulations in both amplitude and phase angle, and frequency ramps have not been addressed either.

1.2.3 Associated Standards and Guides

IEEE C37.118-2005 standard defines synchrophasor measurements used in the power system applications [5]. This standard specifies the compliance requirements for PMUs with respect to the phasor magnitude, frequency, phase angle, harmonics distortion, and out-of-band interference. It specifies the accuracy requirement of PMUs in terms of a single error parameter, defined as the Total Vector Error (TVE). This error combines the phase (timing) error with the magnitude error. It should be pointed out that the performance requirements described in IEEE C37.118-2005 are for steady-state tests, in which the test signals are held constant in magnitude, angle and frequency during each test at values found in a possible operating state of a power system.

In general, power system voltage and current waveforms are not static sinusoids. Instead they contain sustained harmonics and noise. Particularly during system disturbances, oscillations and step changes in the magnitude and phase angles of the waveforms may occur because of faults, switching operations and electromechanical

transients of machine rotors. The working groups of the PSRC are updating the old standard with adding the dynamic performance requirements. Their tasks include two new standards: the PC37.118.1 which specifies the performance requirements for the synchrophasor measurement [52]; the PC37.118.2 which specifies the communication protocols and requirements for the synchrophasor measurement [53]. The Performance and Standards Task Team (PSTT) of the NASPI issued a PMU system testing and calibration guide [54]. This guide describes test environments and procedures for PMU in compliance with performance requirements specified in IEEE C37.118-2005. In addition to the steady-state tests, the performance requirements of PMUs under dynamic conditions are included as well.

1.3 Research Approach

A breakdown of research approach in this dissertation is as follows:

- Study the characteristics of voltage and current waveforms during power system transients. Analyze the effect of power system transients on phasor behavior. Based on better understanding the fundamental properties of the signals that need to be monitored, and corresponding signal processing techniques, define the specific requirements for a reference phasor estimator under power system transient.
- Develop an adaptive algorithm to improve the accuracy of synchrophasor

measurements for better tracking dynamic transients during power system disturbances [55]. Utilize a wavelet method to pre-analyze the waveform spanning the window of observation to identify and localize the discontinuities which affect the accuracy of phasor computation. Detect and further characterize the singularity of signals using Lipschitz Exponent (LE), and make make improvement for better resolving the specific impacts on the measurement raised in a power system.

- Propose a new phasor estimation algorithm for real-time applications featuring better dynamic performance, capable of eliminating decaying DC components, flexible window size and low computation burden [56]-[59]. Conduct reaserch based on recursive wavelet approach, which was introduced in protective relaying for a long time. Construct a new wavelet function, which is a complex function whose wavelet transform coefficients (real part and imaginary part) contain both phase and magnitude information of the input signal. Based on such approach, derive the algorithm for estimating the power system frequency and synchrophasor.
- Develop a test methodology for evaluating the dynamic performance of PMUs when exposed to a step change of input signals [60], [61]. Use the adaptive window scheme to achieve high accuracy of reference phasors. Apply an

interleaving technique on output phasors to equivalently increase the reporting rate and precisely depict the transient behavior of a PMU under the step input. Perform four types of tests with balanced and unbalanced three-phase step signals as reference signals to characterize the step responses. Develop a test plan based the dynamic test system to automate step test procedures.

- Design a laboratory setup using NI-PXI system for performing the conformance tests on synchrophasor devices. Propose the test methodology for how to implement the tests. Develop a reference PMU measurement approach using proposed phasor estimation algorithms and test techniques. Conduct the accuracy study to exhibit the superiority. Test results will be given at the end.

1.4 Organization of the Dissertation

The dissertation is organized as follows. A background of the synchrophasor technology is introduced in Section 2. Section 3 describes the adaptive phasor estimation for power system transients using wavelet transform techniques. A new algorithm for estimating power system frequency, magnitude and phase while eliminating the impact of decaying DC component in real time is proposed in Section 4. Section 5 describes a test method for characterizing PMU dynamic behavior using step change signal. Section 6 describes a comprehensive laboratory setup based on a NI-PXI platform for implementing reference algorithms and evaluating the performance of synchrophasor

devices. The conclusions of the dissertation are given in Section 7. References and Appendices are attached at the end.

2. SYNCHROPHASOR TECHNOLOGY FUNDAMENTALS

2.1 Introduction

The problems to be resolved in this dissertation are discussed in the previous section, in which many new concepts and terminology are involved. This chapter introduces the fundamentals of the synchrophasor measurement and associated technology. The techniques for transferring synchrophasor data in the wide area solution and the applications using synchrophasor data in power system are described as well. This may help to explain the existing issues presented in the previous section from another point of view. In Section 2.2, the concept of synchrophasor measurement is introduced [62]. The main components, such as PMUs, time clocks and PDCs and their functionalities are described in detail in Section 2.3. Section 2.4 presents the applications using phasor data for power system monitoring, protection and control to enhance system reliability [7].

2.2 Synchrophasor Measurement Concept

A phasor is a complex number with magnitude and phase angle that is used to represent a sinusoidal signal under a specific frequency (50 Hz or 60 Hz) at a specific point of time. As shown in Figure 2, the phase angle is the distance between the sinusoidal peak of the signal and a specified reference point of time (for example time = 0) and is expressed using an angular measure. The phasor magnitude is related to the

amplitude of the sinusoidal signal.

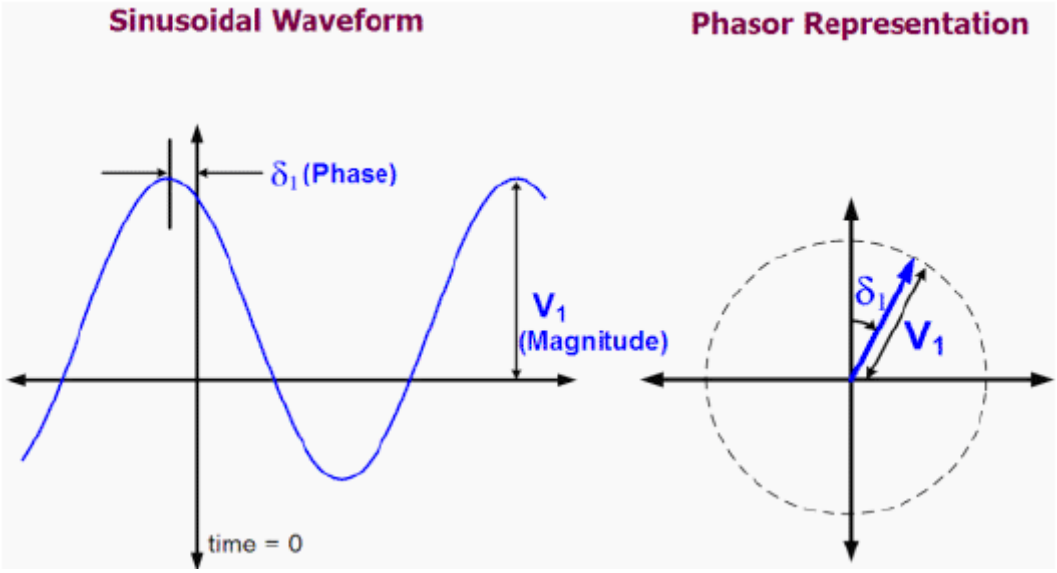

Figure 2 Phasor representation for a sinusoidal waveform [7]

When a phasor measurement is time stamped against the UTC time by GPS, it is called a synchrophasor. This allows measurements in different locations to be synchronized and time-aligned, then combined to provide a precise, comprehensive view of an entire region or interconnection. Usually GPS receiver is used to provide UTC time to synchronize the phasor measurement. GPS receiver provides both PPS and time code (IRIG-B) outputs, as shown in Figure 3. PPS is used to synchronized samples and adjust the local time against the pulse every second. The demodulated IRIG-B signal which is a DC shift pulse chain is similar to PPS but contains time code, which can be

used to timestamp the measurements directly.

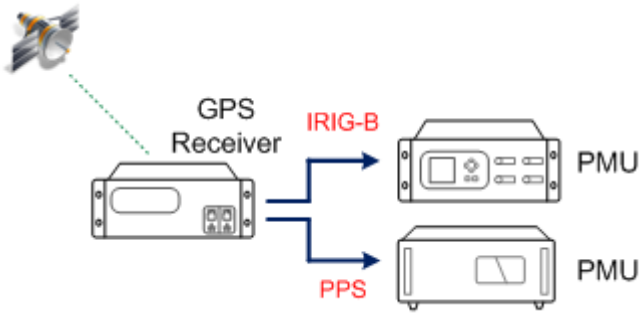

Figure 3 Time synchronization for phasor measurement

Figure 4 gives an example of phasors measurement taken at different locations. With the time reference the phasor measurements are synchronized, then made comparable. The phase angle difference between two sets of phasor measurements is independent of the angle reference. How time skews in the sample synchronization and subsequently in the synchrophasor measurements and analysis process can induce errors in the phase angle difference computations is shown by Figure 5. Basically the phase angle difference between two sets of measurements is approximately ten degrees. However, when one of these two phase angle signals is skewed by one second, the computed phase angle difference is approximately five degrees. This may introduce large errors to application results based on such measurements.

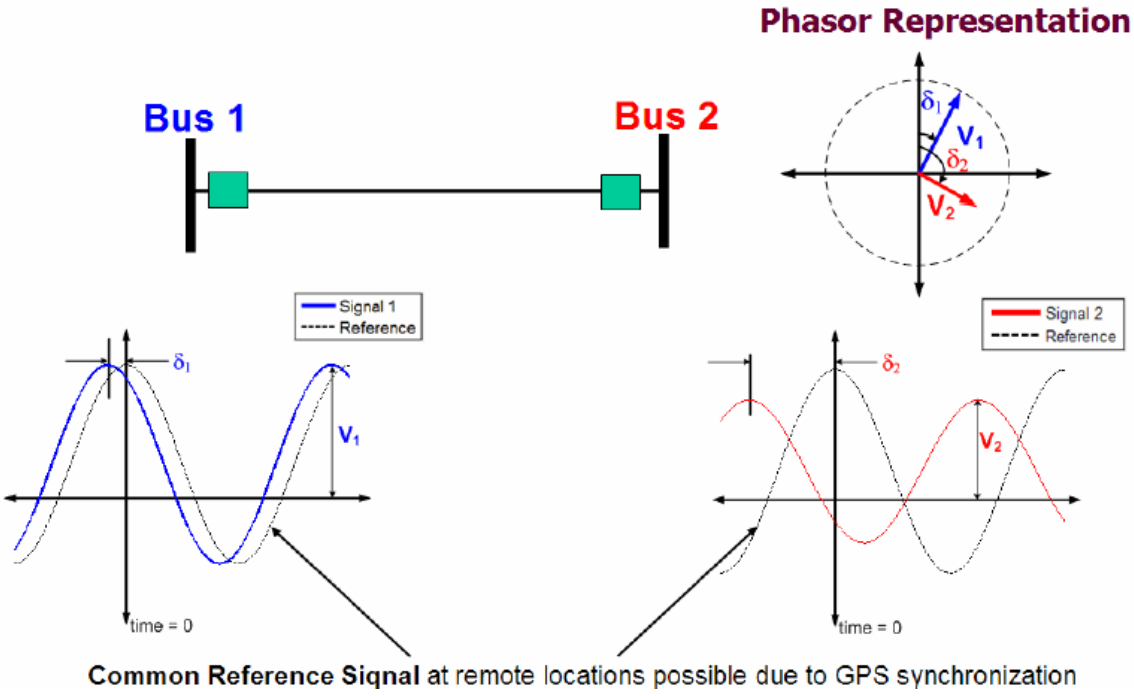

Figure 4 Phasor measurement at remote locations [7]

Compared to the traditional Supervisory Control and Data Acquisition System (SCADA), the synchrophasor technology has the following advantages:

- Phasor technology provides high resolution (sub-second) time synchronized data which is applicable for wide area monitoring; real time dynamics and stability monitoring; dynamic system ratings to operating power system closer to the margin to reduce congestion costs and increasing asset utilization; and improvements in state estimation, protection, and controls.
- Traditional SCADA/EMS systems are based on steady state power flow analysis, and therefore cannot observe the dynamic characteristics of the power system –

phasor technology is the “MRI quality” of the power systemindustry providing the high sub-second visibility required for observing dynamic behavior and, therefore, overcoming the limitations of the old “x-ray quality” visibility that traditional SCADA-based systems offer.

- Phasor measurements directly provide the phase angles at the high sub-second rate. These phase angles have traditionally been obtained from state estimators which are inherently slow (typically every 5-10 seconds) and susceptible to errors due to outdated or inaccurate models required by the state estimation process.

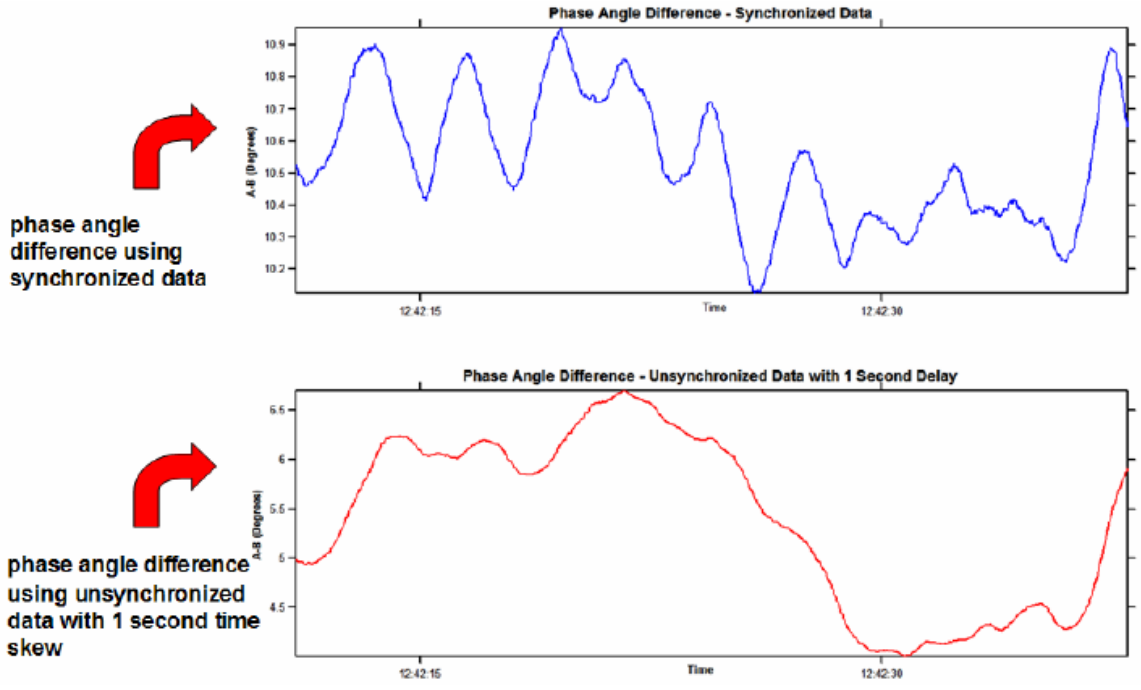

Figure 5 Errors in phase difference caused by time skews in measurements [7]

2.3 Devices and Network

2.3.1 Phasor Measurement Units

A PMU is a standalone device that measures 50/60 Hz AC voltage and/or current signals to provide phasor and frequency measurements. The analog AC waveforms are digitized by an analog to digital converter for each phase and a phase-lock oscillator and a GPS reference time source, often called pulse per second (PPS) provides high-speed time synchronized sampling. A PMU calculates line frequency, as well as voltage and current phasors at a high sampling rate and streams those data, along with the associated GPS time stamp, over networked communication lines. The synchrophasors can be single phase or symmetrical component values.

The synchrophasor measurement functionality need not be the sole function or purpose of a device; for instance, many digital relays have PMU functionality but their primary purpose is to serve as a relay rather than as a PMU. Any device that incorporates this functionality — such as digital fault recorders (DFRs) and digital relays — is considered a PMU device, i.e. PMU-enabled IED. Other unrelated functions of the device must be shown not to affect the performance of the PMU component, and equally importantly the PMU functions must not affect the other functions of the device. The main components of a PMU or PMU-enabled IED include analog input signal interface, data acquisition system, phasor estimation module and post-processing module for

output data. Figure 6 shows the hardware structure of an IED. Each module, particularly the phasor estimation algorithm has impact on the accuracy performance. For their use in various applications, the synchrophasor and frequency values must meet the general definition as well as the minimum accuracy requirements given in standards [5], [52] and [53].

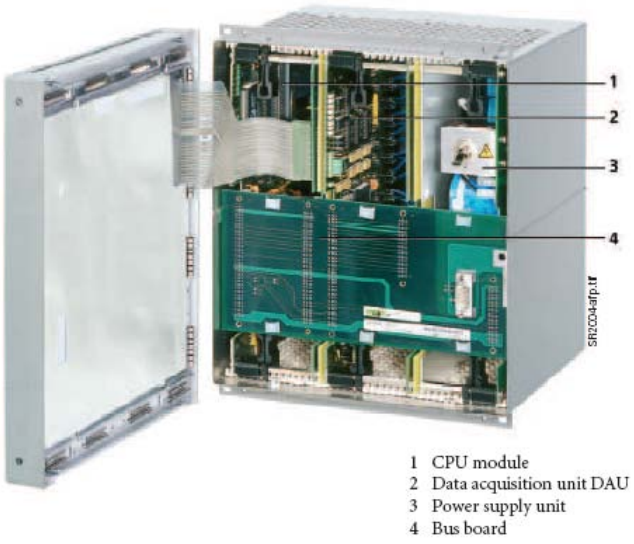

Figure 6 Hardware modules of an IED [9]

PMUs and PMU-enabled IEDs are typically installed in a substation or at a power plant. Each phasor requires three separate electrical connections (one for each phase), to either measure a current (from a line or power transformer bank) or a voltage (from either line or bus PTs). A typical PMU installation is shown in Figure 7.

A PMU also performs pre- and post-processing of the data collected, including proprietary phasor computation algorithms, anti-aliasing filtering, and other signal processing measures. As of today there are thousands of DPRs and DFRs deployed on the US grid that can be upgraded to PMU functionality. These upgraded PMU-enabled IEDs can be used for high-speed grid monitoring, automated operations, forensic analysis, and model calibration. A list of IEEE 37.118 compatible, PMU-capable, upgradable DFRs and DFRs (according to manufacturers' claims) can be found at [63].

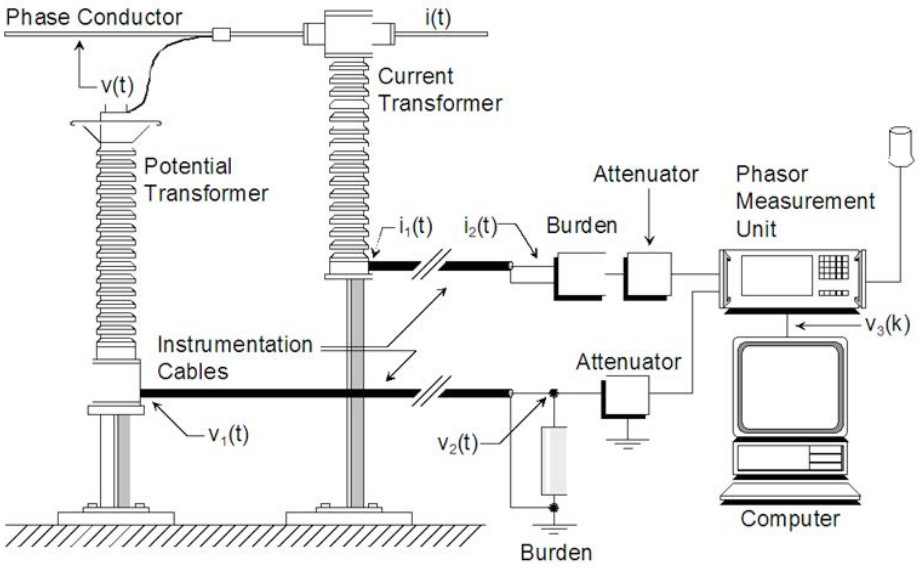

Figure 7 A typical PMU installation [6]

2.3.2 Time Synchronization Options

A PMU requires a source of UTC time and high accuracy timing signal to provide

synchronized measurements. According to the IEEE C37.118 standard, the accuracy of a synchrophasor measurement shall not exceed 1% of TVE, which corresponds to a phase angle error of 0.57 degrees. If we only consider the phase angle error, the error of 0.57 degree corresponds to approximately 26 μs at 60 Hz and 32 μs at 50 Hz. The existing methods include the direct GPS signal [64], IRIG-B/PPS [65] and IEEE 1588 [66]-[68]. For using direct GPS signal, an IED must be equipped with GPS receiver for decoding the time signal. For using IRIG-B and PPS, the receiver must be local to the IEDs. Using IEEE PC37.238 [68], the receiver can be either local or remote to the IEDs because the time code defined in IEEE PC37.238 can be distributed over communication network.

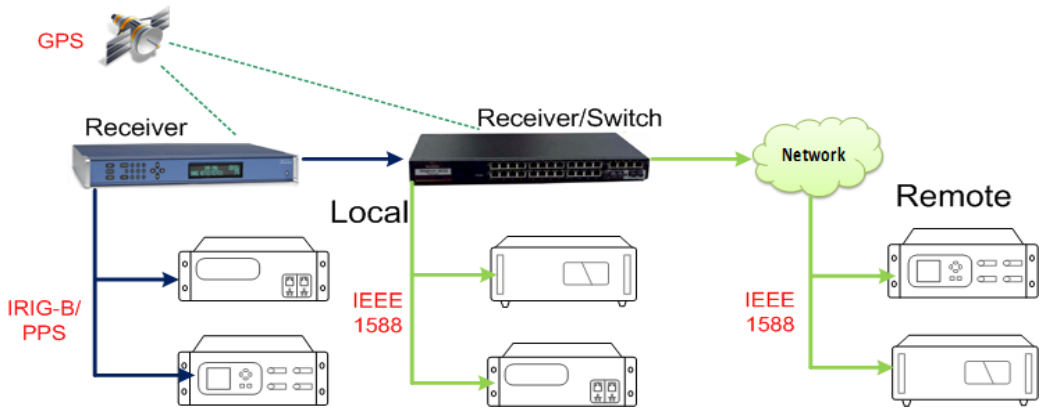

Figure 8 Time synchronization options

- **GPS signal** – A direct way for a PMU to refer UTC time is using a GPS signal. Such PMU should be equipped with internal or external GPS receiver, which is

specially designed to receive and synchronize a local timing reference to UTC using the GPS signal. The GPS system is referenced to atomic clocks maintained by the U.S. military. These clocks are very accurate time and frequency references, and are maintained within a known offset to UTC. A good GPS time receiver will incorporate averaging and holdover to accommodate short deviations and signal dropouts due to atmospheric disturbances and other causes. It will also provide notification if it loses lock with the GPS signal, so the synchronization status is always known to PMUs.

- **IRIG-B/PPS** – IRIG-B is commonly used by PMUs for synchronizing to UTC time. It may be provided in a level shift, a 1 kHz amplitude modulated signal, or in the bi-phase Manchester modulated format (modulation type 2, B2xx). If the amplitude modulation is used, it may need to be supplemented with a 1 PPS pulse train to achieve the required accuracy. The IRIG-B amplitude modulated format is commonly available and hence is the most readily implemented. The newer Manchester format is more compatible with fiber optic and digital systems and provides complete synchronization without additional signals. The clock reference is provided once per second in seconds through day of year in a binary coded decimal (BCD) format and an optional binary second-of-day count. A PPS in timing systems is a pulse train of positive pulses at a rate of 1 Hz. The rising

edge of the pulses coincides with the seconds change in the clock and provides a very precise time reference. The pulse widths vary from 5 μs to 0.5 s, and the signal is usually a 5 V amplitude driving a 50 ohm load.

- **IEEE 1588 PTP** – is a protocol used to synchronize distributed clocks with an accuracy of less than 1 microsecond via Ethernet networks. GPS is a highly accurate solution but does not scale well due to cost and complications of attaching antennas to every device. Using an Ethernet network to propagate timing signals eliminates the extra cabling requirement of GPS and IRIG-B. The first version of IEEE 1588 was found that the original design does not scale well for large switched networks. The processing and traffic congestion can occur at the timing master and cascaded network switches could cause inaccuracies due to jitter that occurs as the packets traverse through the switches. The second generation solves the problems by a. using mechanisms that increase accuracy by accounting for switching time and peer to peer propagation delays that occur as the timing signals traverse the network; b. using “transparent clocks” in Ethernet switches that eliminate the need for end-to-end delay measurement, reducing traffic congestion and eliminating switch jitter. With IEEE 1588, the cabling infrastructure requirement is reduced. The convergence of timing and data information networks can be carried out right to the network edge and converted

to IRIG-B for synchronization of existing devices that are not capable of IEEE 1588, allowing them to be kept in service even while updating the timing and data network infrastructure.

2.3.3 Phasor Data Concentrators (PDCs)

A PDC collects phasor data from multiple PMUs or other PDCs, aligns the data by time-tag to create a time-synchronized dataset, and passes this dataset to other information systems. A PDC also performs data quality checks and missing flags or problematic data (waiting for a set period of time, if needed, for all the data to come in before sending the aggregated dataset on). Some PDCs also store phasor data and can down-sample it so that phasor data can be fed directly to applications that use data at slower sample rates, such as a SCADA system.

The Performance Standards Task Team of NASPI is drafting a document that defines the functional and performance requirements for PDC [69], [70]. The main functions include:

- Correlate phasor data by time tag and then broadcast the combined data to other systems;
- Conform to streaming protocol standards (e.g., IEEE C37.118) for both the phasor data inputs and the combined data output stream;
- Verify the integrity and completeness of data streams from PMUs and properly

handle data anomalies

- Buffer input data streams to accommodate the differing times of data delivery from each PMU.

The functions of a PDC can vary depending on its role or its location between the source PMUs and the higher-level applications. There are three levels of PDCs, as shown in Figure 9:

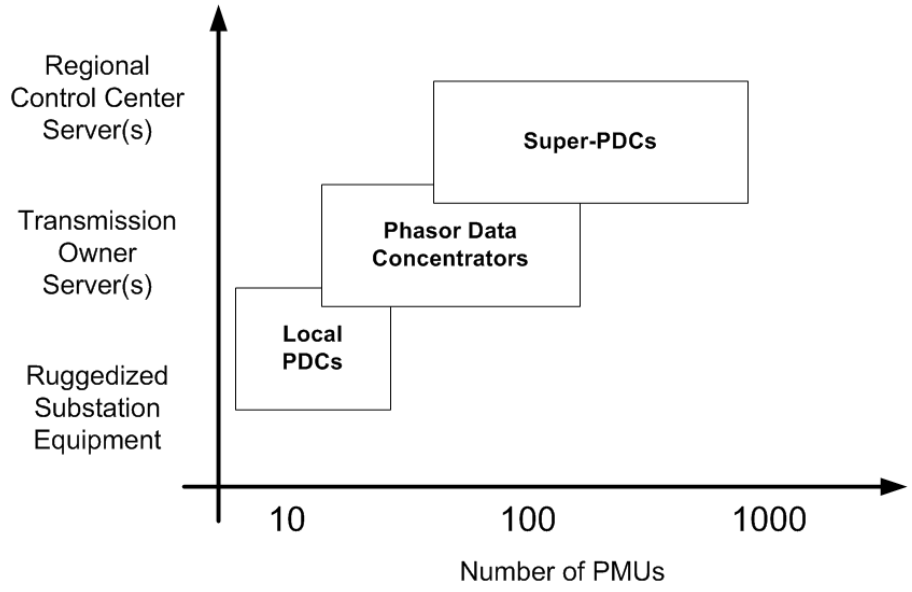

Figure 9 Three levels of PDCs [54]

- **Local PDC** – manages the collection and communication of time-synchronized data from local PMUs, sends it to higher level concentrators, and stores the data for use within the substation. A local PDC may be located physically close to

PMUs (typically at a substation) and store a small cache of local measurements to prevent against network failure, and should be the source of data for local automated control functions. A local PDC is generally a hardware-based device that should require limited maintenance and can operate independently if it loses communications with the rest of the synchrophasor network.

- **Corporate PDC** – operates within a control room where it aggregates data from multiple PMUs and PDCs. It must conduct real-time data quality checks and calculations at very high speed with real-time sample rates currently at 30-240 samples per second and heading higher.Real-time calculation must be completed very quickly, before the next set of values arrive. PDCs typically utilize threading and other parallel computing techniques available within modern operating systems to manage multiple connections at high speeds. PDCs must be adaptable to new protocols and output formats as well as interfaces with data-using applications. PDCs should incorporate inter-utility standards to allow for efficient machine-to-machine, program-to program-compatibility. It is expected that the grid operators that host PDCs will demand these capabilities from PDC vendors, and that these capabilities will be written into specifications and tested for effective interoperability performance before acceptance.
- **Super PDC** – operates on a regional scale, handling phasor measurements from

several hundred PMUs and multiple PDCs. It collects and correlates phasor data from remote PDCs and PMUs and makes them available as a coherent, time-synchronized dataset to applications such as wide-area monitoring and visualization software, energy management systems and SCADA applications. A super-PDC also feeds the data into a central database for long-term data archiving (data historian function). Super-PDCs are software implementations, running on mainstream server hardware, as these larger devices need to scale rapidly to serve growing utility and regional deployment of PMUs and diverse phasor data applications.

PDCs are commercially available from several vendors. Based on their performance history, these PDCs are generally considered to be production-grade systems. Even so, PDCs have not yet been performance-benchmarked. While it is likely that the SGIG projects will accelerate the development of PDC performance and test standards, there are currently no formal standards for evaluating and rating PDCs.

2.3.4 Synchrophasor Data Network

A basic synchrophasor measurement network consists of PMUs and PMU-enabled IEDs, PDCs, gateways, data storage and applications, as given in Figure 10. A standard for synchrophasor data transfer for power systems has been initialized by PSRC[53]. It defines the format of synchrophasor data and specifies the requirements of network for

data transfer. The functions of PMU and PDC have been described in previous sections.

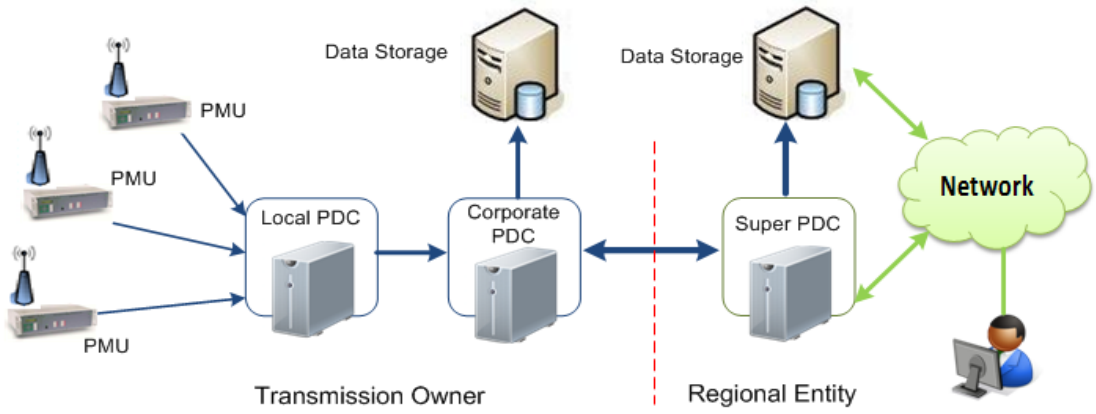

Figure 10 A basic synchrophasor network

2.4 Applications to Power System

According to the function of power system applications, the synchrophasor based applications can be classified into three categories [7]:

- Applications to support real-time grid operations by providing wide-area visualization and increased state awareness,
- Applications to improve system planning and analysis, including power system performance baselining, event analysis and model validation, and
- Response-based control applications that use real-time wide area information to take automated control actions on the power system.

Real-time applications require real-time data collection and processing with

immediate analysis and visualization or are used as control signals for real-time controls applications. Planning and post-event analysis applications use archived data and the analysis may be conducted off-line days or months after the data were collected. Figure 11 summarizes the applications using synchrophasors for different roles in power system including the roles of planners, operators, researchers and reliability coordinators. The rest of this section will briefly introduce principal applications groups in each of three categories.

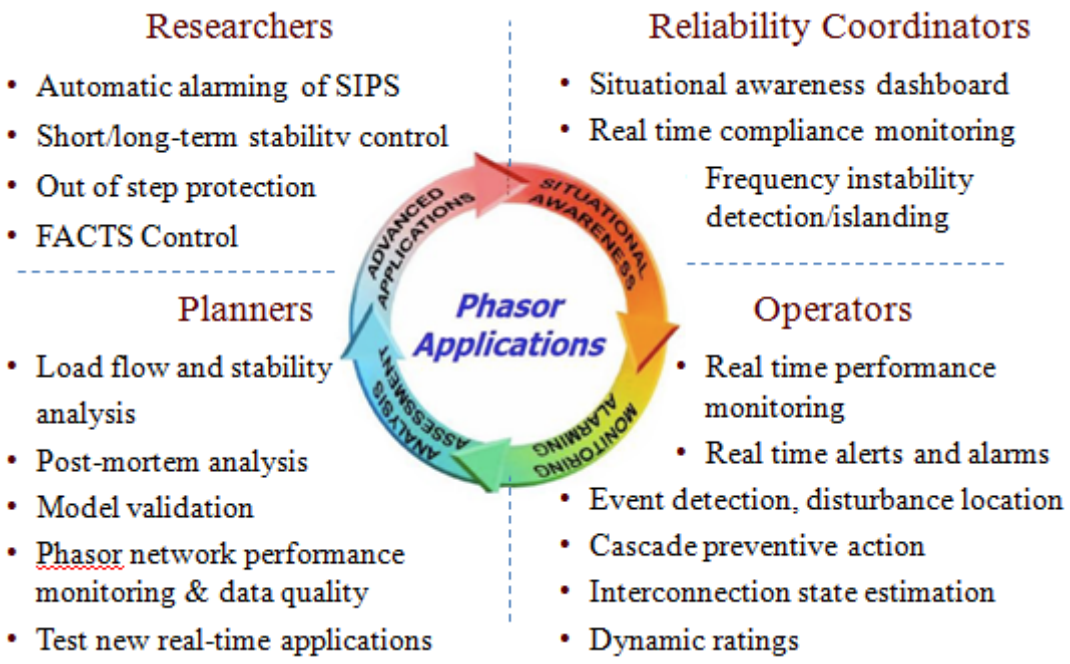

Figure 11 Synchrophasor applications for difference users

2.4.1 Real-time Operations

All real-time operations using phasor data offer high sampling speed, new granularity into phase angles and other grid conditions, and time synchronization. These measurement characteristics also enable exceptional visualization, analytics and alarming — all of which improve operators' ability to see and understand what is happening on the bulk power system, anticipate or identify potential problems, and identify, evaluate, implement and assess remedial measures. However, phasor applications must synthesize and summarize large amounts of phasor data for operators, preventing information overload and presenting actionable information in an easily understandable manner so that quick and reliable decisions can be made.

Most power system operators today have very little visibility into power system dynamics such as power oscillations, voltage stability indications, and system angular stress. Large-scale integration of renewable resources will present an additional challenge to the system operators, as large and fast power changes by intermittent generators can dramatically shift generation patterns and operating conditions. Visibility of power system dynamics is becoming even more critical as the power system grows with inclusion of more variable resources with less offsetting machine inertia to stabilize the system.

There are several applications for enhancing the wide-area situational awareness of

power grids, such as the synchronized measurement and analysis in real time (SMART) tool by Southern California Edison (SCE), real time dynamic monitoring system (RTDMS) and PowerWorld Retriever. Let us take RTDMS for example. This software is a phasor data-based platform used by grid operators, reliability coordinators, and planning and operations engineers for real-time wide-area visualization, monitoring and analysis of the power system. RTDMS offers a real-time dashboard with indicators of key grid metrics for situational awareness.

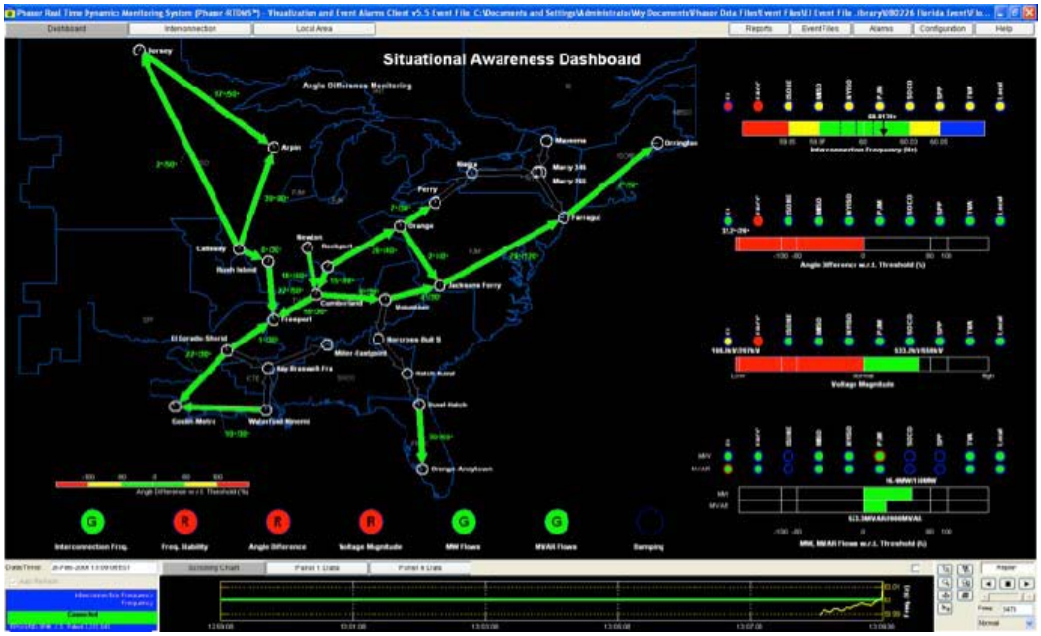

Figure 12 A screen shot of RTDMS for eastern interconnection

Figure 12 shows a screen shot of RTDMS for Eastern Interconnection after start of Florida grid disturbance [7]. It is able to identify and visualize the development of a grid disturbance, showing the difference in grid conditions.

Other real-time applications such as state estimation, frequency stability monitoring, power oscillation detection, voltage monitoring and operation planning are briefly describes as follows:

- State Estimation – Snapshots of data from PMUs can integrated into an orthogonal state estimator by feeding PMU measurements (e.g., voltage and current) directly into the state estimator measurement vector and the Jacobian matrix it uses to solve the network. Alternatively, a state estimator can use derived PMU measurements of voltage angle differences and branch factor angle measurements, thus eliminating the requirement for synchronizing state estimator and PMU angle references. This approach enables the state estimator to calculate the network solution based on both PMU and conventional measurements simultaneously, with the advantage that the phasor data offer redundant system condition measurements and enable better solution accuracy.

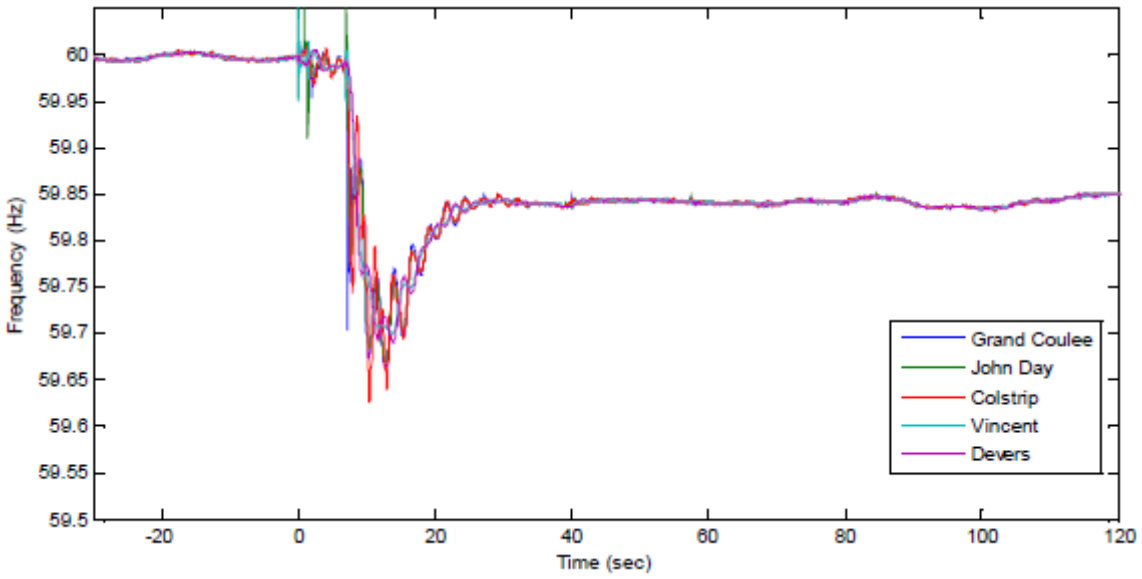

Figure 13 Frequency deviations during a large generation outage

- Frequency Stability – System frequency is the key indicator of the load-resource balance. The size of the frequency deviation is well correlated with the size of generation loss. Figure 13 shows an example of frequency response to a generation outage. System frequency is also a good indicator of integrity of an interconnection during system events involving separation or islanding. If a bus frequency in one part of the system stays at 60.5 Hz while frequency in another part of the system holds at 59.5 Hz for several minutes, it is a sure indication of the system separation. PMU frequency plots provide a good indication of the lost generation, for an example, a frequency drop of 0.1 Hz is typical in the WECC for 800 MW generation losses. Also, the propagation of the frequency drop can

be used to identify where the generation drop occurred.

- Power Oscillation – Detection of power system oscillations and ambient grid damping are among the premier applications that require the high-speed data that PMUs provide and conventional SCADA does not. Low-frequency oscillations occur when an individual generator or group of generators swing against other generators operating synchronously on the same system, caused by power transfers and high-speed, automatic turbine controls attempting to maintain an exact frequency. Synchrophasor data (bus frequency, angles, line loading and voltage) are critical to detect potential and actual oscillations within the bulk power system. Inter-area oscillations can be seen by examining bus voltages and frequencies, so most methods of oscillation detection are applied to the path or flow gate. Oscillation detection methods calculate the damping of a ring down during a system disturbance. The energy of power oscillations indicates whether an oscillation is growing or dissipating. A build-up in energy signals growing oscillatory activity, and can alert an operator to check other indicators.
- Voltage Monitoring – Phasor systems can be used to monitor, predict and manage frequency and voltage on the bulk power system. One of the most promising near-term synchrophasor applications is for trending system voltages at key load center and bulk transmission busses. Voltage trending and voltage

instability prediction are highly desirable uses for synchrophasor systems and a high priority for phasor data applications. Many transmission systems are voltage stability-limited, and voltage collapse can happen very quickly if stability limits are reached. Voltage instability occurs when either the system has inadequate reactive reserves, or the transmission system cannot deliver reactive power from the source to where it is needed. Monitoring system voltage using phasor measurements of voltage profile, voltage sensitivities, and MVar margins allow operators to watch voltage levels in real-time, while a trending application would provide an early indication of voltage instability vulnerability.

- Operation Planning – Phasor data offer great value for hour-ahead and day-ahead operations planning. These data can be used to improve models — both to refine models of individual assets and groups of assets (e.g., combustion turbines or wind power plants) to improve understanding and representation of interconnection-wide behavior. Phasor data snapshots of past system conditions can be used to improve development and analysis of system operating conditions under a variety of normal and potential contingency operating scenarios. Phasor data can also be used to identify and diagnose odd system conditions or behaviors. For instance, BPA planners used phasor data to identify the fact that several of its generators were operating with their governors' automatic controls

turned off.

2.4.2 Off-line Applications

The off-line applications using synchronized phasor measurements including system model validation, event analysis, special protection and islanding, and baselining system performance.

- System Model Validation – Planners are using phasor data to improve static system models. The high-speed observations of grid conditions allow modelers to calibrate models to better understand system operations, identify errors in system modeling data or in model algorithms, and fine-tune the models for online and off-line applications, such as power flow, stability, short circuit, OPF, security assessment, modal frequency response, and more.
- Event Analysis – Synchronized wide-area data is essential for disturbance analysis, as evidenced by the August 14, 2003 blackout investigation [4]. Data synchronization is critical for the sequence of event reconstruction, particularly for complex events where many switching operations occur in short time frame.
- Special Protection and Islanding – Phasor data can be used to design and test special protection schemes (SPS) and islanding. Ultimately it may be possible to use real-time phasor data that reveals the location and causes of system stress to drive automated control and execution of special protection schemes, including

even the real-time design and operation of system islanding in the face of a potential cascade.

- Baselining System Performance – it identifies and understands phase angles under a variety of system conditions. To be most useful and informative, these analyses require extensive records of phasor measurements across a large region, covering a wide variety of loads, equipment status, and other system conditions. Baselining entails using historic grid condition data to correlate system performance relative to the measured angular separation. PMU data are then used to structure power system simulations to predict how system performance relates to the phase angles under large disturbance events. Ideally, this is done using system models that have already been calibrated and validated with phasor data to improve their predictive capability.

2.4.3 Wide-area Controls

Wide-area synchronized measurements enable unprecedented opportunities for wide-area stability control applications. Wide-area measurements provide much greater observability of the system state, thereby leading to better and faster decisions. Since PMU measurements are instantaneous and have high resolution, phasor data can be used to activate local or centralized control of corrective measures for angular stability, voltage stability, low-frequency oscillations and thermal constraints.

The following practical control applications, all requiring high-speed phasor data, are now under study:

- Fast Reactive Switching – Synchronous generators (in voltage control mode) and Static Var Compensators (SVC) provide reactive power reserves that can be deployed during the disturbances. Studies show strong correlation between the reactive margins on voltage stability-limited paths and reactive power response and reactive power reserves. Switching shunt in capacitors can be done to increase the reactive reserves of generators and SVCs.
- Coordinated Secondary Voltage Control – It is not uncommon to have several reactive power resources in electrical proximity to each other. Coordination of voltage set-points is often required to ensure that appropriate reactive power reserves are maintained with equitable reactive sharing through secondary voltage controls. Synchrophasors or SCADA can be used for slow loop control, but with large-scale wind integration, there is greater need for fast coordination of voltage schedules among clustered wind power plants and switched capacitors to maintain dynamic reactive reserves.
- Inter-Area Oscillation Damping Controls – Wide-area oscillations can be dampened using automated controls, but this requires high-speed data and observability such as that offered by a synchrophasor system. After excessive

oscillatory activity was observed during the 2006 summer heat wave, western grid operators are revisiting the feasibility of oscillation damping controls facilitated by phasor data [7].

- Equilibrium State Control – The power system must have a stable equilibrium (target state) to return to following a disturbance event. The more secure the target state, the more likely the system transient oscillation will be damped and the less strong oscillation control will be needed. In effect, the network and transfer demands are brought into balance to assure that there is a stable equilibrium (power flow) condition.

Phasor-driven wide-area controls has been a popular research topic in the last decade, including response-based System Integrity Protection Scheme (SIPS) and inter-area oscillation damping for adaptive islanding. Yet very few control applications are now in use. This is the least mature set of applications, although it offers great benefit for grid reliability.

2.5 Summary

- Phasor is an equivalent representation of sinusoidal waveform. With angle reference and global time synchronization the synchronized phasor measurements are widely used to reflect the operating status of power grid;
- Various PMUs and PMU-enabled IEDs provide synchrophasor measurement

with different accuracy performance.

- IEDs can be synchronized using different options, such as GPS, IRIG-B/PPS and IEEE PC37.238, which provide variant levels of accuracy.
- In a synchrophasor solution, PMUs may be from different vendors using different time synchronization options and connected through different PDCs. This may cause interoperability issues.
- Power system applications using synchrophasor measurement have different requirements in accuracy and response. The quality of synchrophasor measurement has direct impact on the application performance.

3. ADAPTIVE SYNCHROPHASOR ESTIMATOR*

3.1 Introduction

New applications using synchronized phasor measurements for enhancing the power grid reliability and security become an important part of the overall smart grid deployment [85]. The examples mentioned in the previous section such as real time dynamic state monitoring, state estimation, model validation, and instability detection/islanding are improving wide area visualization, protection and control [71]-[84]. The accuracy of phasor measurements becomes an essential aspect that may directly affect the application performance, and hence may have profound impact on the entire system.

As addressed in Section 1.1.1, the conventional Fourier filter based phasor estimation algorithms have difficulties in processing dynamic sinusoidal waveform distortions, such as modulation, frequency drift and particularly abrupt change in magnitude. Section 1.2.1 discusses the existing solutions for improving the accuracy of phasors computation under transient conditions. However, they hardly solve the issue of

---

* Part of the material in this section is reprinted from "An adaptive phasor estimator for power system waveforms containing transients" by Jinfeng Ren and Mladen Kezunovic, *IEEE Trans. Power Delivery* (Under review), paper no. TPWRD-00376-2011 ©2011 IEEE, with permission from IEEE.

dealing with step change signals caused by electromagnetic transients.

For the rest of this section the effect of power system transients on phasor behavior is analyzed firstly. A wavelet method is used to pre-analyze the waveform within an observation window in Section 3.3. It can detect and localize various disturbances while discriminating the valid signal step changes from noise. In Section 3.4, once a valid discontinuity is localized, an adaptive window containing valid data is used to fit a quadratic polynomial model in the sense of least square error. The signal model has perfect accuracy when representing the magnitude and phase angle modulated signals. The algorithm implementation and application studies are presented in Section 3.5 and 3.6 respectively, and summary is outlined at the end.

3.2 Power System Transients

Faults and switching operations produce discontinuous points such as steps and ramps in voltage waveforms respectively due to electromagnetic transients. Typically the phasor estimation is determined over one cycle of nominal power frequency. The discontinuities in waveforms caused by the transients may occur within an observed data window. In this case the accuracy of the phasor output estimated over such data window is affected by the discontinuities, and it can neither represent the pre-state nor the post-state accurately.

An example for computing the phasors representation of a waveform with an abrupt

step in the amplitude and phase angle is given in Figure 14. The step forms a boundary which separates the pre-disturbance from the post-disturbance segment. Assuming the observing window spans *N* samples, as the computation window moves forward when new samples are obtained, the data window *k* and *k*+*N* are the windows closest to the boundary containing only the samples belonging to the pre-disturbance and post-disturbance respectively.

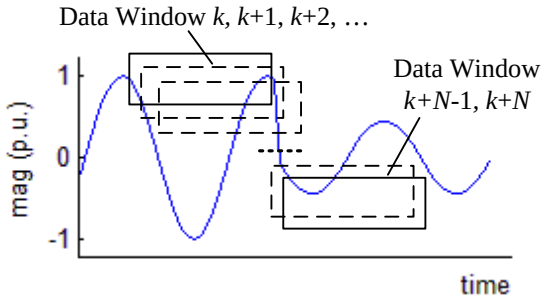

Figure 14 Moving windows for a waveform with steps in magnitude

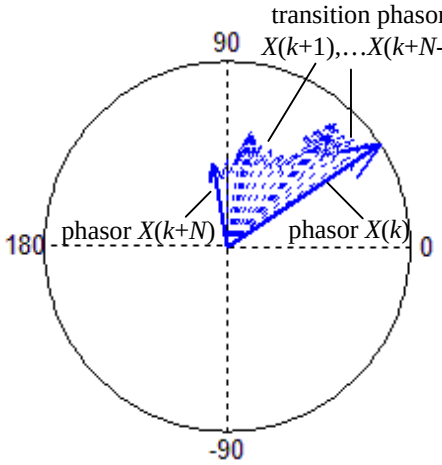

Figure 15 Evolution of phasor measurements over transient period

The phasors calculated through the windows k+1to k+N-1 represent neither the pre- nor post- segments. Figure 15 shows the phasors during the transition period. Use of such phasor estimates for any type of protection or control applications may be inappropriate. A technique for identifying the discontinuities while eliminating their impact on the accuracy of outputs will be described. The technique can be also used to flag such invalid phasor measurements.

Power swing may occur followed by disturbances such as fault, line switching, generation tripping, loss of load or other system disturbances. During power swing the amplitude and phase angle of the voltage and current are modulated with a low frequency signal which corresponds to the deviation of rotating speed among generators. Let consider an example of oscillations caused by a three-phase fault. The waveform of phase-A voltage and its amplitude envelop are given Figure 16 (a). The relay operation was delayed and the oscillation started after the fault was cleared. A DFT-based algorithm is used to compute the phasors. This algorithm is the widely used technique in presently available PMUs though it has difficulty in dealing with sinusoids with changing parameters. Figure 16 shows the dynamic behavior when the algorithm is exposed to the steps and modulations. The phase estimates and total vector error (TVE), which is defined in [5] is given in Figure 16 (b) and (c) respectively. In this example the TVE reaches 2.6% during oscillation, which may hardly meet some applications

requirements. The accuracy during power swing needs to be improved.

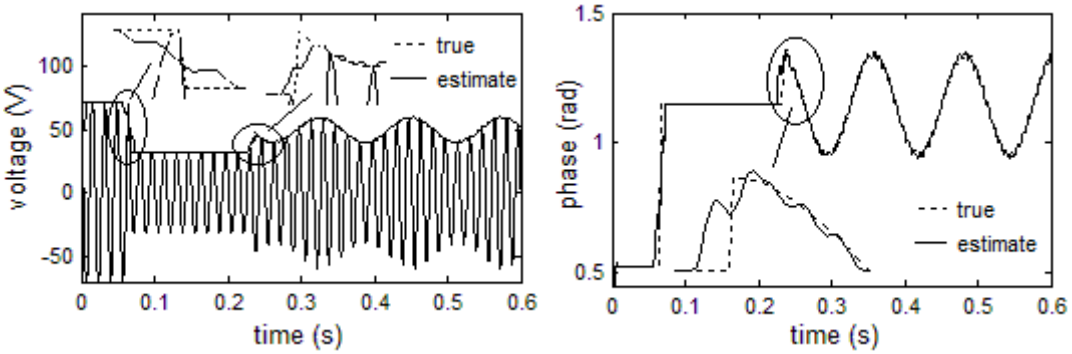

(a) Voltage waveform and amplitude estimate (b) Phase angle estimate

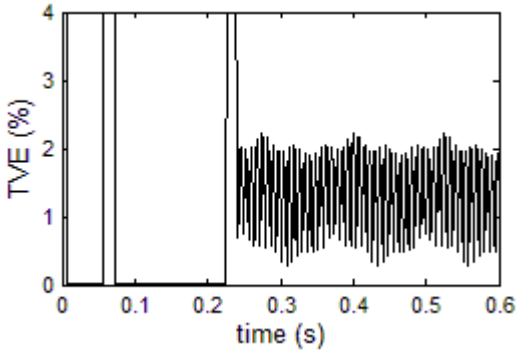

(c) TVE

Figure 16 An oscillation example and estimated phasors by DFT-based algorithm

3.3 Disturbance Identification and Localization

The step in a waveform discussed above is one class of edges, a.k.a. singular points as called in mathematics, which exist among different segments of the waveform. In the area of image processing the edges contain a lot of critical information and the detection

of them plays a significant role in the discipline. Many techniques have been proposed to detect and further characterize the singularity of signals [86], [87]. This study utilizes such principles and makes improvement for better resolving the specific problems identified in a power system.

3.3.1 Lipschitz Exponent

The local regularity of a function can be mathematically measured with Lipschitz Exponent α, i.e. LE α, which is defined as follows [86].

Definition 1: A function $f(t)$ $t \in (c,d)$ is described to be Lipschitz α at point t_0, if there exists a constant K and a polynomial $P_n(t)$, such that $\forall t \in (c,d)$, the following is held:

$$| f(t) - P_n(t) | \leq K | t - t_0 |^{\alpha} \tag{3.1}$$

Based on above definition one can easily prove that for a positive integer n, if $f(t)$ is LE $\alpha > n$, then $f(t)$ is n times differentiable at point t_0 while the polynomial $P_n(t)$ is the first n+1 terms of the Taylor series of $f(t)$ at t_0. LE indicates the differentiability of a function. Furthermore, if the LE α of $f(t)$ satisfies $n < \alpha < n$+1, then we learn that $f(t)$ is n times differentiable at t_0 but its nth derivative is singular at this point and the LE characterizes its regularity.

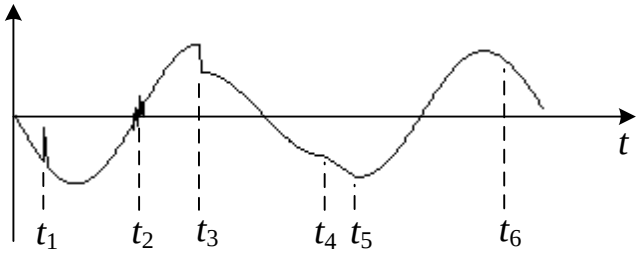

Figure 17 An example of sinusoidal waveform containing various components

Figure 17 shows a sinusoidal waveform containing some components, including noise, step edge and ramp edge at different locations (t_1, t_2, … , t_5), which can be easily found in voltage and current measurements of the real power system. Mathematical functions which represent these signal components and heir corresponding local Lipschitz regularities are given in Table 1. Ideally the voltage and current waveforms are pure sinusoidal. They are usually contaminated by a variety of noise, among which the impulse noise and white noise are the most two common kinds. Sometimes step and ramp edges may occur in voltage waveform due to the electromagnetic transients during faults and switch operations. From Table 1 we know that the different functions can be discriminated with their LEs. The following sections will present the method for estimating the exponents approximately.

Table 1 Specific functions and their Lipschitz exponents

Location	Function	L. E.
t_1	Dirac (Impulse)	α = -1
t_2	White Noise	-1<α < -0.5
t_3	Step	α = 0
t_4, t_5	Ramp	α = 1
t_6	Sinusoidal	α >> 1

3.3.2 Wavelet Function and Transform Coefficient

The wavelet transform has been proven to be an effective mathematical tool to analyze the regularity of a signal because of its remarkable capability of the localization in both time and frequency domain. A wavelet is defined as a function $\psi(t) \in L^2(R)$ whose Fourier transform $\Psi(\omega)$ satisfies the admissibility condition:

$$\int_{-\infty}^{+\infty} \frac{|\Psi(\omega)|^2}{|\omega|} d\omega = C_\Psi < \infty \tag{3.2}$$

In time domain this condition implies:

$$\Psi(\omega)\big|_{\omega=0} = \int_{-\infty}^{+\infty} \psi(t) dt = 0 \tag{3.3}$$

Denote s and u as the scaling factor and time shifting factor respectively. A set of wavelet functions can be derived by dilating and translating the mother wavelet $\psi(t)$,

$$\psi_{u,s}(t) = s^{-1} \cdot \psi(\frac{t-u}{s}), \quad s > 0 \tag{3.4}$$

Definition 2: The wavelet transform of a function $f(t)$ with regard to time shift u and scale s is defined as,

$$Wf(u,s) = f(t) * \psi^*_{u,s}(t) = s^{-1}\int_{-\infty}^{+\infty} f(t)\psi^*(\frac{t-u}{s})dt \quad (3.5)$$

Where $Wf(u, s)$ is denoted as the transform coefficient. Let scale factor s change along the dyadic sequence of 2^j (j=1, 2…), we have the dyadic wavelet function $\psi_{u,2j}(t)$ and its dyadic wavelet transform coefficient $Wf(u, 2^j)$. For simplicity we designate as $Wf(u, j)$ for the rest of this study.

It has been proven that input signal can be perfectly reconstructed with the dyadic transform coefficient. Besides, it leads to efficient numerical implementations. The component of interest in the input signal, called the edge in this study, can be exposed over the transform coefficient by selecting a proper wavelet and transform scales.

3.3.3 Measuring Signal Regularity with Wavelet Transform

Assume the wavelet holds n vanishing moments, i.e. n times differentiable. That is for all positive integer $k < n$, $\psi(t)$ satisfies

$$\int_{-\infty}^{+\infty} t^k \psi(t)dt = 0 \quad (3.6)$$

Theorem 1: Let n be a positive integer and $\alpha \le n$. If $f(t)$ is Lipschitz α at t_0, then there exists a constant A such that for all point t in a neighborhood of t_0 and any scale s, the wavelet transform of $f(t)$ with regard to $\psi(t)$ (with n vanishing moments) holds

$$|Wf(u,s)| \le A(s^\alpha + |u - t_0|^\alpha) \quad (3.7)$$

Theorem 2: $f(t)$ and it wavelet transform is well defined over (c, d), and let $t_0 \in (c, d)$. Suppose that there exists a scale s_0 and a constant C, such that for t $\in$ (c, d) and s< s_0, all

the modulus maxima of $Wf(u, s)$, denoted as $Wf_{\max}(u, s)$, belong to a cone defined by

$$\left|t - t_0\right| \le C \cdot s \tag{3.8}$$

Then at all points $t_1 \in (c, d)$, $t_1 \neq t_0$, $f(t)$ is uniformly Lipschitz n in a neighborhood of t_1. Let $\alpha \le n$ be a non-integer. The function $f(t)$ is Lipschitz α at t_0, if and only if there exists a constant A such that at each modulus maxima is in the cone defined by (3.8)

$$\left|Wf_{\max}(u, s)\right| \le A \cdot s^{\alpha} \tag{3.9}$$

The proof of the above theorems has been given by Mallat [86]. He pointed out that the maxima of the wavelet transform modulus can reflect the locations of the irregular structures. If we rewrite equation (3.9), then:

$$\log_2(\left|Wf_{\max}(u, s)\right|) \le \log_2(A) + \alpha \log_2(s) \tag{3.10}$$

From (3.10) one can see that the Lipschitz regularity at point t_0 is the maxima slope of straight lines that remain above $\log_2(|Wf_{\max}(u,s)|)$ on a logarithmic scale s.

The dyadic wavelet transform ($s = 2^j$) for scale j and j+1 can be obtained from (3.10)

$$\log_2(\left|Wf_{\max}(u, j)\right|) \le \log_2(A) + \alpha \cdot j \tag{3.11}$$

$$\log_2(\left|Wf_{\max}(u, j+1)\right|) \le \log_2(A) + \alpha \cdot (j+1) \tag{3.12}$$

Subtract (3.12) from (3.11) the LE α can be approximately estimated by the following equation

$$\alpha \cong \log_2 \frac{\left|Wf_{\max}(u, j+1)\right|}{\left|Wf_{\max}(u, j)\right|} \tag{3.13}$$

Equation (3.13) shows that the Lipschitz α of a signal at any point can be

approximately estimated by its modulus maxima of dyadic wavelet transform over adjacent scales. Based on LE one can identify the types of singularities. For example, if $|Wf_{max}(u, j+1)| = |Wf_{max}(u, j)|$, i.e. $\alpha=0$ it implies the signal is discontinuous at this point, such as step change; if $|Wf_{max}(u, j+1)| < |Wf_{max}(u, j)|$, i.e. $\alpha<0$, it implies that the signal is more singular than discontinuity at this point, such as Dirac and white noise; if $|Wf_{max}(u, j+1)| > |Wf_{max}(u, j)|$, i.e. $\alpha>0$, it means the signal is at least continuous such as ramp, or smooth such as sinusoid.

3.3.4 Modulus Maxima Detection and Localization

In mathematics the inflection points of a function correspond to the local extrema of the first derivative of the function or to the zero crossings of the second derivative of the function. Based on this, Canny developed a computational approach for edge detection using smooth functions [88].

Let f be the original signal and F be the smoothed one by function θ, for example the Gaussian function whose integral is equal to one and it converges to 0 at infinity. In the sense of filtering $F = f * \theta$, where * stands for the convolution operator. Suppose that θ is twice differentiable and define ψ and ψ' as the first- and second-order derivative of θ, respectively. In this case the detection of edges is equivalent to locating the inflection points of the smoothed F. That is to find the local extrema of $f*\psi$ or zero crossings of $f*\psi'$. Both local extremum and zero crossing give location information of the inflection

point and detecting them is a similar procedure. However the local extremum approach has some important advantages. An inflection point of F can be either a maximum or a minimum of the absolute value of $f * \psi$. The maximum is sharp variation point of F, which is the point of interest, whereas the minimum corresponds to slow variation. With a second derivative operator ψ' it is difficult to distinguish these two types of zero crossings. On the contrary, with the first derivative ψ one can easily detect the sharp variation points by only locating the local maxima of $|f * \psi|$, which is the modulus of $f * \psi$. Besides, finding a maximum point is much easier than locating a zero crossing point.

In the frequency domain, the smooth function θ features a low-pass filter while its first derivative ψ is a band-pass filter. The function ψ can be considered to be a wavelet because its integral is equal to zero by definition. Let ψ_s be the function dilated by scale factor s. The wavelet transform of f under scale s is given by

$$Wf(s) = f * \psi_s \tag{3.14}$$

From above discussion we know that the inflection points with sharp variations can be detected and localized by the modulus maxima of wavelet transform.

3.3.5 Step Identification with LE

After detecting the disturbance points one needs to further identify their types because the sharp variations may either be step or noise. As we discussed the types, or regularities in mathematic terms can be characterized by LE which can be estimated by

the evolution across scales of wavelet transform modulus maxima $|Wf_{\max}(u, j)|$.

To achieve this goal we construct a cubic order B-Spline function as the smooth function and its first-order derivative as the wavelet function, i.e. a quadratic B-Spline wavelet. This wavelet possesses desirable properties, such as the compact support, symmetry and biorthogonality [89]. It has a simple analytical form in frequency domain. The filter length for scaling function and wavelet function are 4 and 2 respectively. This feature results in an efficient numerical implementation for the multi-scale decompositions. For example, if one performs wavelet transform in two scales, $12N$ multiplications and summations will be required, where N is the length of input data.

In Figure 18 four types of singularities, Dirac, white noise, step, and ramp are shown in (a) designated as p1-p4 respectively. Their transform coefficients of quadratic B-Spline wavelet from scale 1 to 3 are given in (b) –(c). From Figure 18 we can observe that for the Dirac and white noise the maxima of wavelet transform coefficient decrease along the evolution of scales while for the step and ramp they increase along the evolution of scales.

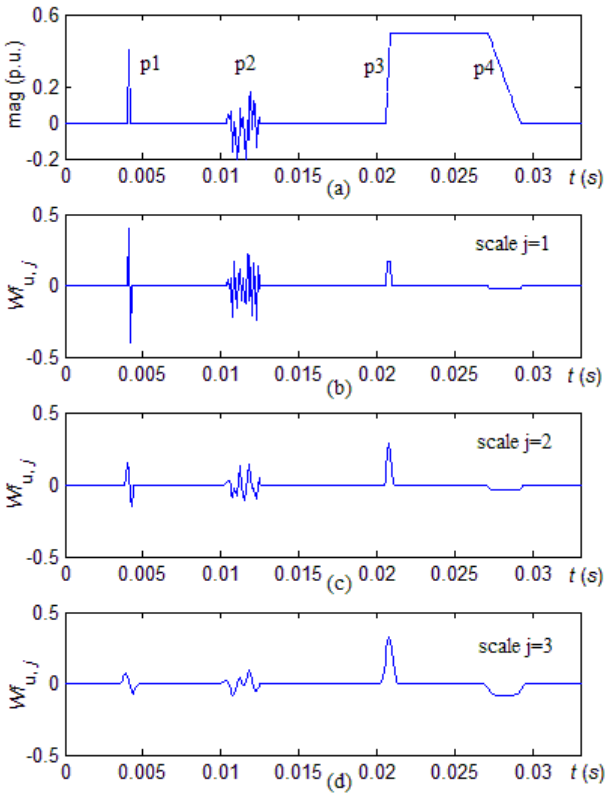

Figure 18 Singularities and their coefficients of wavelet transform across scales

This can be clearly seen by the ratios of wavelet transform modulus maxima for adjacent scales given in Table 2, where $|Wf_{max}(j)|$ stands for the modulus maximum under scale j. The LE estimates by (3.13) are given as well. It has to been pointed out that magnitude steps in voltage waveforms are usually smoothed to appear as a ramp due to their travelling along the transmission lines. As a result the LE will fall into the range between 0 and 1. For simplicity let designate such singularities as steps for the rest of the study.

Table 2 Ratios of wavelet transform modulus maxima and LEs

Type	$\|Wf_{max}(2)\|/\|Wf_{max}(1)\|$	$\|Wf_{max}(3)\|/\|Wf_{max}(2)\|$	LE α
p1	0.38	0.45	-1.42/-1.12
P2	0.21	0.33	-2.26/-1.58
P3	1.75	1.11	0.81/0.15
P4	2.00	2.00	1.00/1.00

3.3.6 Implementation and Threshold

Let $f(k)$ be the samples of the input signal and N be the length of the observed data window. Suppose $f(k)$ is properly processed using low-pass filter to comply with the Sampling Theorem. The process of disturbance detection will be performed to each observed data window (denoted as $f_N(k)$) before directly estimating the phasor over it. The implementation procedure for disturbance detection is:

(1) Detect the singularity of the input signal to see if any disturbance occurs within this window span. Perform wavelet transform using the quadratic B-Spline wavelet in scale 1 to obtain the have coefficient $Wf(k,1)$ (k=1, 2 … N). Under normal conditions, the signal is sinusoidal, thus the coefficient $Wf(k,1)$ has no local modulus maxima. If there is no modulus maximum the process is terminated and data will be handed over to the next process, such as phasor estimation; If the modulus maxima $Wf_{max}(k,1)$ exist then there are singularities within the window and locations can be found by $Wf_{max}(k,1)$ as well.

(2) Identify the type of singularities. The singularities can be either the real transient disturbances (abrupt steps) or the noise caused by a variety of interferences brought into the measurements. To further distinguish them the wavelet transform coefficients in scale 2 is computed and the modulus maxima $Wf_{max}(k,2)$ are found.

If $|Wf_{max}(k,2)| / |Wf_{max}(k,1)| \geq 2^{\alpha=0} = 1$, the singularity is a step, the data will be turned over to the process of the step handler;

If $|Wf_{max}(k,2)| / |Wf_{max}(k,1)| < 2^{\alpha=-0.5} = 0.707$, the singularity is a noise, then the process is terminated and data is turned over to the process for phasor estimation.

3.4 Adaptive Phasor Estimation Scheme

Typically PMUs generate synchrophasors at submultiples of the nominal power system frequency. One cycle period of the input signal is commonly used as the length of the data window for phasor computations. The samples of voltages and currents in a window span are obtained at the same rate as the output phasors. And the position of window is either centered, or sided (at the beginning or the end) at fixed points corresponding to timestamps. The abrupt steps in input signals may affect the accuracy of phasor outputs, particularly when the data window crosses the step point. The method for detecting the transient disturbances has been discussed. This section will introduce an adaptive data window for avoiding or minimizing the impact of disturbances and present a signal model for accurately estimating phasors during transients.

3.4.1 Adaptive Data Window

Suppose that the occurrence of a step change within a span of data window has been identified and localized. Let *N* be the length of the window. As shown in Figure 19 the window for time stamp t_k (denoted as window t_k) contains a step change in waveform. The phasor computed over this window will represent neither the past (normal) state nor the present (faulty) state because it contains partial samples of both states. Since the position of the step change within this window has estimated, we can use the data either before or after the step point.

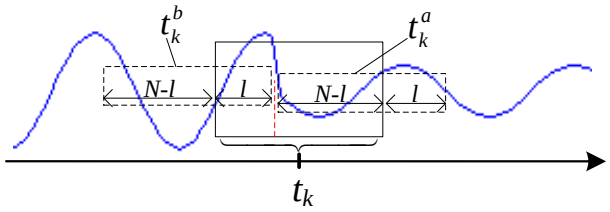

Figure 19 Occurrence of a step change in a data window

To use the data before the singular point the partial data with the length of *l* in window t_k combining the data with the length of *N-l*, which is usually stored in a buffer with continuous sampling, forms the window t_k^b. It should be pointed out that the amplitude of the phasor estimated over the window t_k^b represents the past state while the phase angle starts showing the transition due to the selection of angle reference.

To use the data after the singular point, the window t_k^a is formed by using the partial data with the length of *N-l* in window t_k, and combining the data from the next sampling window with the length of *l*. In this case both the amplitude and phase angle will represent the present state. The phasor output will be delayed because of the wait due to acquiring data *l* in the next sampling window.

Which data window will be used in the algorithm can be determined by the specific requirements of the applications. For example, some applications that require the least output latency may use the window t_k^b; some applications that require a rapid detection of the disturbance state, but can tolerate the delay to a certain level, may use the window t_k^a. How to select the data window for a specific application will not be discussed here. Nevertheless, a simple rule will be followed and it will be used in the algorithm for the rest of the considerations: if the singular point occurs in the first half of the window, as shown in Figure 19, window t_k^a will be used for computing the phasor; if the singular point occurs in the second half of the window, window t_k^b will be used. Based on this rule the maximum delay for using window t_k^a will be half cycle, i.e. *N*/2 times sampling interval.

3.4.2 Phasor Estimation Algorithm

The conventional DFT-based algorithms usually assume a sinusoidal signal model with constant amplitude and phase angle over the observation window. This assumption

is not very rigorous for the signals during power system transients. For better describing the signal in transient state a model with changing amplitude and phase angle is employed:

$$y(t) = a(t) \cdot \cos[2\pi f_0 t + \varphi(t)] \tag{3.15}$$

where f_0 is the nominal frequency, the amplitude $a(t)$ and phase angle $\varphi(t)$ are functions of time. Rewrite (3.15) as

$$y(t) = a(t) \cdot \cos[\varphi(t)]\cos(2\pi f_0 t) - a(t) \cdot \sin[\varphi(t)]\sin(2\pi f_0 t) \tag{3.16}$$

For an observation interval, the $a(t)\cos[\varphi(t)]$ and $-a(t)\sin[\varphi(t)]$ are the envelopes of the nominal frequency components $\cos(2\pi f_0 t)$ and $\cos(2\pi f_0 t)$ respectively. Using the quadratic form to approach the envelopes spanning the observation interval we have,

$$y(t) = (q_0 + q_1 t + q_2 t^2) \cdot \cos(2\pi f_0 t) - (r_0 + r_1 t + r_2 t^2) \cdot \sin(2\pi f_0 t) \tag{3.17}$$

where q_0, q_1, q_2, r_0, r_1, r_2 are the coefficients of quadratic form.

According to the synchrophasor standard C37.118 the amplitude A_1 and phase angle φ_1 are computed over the observation window at the timestamp t_k, which is the point t = 0 in the window. This is also the reference point for computing phase angle. From (3.15) we have $A_1 = a(t)|_{t=0}$, $\varphi_1 = \varphi(t)|_{t=0}$.

Let $\theta(t) = 2\pi f_0 t + \varphi(t)$, then the frequency at the reference point can be represented with

$$f_1 = \left.\frac{d\theta(t)}{2\pi dt}\right|_{t=0} = f_0 + \left.\frac{\varphi'(t)}{2\pi}\right|_{t=0} \tag{3.18}$$

Estimating the quadratic coefficients in (3.17) can be achieved by resolving the linear regression problem. Suppose that the solution depends linearly on the data $\sum_j^M \gamma_{ij} x_j = y_i$ (i = 1, 2… N), that is N linear equations in M unknown coefficients x_1, x_2… x_M, with $N>M$. Rewrite this in matrix form as $H \cdot X = Y$. The fitting variables X are determined in the least square error sense by solving the quadratic minimization problem $argmin||Y-H \cdot X||^2$.

For (3.17) the H matrix is H = [cos($2\pi f_0 t_i$) -sin($2\pi f_0 t_i$) $t_i$cos($2\pi f_0 t_i$) -$t_i$sin($2\pi f_0 t_i$) t_i^2cos($2\pi f_0 t_i$) -t_i^2sin($2\pi f_0 t_i$)], (i = 1, 2… N). The corresponding fitting variable X vector is $X = [q_0\ r_0\ q_1\ r_1\ q_2\ r_2]^T$, where T stands for the transpose. For a N-sample window the H matrix is a N×6 matrix while the fit data Y is a N×1 vector. The position of the phase reference in a given observation window can be determined by assigning time vector $\bar{t}$. If the timestamp is located in the middle of the window let $\bar{t} = [-t_{N/2-1}, \cdots, 0, \cdots t_{N/2}]$; if the timestamp is located at the beginning or the end of the window, assign $\bar{t} = [0, t_1, \cdots t_{N-1}]$ or $\bar{t} = [-t_{N-1}, \cdots, t_1, 0]$, respectively.

After obtaining the fit coefficients, the amplitude and phase angle over the observation window can be computed by the following equations:

$$A_1 = (q_0^2 + r_0^2)^{1/2} \tag{3.19}$$

$$\varphi_1 = \arctan(r_0 / q_0) \tag{3.20}$$

$$f_1 = f_0 + \frac{q_0 r_1 - r_0 q_1}{2\pi(q_0^2 + r_0^2)} \tag{3.21}$$

And the rate of change of frequency $R_f = \mathrm{d}f_1/\mathrm{d}t$. The derivation of the above equations is given in the Appendix A.

3.4.3 Study of Model Accuracy

Equation (3.17) uses the quadratic form to approach the envelope of the slow changing in an observation interval. The adequacy of such approximation is investigated to ensure the model is capable of representing the voltage and current signals measured from the real system. The new synchrophasor standard C37.118.1 (being balloted) defines dynamic signal models and corresponding specification requirements. The dissertation uses the signal models and test conditions defined in the standard draft to study the accuracy of a phasor estimation algorithm.

Two types of signals representing the power oscillation and frequency ramp are given as follows:

a. Power Oscillation

$$y_1(t) = A_m[1 + k_x \cos(2\pi f_m t)] \cdot \cos[2\pi f_0 t + k_a \cos(2\pi f_m t - \pi)] \qquad (3.22)$$

where A_m is the constant amplitude, f_m is the modulation frequency, and k_x and k_a are modulation factors for amplitude and phase angle respectively.

b. Frequency Ramp

$$y_2(t) = A_m \cos(2\pi f_0 t + \pi f_d t^2 + \varphi) \qquad (3.23)$$

where f_d is the rate of frequency change and φ is the initial phase.

0.1% white noise (SNR 60 dB) is added to the test signals. We use one cycle as the observation interval for the phasor measurement. The TVE and the frequency error Δf are used to measure the estimation accuracy. Abundant scenarios that may be observed in real system are studied as summarized in Table 3. The test conditions are more severe than these required by the standard. The maximum values of TVE and frequency error, which correspond the most rigorous conditions, are given in Table 3. For example, as related to type "*a*", the most rigorous condition is f_m=12 Hz, k_x=k_a=0.2. The typical TVE and frequency error are at the level of 0.01 % and 1 mHz respectively. The results demonstrate that the model approach is adequate for representing the power signal under transient conditions.

Table 3 Results for accuracy studies

Type	Conditions (100% rated magnitude and f_0 at start)	Max TVE (%)	Max $\|\Delta f\|$ (Hz)
a	f_m: 0.1 Hz to 12 Hz k_x: 0 to 0.2, k_a: 0 to 0.2.	0.028	0.046
b	f_d: ±0.1 Hz to ±1 Hz Ramp range: ±5 Hz	0.032	0.026

3.5 Implementation of Adaptive Estimator

The adaptive phasor estimation approach has been implemented for real-time use in the synchrophasor measurement test system, which was developed on a PC-based PXI

platform (by National Instruments) and used for PMU calibration and testing [60]. The system consists of a controller, time synchronization clock and data acquisition modules. It is capable of performing synchronous sampling for eight channels at up to 500 kHz. The implementation flow chart of the adaptive scheme is shown in Figure 20, where the "valid" means that the input samples within the observation window have discontinuity caused by electromagnetic disturbance instead of noise.

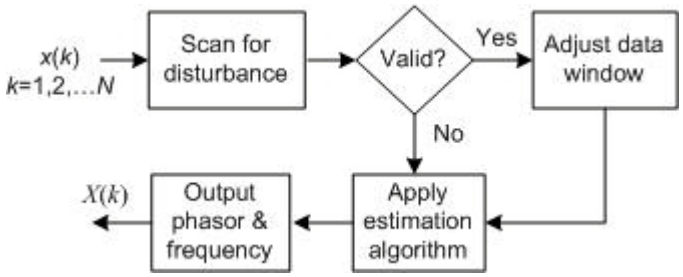

Figure 20 Implementation flow chart for the adaptive approach

Solving the quadratic minimization problem $argmin||Y\text{-}H\cdot X||^2$ is equivalent to solving $\partial \| Y - HX \|^2 / \partial X = 0$, That is

$$-2H^T(Y - HX) = 0 \tag{3.24}$$

Let designate $H^T \cdot Y$ as Z, and $H^T \cdot H$ as G. If we rewrite (3.24), we have

$$G \cdot X = Z \tag{3.25}$$

where G is 6×6 matrix, and Z is 6×1 vector. Then the fitting variables X can be estimated by solving equation (3.25). For efficient implementation, the coefficient matrix G can be

calculated in advance and decomposed into LU matrices for fast computation. It has been proven that the matrix G is nonsingular.

For a given size of data window N, the disturbance check requires about $12N$ multiplications and summations while phasor estimation requires $6N+30$ multiplications and $6N+20$ summations. The computation burden is very low. We have demonstrated that the adaptive approach can be realized in real-time.

3.6 Application Studies

We use voltages and currents generated from the time domain program ATP/EMTP to evaluate the performance of the adaptive phasor estimator under transient conditions. The power system model is a 230 kV power network created by IEEE Power & Engineering Society's PSRC [90]. The files recording voltage and current waveforms are read by program and fed to algorithms. Two scenarios are considered: one is a transmission line fault followed by tripping of faulted line that caused power swing; another is an out of step due to a loss of load. We use 1.92 kHz sampling frequency and one cycle data window. The estimates from three algorithms are compared; the adaptive phasor estimator (denoted as APE), the DFT-based algorithm and the four-parameter algorithm (denoted as FPA) in [12].

3.6.1 Power Swing Followed by Three-phase Fault

We use one phase voltage (from secondary side of instrument transformer) as the

input fed to the phasor estimation algorithms. As shown in Figure 21 two disturbances occurred at t_1 and t_2 which stand for the three phase fault and the clearance of fault respectively, and oscillations followed. The estimated amplitude, phase angle, frequency and TVE in the vicinity of t_1 and t_2 for the three algorithms are given respectively in Figure 22 (a)-(d) at an appropriate zoom. One can see that the DFT and FPA suffer step effects when exposed to the disturbances, particularly for the frequency estimation. In Figure 22 (d) the TVEs exceed 10% during transitions.

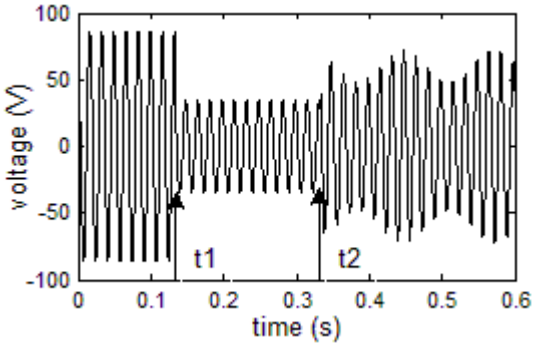

Figure 21 Voltage waveform under fault and power swing condition

The proposed method is capable of detecting the disturbances and computing phasors with adaptive windows. In this case the phasor estimates can follow the input changes very well. The maximum TVEs for DFT, FPA and APE during oscillation are 2.42, 0.89 and 0.12 respectively.

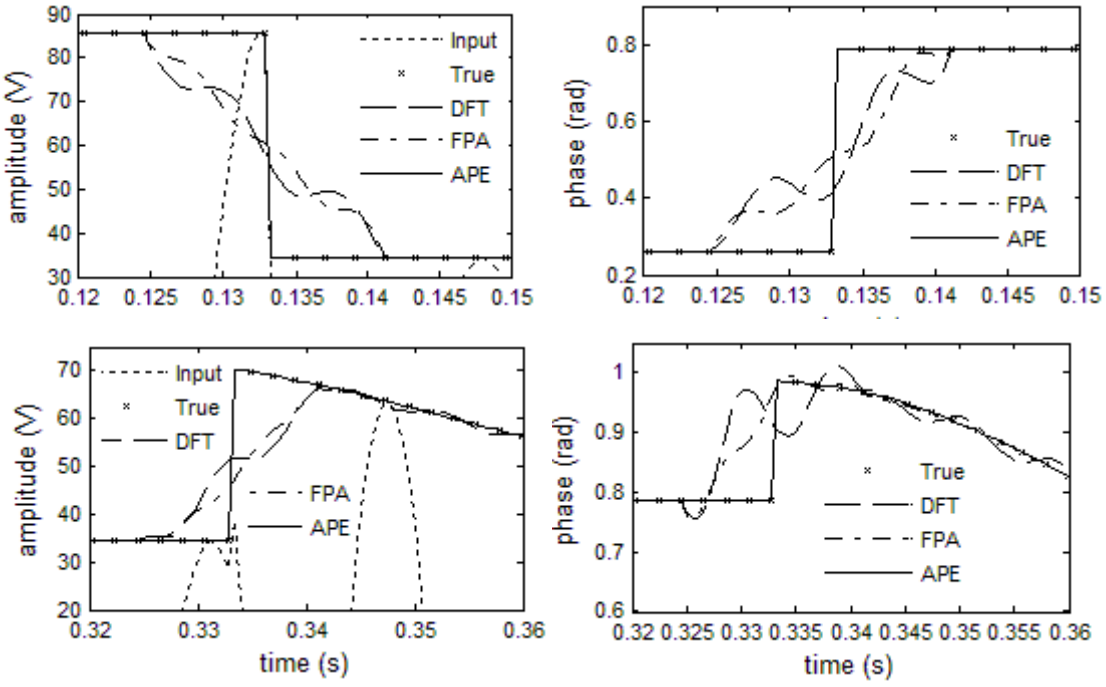

(a) Amplitude estimates (b) Phase estimates

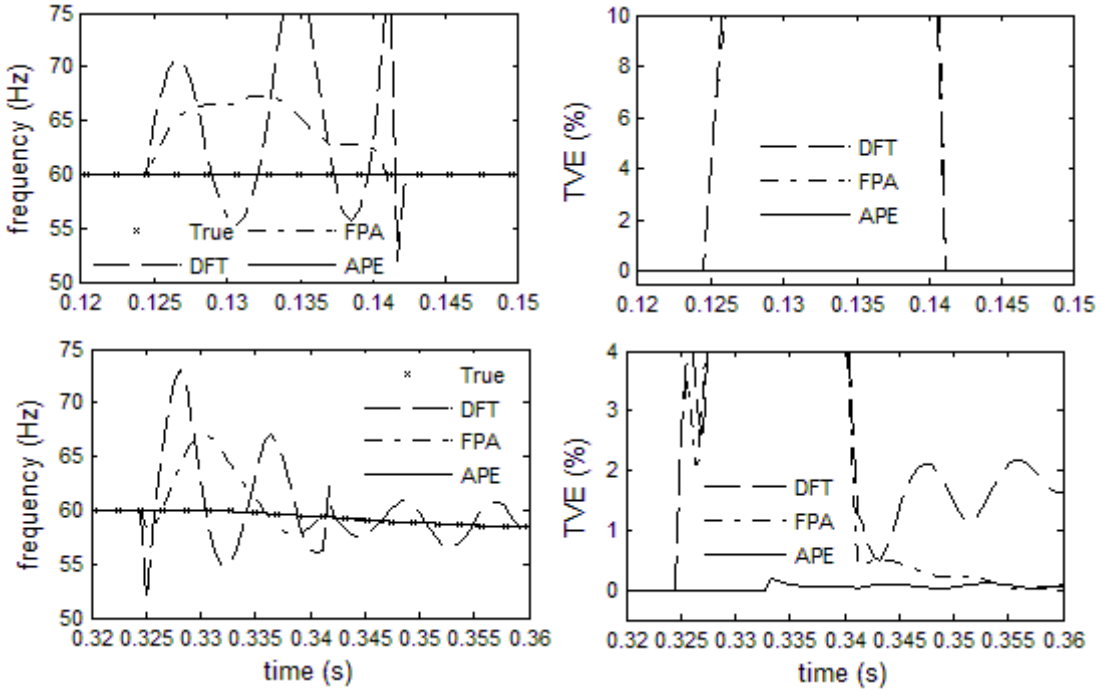

(c) Frequency estimates (d) TVE

Figure 22 Parameter estimates and errors of three algorithms at t_1 and t_2

3.6.2 Out of Step Caused by Loss of Load

One phase current (from secondary side of instrument transformer) is fed to the phasor estimation algorithms. Figure 23 shows the current waveform measured during disturbances. The estimated amplitude, phase angle, frequency and TVE by the three algorithms are given in Figure 24 (a)-(d). Compared to the DFT-based algorithm, both four-parameter algorithm and the proposed phasor estimation method can follow the input during oscillations. The maximum TVEs for DFT, FPA and APE after t_2 are 4.2%, 1.3% and 0.086% respectively. This proves that the proposed dynamic phasor model achieves better accuracy than that of the four-parameter model. From the TVE results in Figure 24 (d) we can observe that the adaptive method successfully detected and localized the discontinuous point t_1 and t_2 so that their effects on outputs were eliminated.

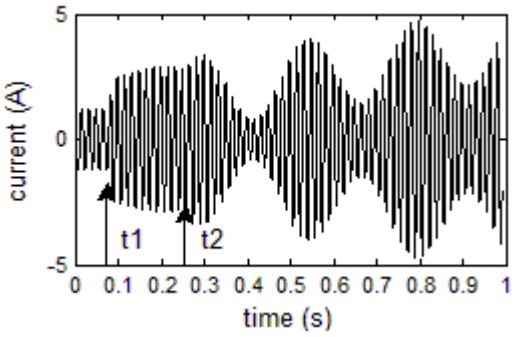

Figure 23 Current waveform under out of step condition

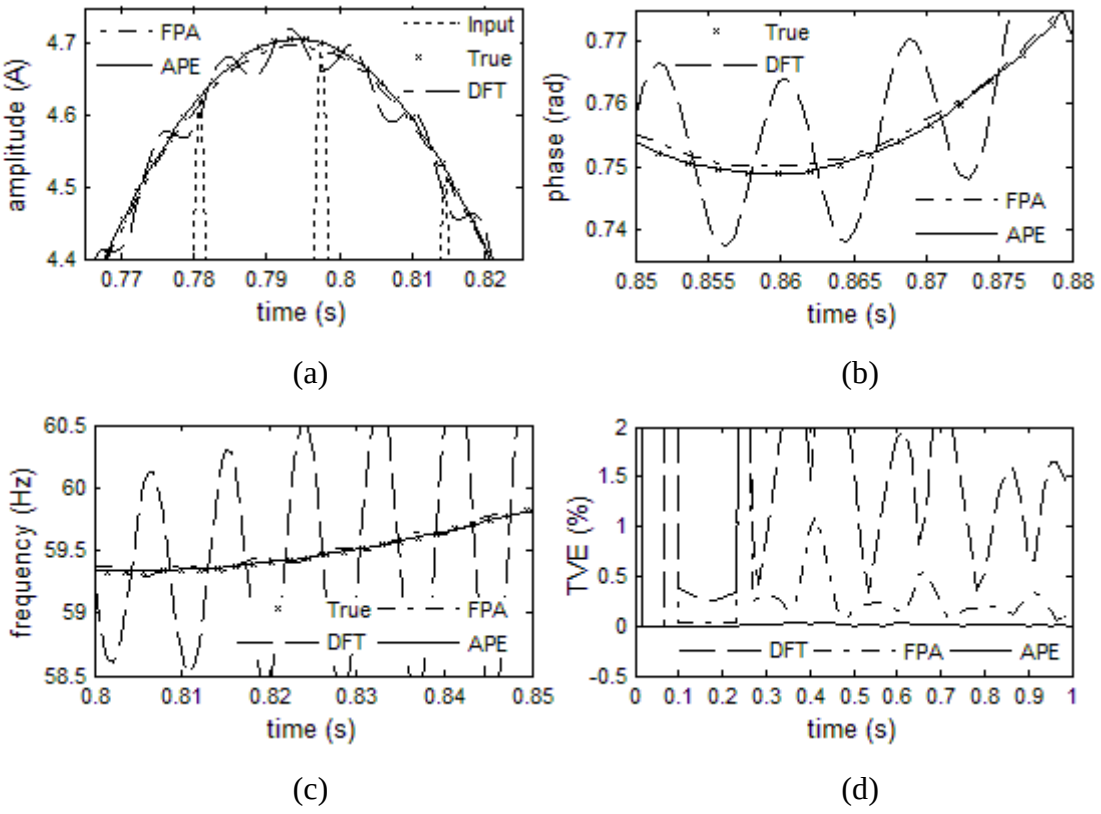

Figure 24 Estimated amplitude, phase, frequency and TVE for three algorithms

3.7 Summary

An adaptive approach for estimating phasor under power system transient conditions in real-time is proposed in the dissertation. The summary is given as follows:

- The wavelet method is able to identify and localize the disturbance while discriminating from various types of noise within a given data window.
- The effect of electromagnetic transients can be eliminated by using adaptive data window.

- The quadratic polynomial model achieves better accuracy during power oscillations.
- The proposed approach can be implemented for real-time synchrophasor estimation. It can also be used as the reference algorithm for testing devices performing synchrophasor measurements.
- The proposed algorithm for disturbance detection can be used to indicate the phasor quality so that the power system applications are able to be aware of whether the phasors they use or the results based on the phasors are valid or not.

4. NEW PHASOR ESTIMATION ALGORITHM*

4.1 Introduction

The phasor frequency, amplitude and phase angle are critical variables used by many algorithms. How to rapidly and accurately estimate frequency and other phasor parameters is still a contemporary topic of research interest.

Discrete Fourier Transform (DFT) is widely used as a filtering algorithm for estimating fundamental frequency phasors [91], [92]. Conventional DFT algorithm achieves excellent performance when the signals contain only fundamental frequency and integer harmonic frequency components. Since in most cases the currents contain decaying DC components this may introduce fairly large errors in the phasor estimation [93], [94].

As addressed in Section 1.2.1, many techniques for the real time estimation of power system frequency have been developed and evaluated in past two decades [15]-[24]. Some methods were developed to improve the performance of DFT based approaches. Such improvements include adaptive methods based on feedback loop by tuning the sampling interval, adjusting data window length, changing the nominal

---

* Part of the material in this section is reprinted from "Real time power system frequency and phasor estimation using recursive wavelet transform" by Jinfeng Ren and Mladen Kezunovic, *IEEE Trans. Power Delivery*, vol. 26, no. 3, pp. 1392-1402, July 2011

frequency iteratively, correcting the gains of orthogonal filters and tuning the weighted factors. Because of the inherent limitation in DFT, at least one cycle of analyzed signal is required, which hardly meets the demand of high-speed response for protection schemes. The methods using consecutive samples of the instantaneous input signal suffer the noise and zero crossing issues. Kalman filter and recursive Least Squares algorithm are well known techniques. Some artificial intelligence techniques, such as genetic algorithm and neural networks have been used to achieve precise frequency estimation over a wide range with fast response. Although better performance can be achieved by these optimization techniques, the implementation algorithm is more complex and intensive in computation.

The techniques developed for eliminating the impact of decaying DC component in phasor estimation include digital mimic filter based methods [25] and parameter estimation based algorithms [26]-[32]. The mimic filter performs well when its time constant matches the time constant of the exponentially decaying component. For parameter estimation based methods, some technique such as the simultaneous equation, partial summation, Taylor expansion and least square method are utilized. Those methods either require additional samples or both voltages and currents, which may cause application problems.

Recursive wavelet approach was introduced in protective relaying for a long time

[95]-[99]. The improved model with single-direction recursive equations is more suitable for the application to real-time signal processing [98]. The band energy of any center frequency can be extracted through recursive wavelet transform (RWT) with moderately low computation burden.

A new mother wavelet with recursive formula is constructed in this study. RWT based real time frequency and phasor estimation and decaying DC component elimination scheme is proposed. Section 4.2 introduces the basic concept of wavelet transform, presents the newly constructed recursive wavelet and its characteristics both in time and frequency domain and describes the process of deriving recursive formula for calculating wavelet transform coefficients. The frequency and phasor estimation algorithm is described in Section 4.3. The analysis of convergence and computation burden is presented in Section 4.3.. The method for eliminating the effect of decaying DC offset is given in Section 4.4. Section 4.5 and 4.6 present the details of performance evaluation and summary respectively.

4.2 Recursive Wavelet Transform

4.2.1 Wavelet Transform Background

Mother wavelet function is defined as a function $\psi(t)$ which satisfies the admissibility condition:

$$C_{\Psi} = \int_{-\infty}^{+\infty} \frac{|\Psi(\omega)|^2}{|\omega|} d\omega < \infty \tag{4.1}$$

i.e. $\Psi(\omega)|_{\omega=0} = \int_{-\infty}^{+\infty} \psi(t)dt = 0$

where $\Psi(\omega)$ is the Fourier transform of $\psi(t)$.

A set of wavelet functions can be derived from $\psi(t)$ by dilating and shifting the mother wavelet, as given below:

$$\psi_{a,b}(t) = a^{-1/2} \cdot \psi(\frac{t-b}{a}), a > 0 \tag{4.2}$$

where a and b are scaling (dilation) factor and time shifting (translation) factor, respectively.

A “good” wavelet is such a function that meets the admissibility condition and has a small time-frequency window area [89]. We construct a mother wavelet function as expressed as follows:

$$\psi(t) = (\frac{\sigma t}{2} + \frac{\sigma^2 t^2}{2} + \frac{\sigma^3 t^3}{3}) e^{(\sigma + j\omega_0)t} u(-t) \tag{4.3}$$

And we designate function $\psi_1(t) = \psi^*(-t)$,

$$\psi_1(t) = (-\frac{\sigma t}{2} + \frac{\sigma^2 t^2}{2} - \frac{\sigma^3 t^3}{3}) e^{(-\sigma + j\omega_0)t} u(t) \tag{4.4}$$

Its frequency domain expression obtained by Fourier transform is given in following expression:

$$\Psi(\omega) = \frac{\sigma(\omega_0 - \omega)^2 - 3\sigma^3}{2 \cdot [\sigma + j(\omega_0 - \omega)]^4} \tag{4.5}$$

Setting $\sigma = 2\pi/\sqrt{3}$, $\omega_0 = 2\pi$ makes the wavelet function $\psi(t)$ admissible, i.e. $\Psi(\omega)|_{\omega=0} = 0$.

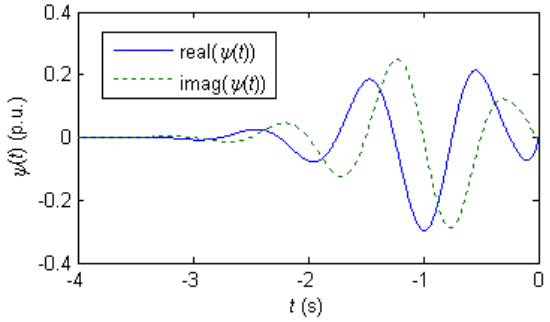

Figure 25 Time domain waveforms of $\psi(t)$

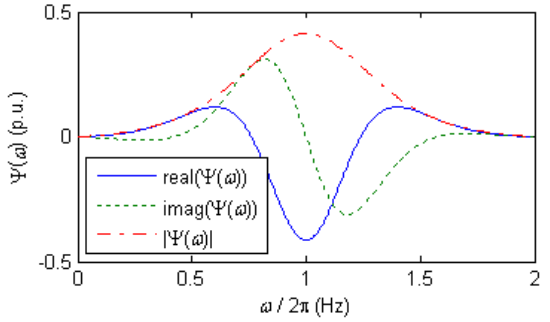

Figure 26 Frequency domain waveforms of $\Psi(\omega)$

One can see that the newly constructed wavelet is a complex function whose time and frequency domain expressions contain real and imaginary parts. Figure 25 and Figure 26 give time and frequency domain waveforms of $\psi(t)$ and $\Psi(\omega)$, respectively. Some performance parameters can be calculated to specify a wavelet function [89]. Time-domain center t^* and window radius Δt of wavelet function $\psi(t)$ are -0.99 s and

0.40 s respectively. As one can see in Figure 26, it features a band-pass filter with the frequency-domain center ω^* and band radius $\Delta\omega$ of 2π rad and 1.38 rad. One of advantages of the wavelet transform is that the quality factor Q, defined as the ratio of frequency center ω^* and bandwidth $2\Delta\omega$, stays constant as the observation scale varies. For $\Psi(\omega)$, $Q = \omega^*/2\Delta\omega = 2.27$. The complex wavelet exhibits good time-frequency localization characteristics. Its time-frequency window area S defined as a product of time window width $2\Delta t$ and frequency band width $2\Delta\omega$ is 2.23 rad·s.

To obtain the center frequency f_c of the band-pass filter, which is defined as the frequency in which the function reaches the maximum magnitude, we have the Fourier transform for the dilated wavelet function $\psi(t/a)$:

$$\Psi(a\omega) = \frac{\sigma(\omega_0 - a\omega)^2 - 3\sigma^3}{2 \cdot [\sigma + j(\omega_0 - a\omega)]^4} \tag{4.6}$$

$|\Psi(a\omega)|$ reaches the maximum value when $a \cdot \omega = \omega_0$, i.e. $a \cdot 2\pi \cdot f_c = 2\pi$. Thus, we have $f_c = 1/a$. That is the scale factor a is reciprocal to the center frequency f_c of the band-pass filter.

4.2.2 Newly Constructed Recursive Wavelet

Since the wavelet function $\psi(t)$ is anti causal which has zeros for all positive time, the wavelet transform coefficient in scale a for a given causal signal $x(t)$ can be expressed as below:

$$W_{x(t)}(a,b) = a^{-1/2}\int_0^b x(t)\cdot\psi(\frac{t-b}{a})^* dt, t>0 \tag{4.7}$$

Let ΔT be the sampling period, n and k are integers. Then $t = n\Delta T$, $b = k\Delta T$. With the observing frequency $f = 1/a$, formula (4.7) can be expressed discretely:

$$W_{x(n\Delta T)}(f, k\Delta T) = \Delta T\sqrt{f}\sum_{n=1}^{\infty} x(n\Delta T)\cdot\psi^*(f(n\Delta T - k\Delta T))$$

$$= \Delta T\sqrt{f}\sum_{n=1}^{\infty} x(n\Delta T)\cdot\psi_1(f(k\Delta T - n\Delta T)) \tag{4.8}$$

Above formula can be expressed using convolution:

$$W_{x(n\Delta T)}(f, k\Delta T) = \Delta T\sqrt{f}[x(n\Delta T) * \psi_1(fn\Delta T)] \tag{4.9}$$

Taking z-transform on both sides, we have,

$$W_x^z(f, Z) = \Delta T\sqrt{f}[X(Z)\cdot\Psi_1(Z)] \tag{4.10}$$

where $W_x^z(f,Z)$, $X(Z)$ and $\Psi_1(Z)$ are z-transforms of discrete sequences $W_{x(n\Delta T)}(f, k\Delta T)$, $x(n\Delta T)$ and $\psi_1(fn\Delta T)$, respectively.

Based on the expression of wavelet function $\psi_1(t)$, we derive its discrete form in terms of observing frequency f,

$$\psi_1(fn\Delta T) = (-\frac{\sigma fn\Delta T}{2} + \frac{\sigma^2(fn\Delta T)^2}{2} - \frac{\sigma^3(fn\Delta T)^3}{3})\cdot e^{(-\sigma + j\omega_0)(fn\Delta T)}u(fn\Delta T) \tag{4.11}$$

Its z-transform is expressed as follows,

$$\Psi_1(Z) = \sum_{n=0}^{\infty}\psi_1(fn\Delta T)\cdot Z^{-n} \tag{4.12}$$

Denote $\alpha = e^{-f\Delta T(\sigma - j\omega_0)}$, we obtain the expression for $\Psi_1(Z)$,

$$\Psi_1(Z) = \frac{\lambda_1 z^{-1} + \lambda_2 z^{-2} + \lambda_3 z^{-3}}{1 + \beta_1 z^{-1} + \beta_2 z^{-2} + \beta_3 z^{-3} + \beta_4 z^{-4}} \tag{4.13}$$

where,

$\lambda_1 = \alpha \cdot [-\sigma f \Delta T / 2 + (\sigma f \Delta T)^2 / 2 - (\sigma f \Delta T)^3 / 3]$, $\lambda_2 = \alpha^2 \cdot [\sigma f \Delta T - 4 \cdot (\sigma f \Delta T)^3 / 3]$

$\lambda_3 = \alpha^3 \cdot [-\sigma f \Delta T / 2 - (\sigma f \Delta T)^2 / 2 - (\sigma f \Delta T)^3 / 3]$, $\beta_1 = -4\alpha$, $\beta_2 = 6\alpha^2$, $\beta_3 = -4\alpha^3$, $\beta_4 = \alpha^4$

From (4.10) and (4.13), we obtain,

$$\begin{aligned} W_x^z(Z) &= \Delta T \sqrt{f} \cdot X(Z)(\lambda_1 z^{-1} + \lambda_2 z^{-2} + \lambda_3 z^{-3}) \\ &\quad - W_x^z(Z)(\beta_1 z^{-1} + \beta_2 z^{-2} + \beta_3 z^{-3} + \beta_4 z^{-4}) \end{aligned} \tag{4.14}$$

According to the properties of inversion of z-transform, we obtain the recursive expression for discretely computing wavelet transform coefficients,

$$\begin{aligned} & W_{x(n\Delta T)}(f, k\Delta T) = \Delta T \sqrt{f} [\lambda_1 x((k-1)\Delta T) \\ & + \lambda_2 x((k-2)\Delta T) + \lambda_3 x((k-3)\Delta T)] \\ & - \beta_1 W_{x(n\Delta T)}(f, (k-1)\Delta T) - \beta_2 W_{x(n\Delta T)}(f, (k-2)\Delta T) \\ & - \beta_3 W_{x(n\Delta T)}(f, (k-3)\Delta T) - \beta_4 W_{x(n\Delta T)}(f, (k-4)\Delta T) \end{aligned} \tag{4.15}$$

In formula (4.15), *f* represents the observing center frequency which is reciprocal to the scale factor *a*. To extract the frequency band energy centered in 60 Hz, for instance, simply apply *f* = 60 to (4.15). One can notice that wavelet transform coefficients can be calculated recursively with the historical data. This type of wavelet transform is so-called the recursive wavelet transform (RWT). Comparing with the RWT in [96] and [98], the proposed RWT requires the historical data and less computation, thus it can be used in real time applications.

4.3 Frequency and Phasor Estimation Algorithm

As discussed in previous section the recursive wavelet (RW) features a complex wavelet whose wavelet transform coefficients (real part and imaginary part) contain both phase and magnitude information of the input signal, based on which the algorithm for estimating the power system frequency and phasor is derived as following.

4.3.1 RWT Based Frequency and Phasor Estimation

Let us consider a discrete input signal that contains *M*th order harmonics with a sampling period ΔT:

$$x(n) = \sum_{m=1}^{M} A_m \cos(2\pi \cdot f_m \cdot n\Delta T + \varphi_m),\ n = 0, 1, 2, \cdots \tag{4.16}$$

where f_m, A_m and φ_m represent the frequency, amplitude and phase angle of *m*th order harmonic, respectively. Denoting the absolute phase angle of the *m*th order harmonic at sample *n* as $\theta_m(n) = 2\pi \cdot f_m n\Delta T + \varphi_m$, one can see that frequency f_m represents the rate of change of θ_m. For simplicity, the sampling period ΔT is neglected when expressing variables for the rest of the paper.

To represent the input signal *x*(*n*) in time-frequency domain apply RWT in scale *a* using (4.15). As derived in Appendix B we have following expression:

$$\begin{aligned} W_{x(n)}(a,k) = &\sum_{m=1}^{M} u_m^c(a, f_m, k) \cdot x_m^c(k) \\ &+ \sum_{m=1}^{M} u_m^s(a, f_m, k) \cdot x_m^s(k),\ k = 0, 1, 2, \cdots \end{aligned} \tag{4.17}$$

From equation (4.17) one can see that the wavelet transform coefficient $W_{x(n)}$ contains information of input signal in both cosine form and sine form, denoted as x_m^c and x_m^s in equation (B.4) and (B.5) respectively, multiplied by weighting factors, denoted as u_m^c and u_m^s in equation (B.6) and (B.7) respectively.

Let $\tilde{f}_m$ represent the initial estimate of frequency variable, and rewrite equation (B.6) using the first order Taylor series expansion. That is

$$u_m^c(a, f_m, k) \cong u_m^c(a, \tilde{f}_m, k) + \left.\frac{du_m^c}{df_m}\right|_{\tilde{f}_m} \cdot \Delta f_m$$

$$= u_m^c(a, \tilde{f}_m, k) + u_m^{c1}(a, \tilde{f}_m, k) \cdot \Delta f_m \tag{4.18}$$

$$u_m^{c1}(a, \tilde{f}_m, k) = -2\pi\sqrt{a}\Delta T^2 \sum_{l=k/a}^{0} l \sin(2\pi\tilde{f}_m a l \Delta T) \cdot Q \tag{4.19}$$

where $Q = [\frac{\sigma}{2}(l\Delta T) + \frac{\sigma^2}{2}(l\Delta T)^2 + \frac{\sigma^3}{3}(l\Delta T)^3] \cdot e^{(\sigma - j\omega_0)\cdot l\Delta T}$.

For simplicity, denote $u_m^c(a, \tilde{f}_m, k)$ and $u_m^{c1}(a, \tilde{f}_m, k)$ as $\tilde{u}_m^c$ and $\tilde{u}_m^{c1}$ respectively. Then we rewrite the equation as follows:

$$u_m^c(a, f_m, k) \cong \tilde{u}_m^c + \tilde{u}_m^{c1} \cdot \Delta f_m \tag{4.20}$$

Following the same procedures we can rewrite equation (B.7S) as follows:

$$u_m^s(a, f_m, k) \cong \tilde{u}_m^s + \tilde{u}_m^{s1} \cdot \Delta f_m \tag{4.21}$$

$$\tilde{u}_m^{s1} = 2\pi\sqrt{a}\Delta T^2 \sum_{l=k/a}^{0} l \cos(2\pi\tilde{f}_m a l \Delta T) \cdot Q \tag{4.22}$$

Then formula (4.17) can be expressed as follows:

$$W_{x(n)}(a,k) \cong \sum_{m=1}^{M} [\tilde{u}_m^c \cdot \tilde{x}_m^c(k) + \tilde{u}_m^{c1} \cdot \tilde{x}_m^{c1}(k)]$$

$$+ \sum_{m=1}^{M} [\tilde{u}_m^s \cdot \tilde{x}_m^s(k) + \tilde{u}_m^{s1} \cdot \tilde{x}_m^{s1}(k)] \tag{4.23}$$

where $\tilde{x}_m^{c1} = \tilde{x}_m^c \cdot \Delta f_m$ and $\tilde{x}_m^{s1} = \tilde{x}_m^s \cdot \Delta f_m$.

Applying RWT to $x(n)$ in a series of scales a_1, a_2, …, a_{4M} we obtain a series of coefficients w_1, w_2, …, w_{4M} that can be expressed in (4.23). Rewrite those equations in matrix form:

$$\begin{bmatrix} w_{a_1} \\ w_{a_2} \\ w_{a_3} \\ w_{a_4} \\ \vdots \\ w_{a_{4M}} \end{bmatrix} \cong \begin{bmatrix} \tilde{u}_{1,a_1}^c & \tilde{u}_{1,a_1}^{c1} & \tilde{u}_{1,a_1}^s & \tilde{u}_{1,a_1}^{s1} & \cdots & \tilde{u}_{M,a_1}^{s1} \\ \tilde{u}_{1,a_2}^c & \tilde{u}_{1,a_2}^{c1} & \tilde{u}_{1,a_2}^s & \tilde{u}_{1,a_2}^{s1} & \cdots & \tilde{u}_{M,a_2}^{s1} \\ \tilde{u}_{1,a_3}^c & \tilde{u}_{1,a_3}^{c1} & \tilde{u}_{1,a_3}^s & \tilde{u}_{1,a_3}^{s1} & \cdots & \tilde{u}_{M,a_3}^{s1} \\ \tilde{u}_{1,a_4}^c & \tilde{u}_{1,a_4}^{c1} & \tilde{u}_{1,a_4}^s & \tilde{u}_{1,a_4}^{s1} & \cdots & \tilde{u}_{M,a_4}^{s1} \\ \vdots & \vdots & \vdots & \vdots & \ddots & \vdots \\ \tilde{u}_{1,a_{4M}}^c & \tilde{u}_{1,a_{4M}}^{c1} & \tilde{u}_{1,a_{4M}}^s & \tilde{u}_{1,a_{4M}}^{s1} & \cdots & \tilde{u}_{M,a_{4M}}^{s1} \end{bmatrix} \cdot \begin{bmatrix} \tilde{x}_1^c \\ \tilde{x}_1^{c1} \\ \tilde{x}_1^s \\ \tilde{x}_1^{s1} \\ \vdots \\ \tilde{x}_M^{s1} \end{bmatrix} \tag{4.24}$$

For simplicity, we represent above matrix in vector form. At sample k we have the following equation:

$$W(k) \cong \tilde{U}(k) \cdot \tilde{X}(k) \tag{4.25}$$

In (4.25) the wavelet coefficient $W(k)$ can be calculated using recursive equation (4.15). For weighting factor $\tilde{U}(k)$, it can be calculated with estimated frequency $\tilde{f}_m$ using equations (B.6), (B.7), (4.19) and (4.22). Solving equation (4.25) we obtain vector variable $\tilde{X}(k)$. Then we can derive the following formula for Δf_m:

$$\Delta f_m = \frac{\tilde{x}_m^c(k) \cdot \tilde{x}_m^{c1}(k) + \tilde{x}_m^s(k) \cdot \tilde{x}_m^{s1}(k)}{(\tilde{x}_m^c(k))^2 + (\tilde{x}_m^s(k))^2} \tag{4.26}$$

After we estimate the frequency adjustment, update frequency with $\tilde{f}_m + \Delta f_m$ and iterate above approximation procedures until either the frequency change reaches the cutoff value, for example $\varepsilon = 0.001$ Hz, or a maximum number of iterations denoted as L is performed. As a result, the real frequency can be estimated at the last iteration. Then the amplitude A_m and phase angle φ_m can be estimated by the following equations:

$$A_m = \sqrt{\tilde{x}_m^c(k) + \tilde{x}_m^s(k)} \tag{4.27}$$

$$\varphi_m = \theta_m(k) - 2\pi \cdot \tilde{f}_m \cdot k\Delta T \tag{4.28}$$

where $\theta_m(k) = \cos^{-1} \tilde{x}_m^c(k)$ or $\theta_m(k) = \sin^{-1} \tilde{x}_m^s(k)$.

The flow chart as given in Figure 27 illustrates the implementation of procedures for the proposed frequency, magnitude and phase estimation algorithm. In practice, a low-pass filter with appropriate cutoff frequency is applied for eliminating high frequency components in voltage and current measurements. As a result, the order of harmonic components can be limited within the range of cutoff frequency. For example, if a third order Butterworth low-pass filter with cutoff frequency 320 Hz is used to pre-filter input signals, in this case the maximum order of harmonics will be limited to five, i.e. $M = 5$. Generally we select m multiples of nominal frequency (i.e. $f_0 = 60$ Hz, m represents the order of harmonics) as initial estimate to start iterations. To achieve high accuracy, scale factors [a_1, a_2… a_{4M}] are required to cover all the frequency components of the signal being analyzed. Therefore, we select $a_m = 1 / (f_0 \times (1+(m-1)/4))$. Extensive

simulations show that proposed algorithm can converge to the real value within three iterations.

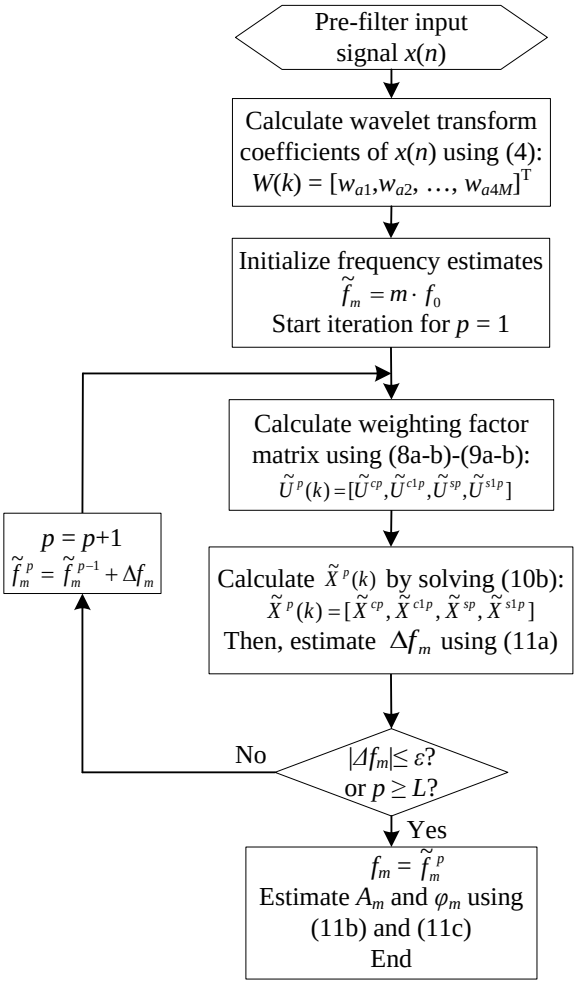

Figure 27 Flow chart of the frequency, magnitude and phase estimation

It should be noted that if only the fundamental frequency component is of interest, i.e. only f_1 is taken into iteration loop, the dimension of scale factors and weighting

matrix will be reduced to 2*M*+2.Obviously, if input signal only contains the fundamental frequency component the solved variables x_m^c and x_m^s ($2 \le m \le M$) will be some numbers close to zero, and then the parameters of those harmonics are meaningless.

4.3.2 Study of Convergence Characteristics

The sampling rate and window length may affect the convergence characteristics because of two factors. One is that these formulae are derived based on the assumption that the error resulting from the discrete computation is negligible. Another is the error introduced by an inherent settling process in recursive equations. Besides, inappropriately selecting window size and sampling rate may cause the weighting factor matrix $\tilde{U}(k)$ to become singular.

To analyze the convergence characteristics, we define the window length l_s as the cycle of the nominal frequency, which is independent of the signal sampling frequency f_s defined as N times nominal frequency f_0 in Hz. The variable l_s and f_s determine the number of samples N_s within a data window, i.e. $N_s = l_s \cdot f_s / f_0 = l_s \cdot N$. Total vector error (TVE) is used to measure the phasor accuracy. Once the amplitude error ΔA_m (in percent of real value) and the phase error $\Delta\varphi_m$ (in degrees) are available, the expression for TVE is given by $TVE_m = \sqrt{(\Delta A_m)^2 + (\Delta\varphi_m / 0.573)^2}$, where 0.573 is the arcsine of 1% in degree.

The signal model in (4.16) is used for the algorithm convergence analysis. In (4.16)

we let f_1 = 60 Hz and M = 5, that is the fundamental frequency component contained in the signal is 60 Hz and the frequency of harmonic noise is up to 300 Hz. Analysis results are given in Figure 28, in which dot represents the convergence while “x” stands for divergence. Results indicate that the window length can be shortened to 0.2 cycle if the sampling rate is 70 samples per cycle (i.e. 4.2 kHz) or higher.

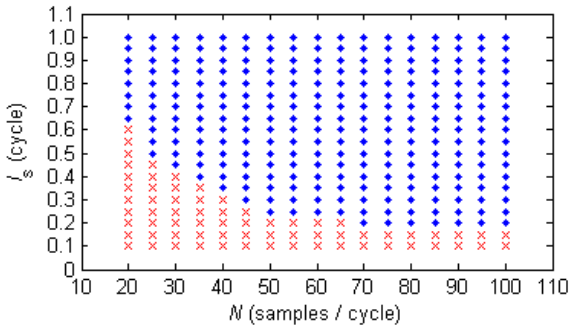

Figure 28 Convergence analysis results

Let us consider a case when the fundamental frequency deviates to 65 Hz and perform the algorithm to estimate frequency, magnitude and phase. Relationships between frequency error, TVE and two variables l_s and f_s are shown in Figure 29 and Figure 30 respectively, in which the signal sampling rate is simulated from 50 to 150 samples per cycle while the window length changes from 0.25 to 1 cycle. One can see that the proposed algorithm achieves high accuracy and fast convergence. Simulations performed in Section 4.5 also show that for a broad range of frequency deviation, such as

55 Hz – 65 Hz, the algorithm can converge to the real value within three iterations. Besides, the sampling rate has barely any effect on the accuracy once it reaches to 50 samples per cycle (i.e. 3 kHz for 60 Hz power system) or higher. Comparing to the conventional DFT based methods this algorithm can shorten the window length to a quarter- cycle.

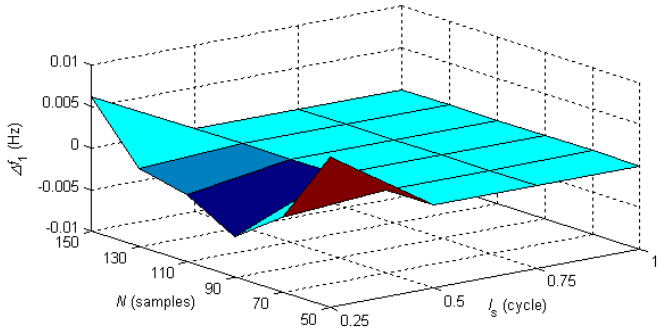

Figure 29 Estimated frequency error for f_1=65 Hz

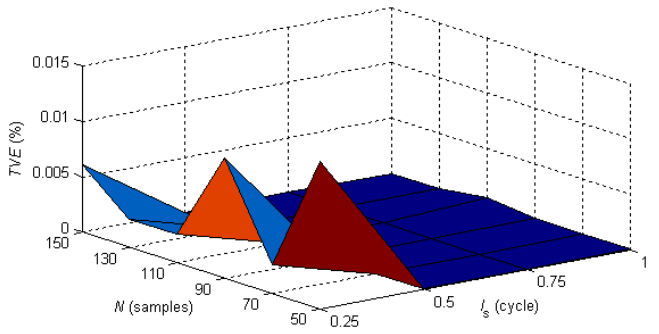

Figure 30 Estimated TVE for f_1=65 Hz

4.3.3 Analysis of Computational Burden

Let us now consider the computation burden of the proposed algorithm. If we use 3 kHz sampling frequency and 0.25 cycle data window as the case performed in convergence analysis and performance tests it approximately requires 6000 multiplications and 5796 summations. Only $68*(2M+2) = 816$ multiplications and $51*(2M+2) = 612$ summations are used for computing RWT coefficients $W_{2M+2}(12)$ (where $M=5$), and $3*(2M+2)^3 = 5184$ multiplications and summations for matrix inverse computation when three iterations are performed. Weighting matrix $U(12)$ with various scales and frequencies can be calculated and stored in advance and can be accessed very fast using a table look-up method. Some mathematical techniques such as Chelosky and LU factorization methods can be adopted to simplify the matrix computation [100], [101]. The computation burden can then be noticeably reduced to $68*(2M+2) + 3*(2M+2)^2 = 1248$ multiplications and $51*(2M+2) +3*(2M+2)^2 = 1044$ summations. Besides, increasing the window length has very small effect on the total computation burden because it only increases the computation burden of RWT coefficients while the matrix dimension stays the same. Based on the analysis one can see the total computation burden is fairly low. It can satisfy the time response requirement of time-critical applications.

4.4 Eliminating Decaying DC Component

Similar derivation procedures can be used to develop the algorithm for eliminating the effect of decaying DC Offset. Let us consider the following signal model that contains the exponentially decaying component:

$$y(n) = x(n) + A_\tau \cdot e^{-n\Delta T \cdot \tau}, \quad n = 0, 1, 2, \cdots \tag{4.29}$$

where $x(n)$ is the signal model defined in (4.16), A_τ and τ represent the amplitude and time constant of DC offset respectively.

Applying RWT in scale a to represent signal $y(n)$ in time-frequency domain as derived in the Appendix B we have:

$$W_{y(n)}(a,k) = W_{x(n)}(a,k) + u_\tau(a,\tau,k) \cdot x_\tau(k), k = 0, 1, \cdots \tag{4.30}$$

From equation (4.30) one can see that the wavelet coefficient $W_{y(n)}$ contains the coefficient for signal $x(n)$ and the weighted decaying DC component. Since the time constant is unknown to u_τ, iterations are required to approximate it.

Let $\tilde{\tau}$ represent the initial estimate and rewrite equation (B.11) using the first order Taylor series expansion, we have

$$\begin{aligned} u_\tau(a,\tau,k) &= u_\tau(a,\tilde{\tau},k) + \left.\frac{du_\tau}{d\tau}\right|_{\tilde{\tau}} \cdot \Delta\tau \\ &= u_\tau(a,\tilde{\tau},k) + u_\tau^1(a,\tilde{\tau},k) \cdot \Delta\tau \end{aligned} \tag{4.31}$$

where $u_\tau^1(a,\tilde{\tau},k) = -\sqrt{a}\Delta T^2 \sum_{l=k/a}^{0} l \cdot e^{-al\Delta T \cdot \tau} \cdot Q$

For simplicity, denote $u_\tau(a,\tilde{\tau},k)$ and $u_\tau^1(a,\tilde{\tau},k)$ as $\tilde{u}_\tau$ and $\tilde{u}_\tau^1$ respectively, and rewrite above formula as follows: $u_\tau(a,\tau,k)=\tilde{u}_\tau+\tilde{u}_\tau^1\cdot\Delta\tau$

Then the equation (4.13) can be expressed as follows:

$$\begin{aligned}W_{y(n)}(a,k)=&\sum_{m=1}^{M}[\tilde{u}_m^c\cdot\tilde{x}_m^c(k)+\tilde{u}_m^{c1}\cdot\tilde{x}_m^{c1}(k)]\\&+\sum_{m=1}^{M}[\tilde{u}_m^s\cdot\tilde{x}_m^s(k)+\tilde{u}_m^{s1}\cdot\tilde{x}_m^{s1}(k)]\\&+\tilde{u}_\tau\cdot\tilde{x}_\tau(k)+\tilde{u}_\tau^1\cdot\tilde{x}_\tau^1(k)\end{aligned}\tag{4.32}$$

where $\tilde{x}_\tau^1=\tilde{x}_\tau\cdot\Delta\tau$.

Applying RWT to $y(n)$ in a series of scales a_1, a_2, …, a_{4M+2} we obtain a series of coefficients w_1, w_2, …, w_{4M+2} that can be expressed as the following matrix:

$$\begin{bmatrix}w_{a_1}\\w_{a_2}\\\vdots\\w_{a_{4M}}\\w_{a_{4M+1}}\\w_{a_{4M+2}}\end{bmatrix}=\begin{bmatrix}\tilde{u}_{1,a_1}^c&\tilde{u}_{1,a_1}^{c1}&\cdots&\tilde{u}_{M,a_1}^{s1}&\tilde{u}_{\tau,a_1}&\tilde{u}_{\tau,a_1}^1\\\tilde{u}_{1,a_2}^c&\tilde{u}_{1,a_2}^{c1}&\cdots&\tilde{u}_{M,a_2}^{s1}&\tilde{u}_{\tau,a_2}&\tilde{u}_{\tau,a_2}^1\\\vdots&\vdots&\ddots&\vdots&\vdots&\vdots\\\tilde{u}_{1,a_{4M}}^c&\tilde{u}_{1,a_{4M}}^{c1}&\cdots&\tilde{u}_{M,a_{4M}}^{s1}&\tilde{u}_{\tau,a_{4M}}&\tilde{u}_{\tau,a_{4M}}^1\\\tilde{u}_{1,a_{4M+1}}^c&\tilde{u}_{1,a_{4M+1}}^{c1}&\cdots&\tilde{u}_{M,a_{4M+1}}^{s1}&\tilde{u}_{\tau,a_{4M+1}}&\tilde{u}_{\tau,a_{4M+1}}^1\\\tilde{u}_{1,a_{4M+2}}^c&\tilde{u}_{1,a_{4M+2}}^{c1}&\cdots&\tilde{u}_{M,a_{4M+2}}^{s1}&\tilde{u}_{\tau,a_{4M+2}}&\tilde{u}_{\tau,a_{4M+2}}^1\end{bmatrix}\cdot\begin{bmatrix}\tilde{x}_1^c\\\tilde{x}_1^{c1}\\\vdots\\\tilde{x}_M^{s1}\\\tilde{x}_\tau\\\tilde{x}_\tau^1\end{bmatrix}\tag{4.33}$$

For simplicity, we represent above matrix in vector form. At sample k we have the following equation:

$$W'(k)=\tilde{U}'(k)\cdot\tilde{X}'(k)\tag{4.34}$$

In (4.34) the wavelet coefficient $W'(k)$ can be calculated using recursive equation (4.15). For weight factor $\tilde{U}'(k)$, it can be calculated with approximate frequency $\tilde{f}_m$ and

time constant $\tilde{\tau}$ using equations (B.6), (B.7), (4.19), (4.22), (B.11) and (4.31) respectively. Solving matrix (4.34) we obtain vector variable $\tilde{X}'(k)$. Then we can derive the formula to estimate $\Delta\tau$:

$$\Delta\tau = \tilde{x}_\tau^1(k) / \tilde{x}_\tau(k) \tag{4.35}$$

And formula (4.26) can be used to estimate Δf_m. After we obtain the time constant and frequency adjustments, update those two variables with $\tilde{f}_m + \Delta f_m$ and $\tilde{\tau} + \Delta\tau$, and iterate above approximation procedures until either the changes of variables reach the cutoff value or a maximum number of iterations is performed. As a result, the real frequency and time constant can be estimated at the last iteration. Then the amplitude A_m and phase angle φ_m can be estimated using equation (4.27) and (4.28) respectively. If we approximate exponential function using the second order Taylor expansion, we obtain:

$$x_\tau(k) = A_\tau \cdot e^{-k\Delta T\cdot\tau} = A_\tau \cdot [1 - k\Delta T \cdot \tau + \frac{1}{2}(k\Delta T \cdot \tau)^2] \tag{4.36}$$

The formula for estimating the magnitude of the decaying DC component is:

$$A_\tau = \frac{\tilde{x}_\tau(k)}{1 - k\Delta T \cdot \tilde{\tau} + \frac{1}{2}(k\Delta T \cdot \tilde{\tau})^2} \tag{4.37}$$

The initial estimate of the time constant $\tilde{\tau}$ can be selected from a wide range: a half cycle to five cycles [25]. Generally we select two cycles as the initial estimate. The expression for x_τ is given in (13). Given the sampling rate N and window size 1/4 cycle the equation (B.10) can be rewritten as $x_\tau = A_\tau \cdot e^{-1/4d}$ ($\tau = f_0/d$, f_0 = 60 Hz) or $x_\tau = A_\tau \cdot e^{-1/d}$ (the window size is 1 cycle). Considering a typical range for the time

constant variable of decaying DC component (d = [0.5, 5]) x_τ would take on the range $0.61A_\tau$~$0.95A_\tau$ or $0.14A_\tau$~$0.82A_\tau$ (A_τ is the amplitude of the decaying DC component), respectively. One can see that the value of x_τ has the same level as its amplitude. Thus the issues of noise and division by zero due to the small value can be avoided. The flow chart for performing the algorithm is similar to the one shown in Figure 27 except for modifying the wavelet coefficients and weighting matrix and introducing time constant variables into iteration loop.

4.5 Performance Evaluation

In this section, performance of the proposed estimation algorithm is fully evaluated with various test conditions covering static state, dynamic state and transient state, and the results are compared with conventional DFT methods, improved DFT-based methods in [15]-[17] and the latest published techniques in [19], [20], [30] and [31]. In the static test, a signal model containing harmonics and noise is used and the performance is verified in a wide range of frequency deviation. The dynamic test uses the scenarios that may occur in real power system. The scenarios including the frequency ramp, short-circuit fault and power swing are simulated using appropriate signal models. In the transient test, three-phase current outputs from ATP/EMTP [90] are used to verify the performance of eliminating the DC offset. All tests are performed with the sampling rate N = 50 samples per cycle, i.e. f_s = 3 kHz, and data window size l_s = 0.25

cycle (12 samples).

4.5.1 Static Test

A signal model in (4.38) containing harmonics and 0.1% (signal-to-noise ratio SNR=60dB) white noise is assumed, where $e(n)$ represents the zero-mean Gaussian noise. Let A = 1.0 p.u., $\varphi = 5^{\circ}$. The fundamental frequency f_1 varies over a wide range from 55 Hz to 65 Hz in 0.2 Hz steps. Frequency error and TVE (total vector error) of the fundamental frequency component are estimated. Comparing to the DFT based methods in [15]-[17] the algorithm can output the frequency and phasor parameters in about 4 milliseconds. The method using three consecutive samples of the instantaneous signal in [19], [20], denoted as MV, achieves the uncertainty of 10 million Hz. But they require higher sampling frequency (6.4 kHz and higher) and the additional time delay (approximately two cycles) introduced by the band pass filtering. The results are shown in Figure 31. The output accuracy can be improved by extending the data window. Simulation results show that the maximum frequency error and TVE can be reduced to 0.05 Hz and 0.17% respectively when l_s is extended to a half cycle.

$$x(n) = \sum_{m=1}^{5} \frac{A}{m} \cos(2\pi \cdot m \cdot f \cdot n\Delta T + m \cdot \varphi) + e(n) \tag{4.38}$$

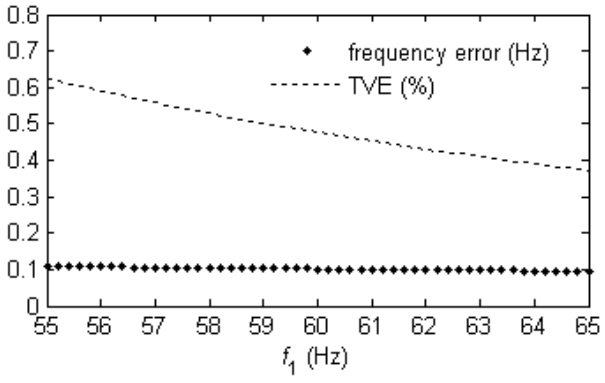

Figure 31 Static test results using a quarter cycle data window

4.5.2 Noise Test

The inherent noise rejection capability of the algorithm is investigated by the noise test. The signal model for static test is used. Let the fundamental frequency take the nominal value (60 Hz). For each level of the Gaussian noise three data windows (quarter cycle, half cycle and one cycle) were applied. The test was conducted using the method MV except applying the variable data windows because the MV has fixed size of data window. Each case was performed 10 times and the maximum value of the frequency estimate error for both RWT and MV, and TVE for RWT are shown in Table 4. As one can expect the better noise rejection can be obtained by slowing down the output response, i.e. prolonging the window span. The accuracy of RWT with one cycle window is in the same level with that of MV. The MV requires extra delay caused by filtering.

Table 4 Test results for noise tests

Noise Level (SNR)	Window l_s (cycle)	RWT $\lvert f_{Error}\rvert$(Hz)	RWT TVE (%)	MV $\lvert f_{Error}\rvert$(Hz)
0.1% (60dB)	0.25	0.16	0.36	0.0043
	0.5	0.042	0.12	
	1.0	0.0029	0.036	
0.32% (50dB)	0.25	0.42	0.94	0.0076
	0.5	0.17	0.40	
	1.0	0.0051	0.064	
1% (40dB)	0.25	0.86	1.60	0.084
	0.5	0.35	1.08	
	1.0	0.068	0.26	
3.2% (30dB)	0.25	1.04	2.73	0.19
	0.5	0.58	1.59	
	1.0	0.10	0.68	

4.5.3 Dynamic Test

a. Frequency Ramp

The following synthesized sinusoidal signal with a frequency ramp is used to perform the frequency ramp tests.

$$x(n) = A \cdot \cos(2\pi \cdot f \cdot n\Delta T + \pi \cdot df \cdot (n\Delta T)^2 + \varphi) \tag{4.39}$$

df is the frequency ramp rate. The signal frequency starts from 59 Hz followed by a positive ramp +10 Hz / sec starting at 0.1 second and ending at 0.3 second, and then stays at 61 Hz for another 0.1 second. Figure 32 shows the estimated frequencies and the true values. The transient behavior at the signal start and each discontinuity are shown as

well. One can see that the outputs follow the inputs very closely and fast. The algorithm is able to output in about four milliseconds with a quarter cycle window. The maximum error during ramp is 0.012 Hz. As discussed in the noise test using more data can improve the tracking accuracy but results in the lower response as a trade-off.

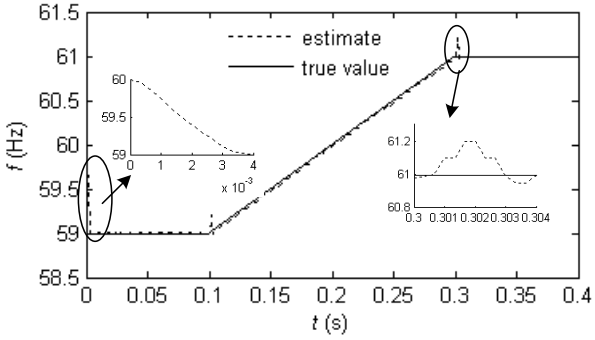

Figure 32 Frequency ramp test results

b. Step Change

To evaluate the dynamic response when exposed to an abrupt signal change, a positive step followed by a reverse step back to the starting value under various conditions is applied to the amplitude, phase angle and frequency of a sinusoidal signal respectively. Studies indicate that under all three types of steps the algorithm shows similar dynamic behavior. The results of the amplitude step (10% of normal value), phase step (π/18 rad) and frequency step (1 Hz) are presented by Figure 33, Figure 34 and Figure 35 respectively. The steps occur at 0.02s and 0.06s. One can observe that

the outputs track the changes in inputs very fast.

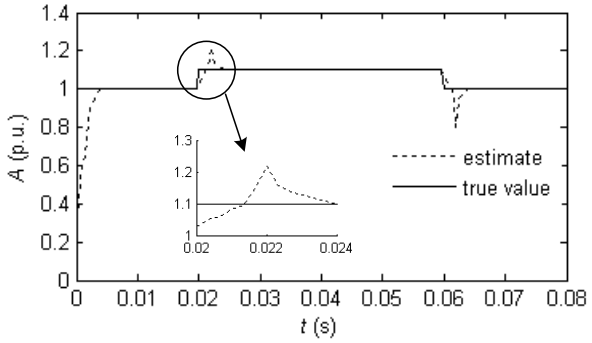

Figure 33 Dynamic response for amplitude step

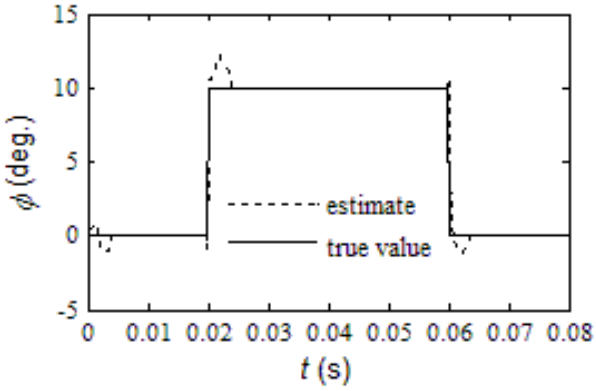

Figure 34 Dynamic response for phase angle step

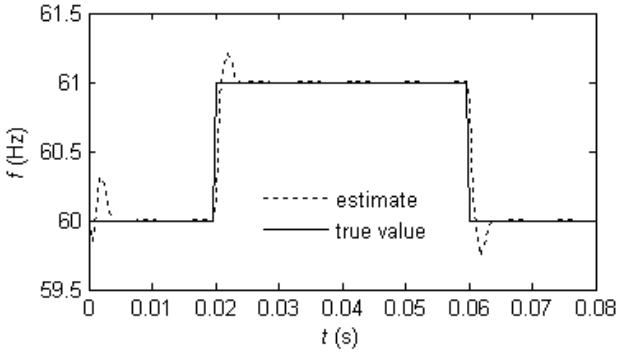

Figure 35 Dynamic response for frequency step

To investigate the effect of pre-filtering on the algorithm dynamic performance a third order Butterworth low-pass filter with cutoff frequency 320 Hz is used to process the input signals. Figure 36 shows the result of amplitude step test. Comparing to Figure 33 which shows the transient behavior without signal pre-filtering, one can see that the low-pass filter enlarges the overshoot and undershoot, and slows the response from 4 milliseconds to 10 milliseconds through it is still faster than the DFT-based methods and instantaneous sample based methods.

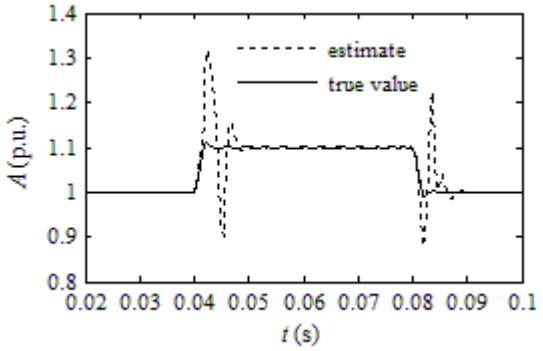

Figure 36 Dynamic response for amplitude step with pre-filtering

c. Modulation

A sinusoidal modulation signal model is used to simulate the transient progress of voltage and current signals during power swing. Its amplitude and phase angle are applied with simultaneous modulation as shown in the following expression:

$$x(n) = A \cdot (1 + k_x \cos(2\pi \cdot f_a \cdot n\Delta T))$$

$$\cdot \cos(2\pi \cdot f \cdot n \cdot \Delta T + k_a \cos(2\pi \cdot f_a \cdot n\Delta T - \pi)) \qquad (4.40)$$

where f_a is the modulation frequency, k_x is the amplitude modulation factor, and k_a is the phase angle modulation factor. Equation (B.12-14) in the Appendix B provides the true value of frequency, amplitude and phase angle for the modulated signal model at output sample *k*.

Table 5 Test results for modulation tests

f_a (Hz)	RWT Δf_{mi}(Hz)	MV Δf_{mi}(Hz)	TVE (RWT)	
			m_i (%)	σ_i(%)
0.1	0.0018	0.0035	0.0070	0.0040
0.5	0.0218	0.0193	0.0805	0.0386
1.0	0.0538	0.0492	0.1612	0.0772
1.5	0.0857	0.1046	0.2417	0.1158
2.0	0.1178	0.1230	0.3227	0.1542

Let k_x = 0.1, k_a= 0.1 radian and modulation frequency vary from 0.1 Hz to 2 Hz in 0.1 Hz step. The results are compared to the instantaneous sample based method MV. The mean of frequency deviation Δf_{mi} obtained by RWT and MV, and the mean m_i and standard deviation σ_i of the TVE by RWT in one second are calculated. As shown in Table 5, the algorithm achieves good dynamic performance when exposed to signal oscillations.

4.5.4 Transient Test

A 230 kV power network is modeled in EMTP to generate waveforms for testing the performance when eliminating decaying DC offset. A three-phase fault is applied and the three-phase currents are used as input signals. Figure 37 shows the phase-A current waveform. One can see that the signal is contaminated with decaying DC component and high frequency noise during the beginning of post-fault. The third order Butterworth low-pass filter with cutoff frequency 320 Hz is used to attenuate the high frequency components. Parameters estimation for the steady state (twenty cycles after the fault occurs) is used as a reference to measure the total vector errors.

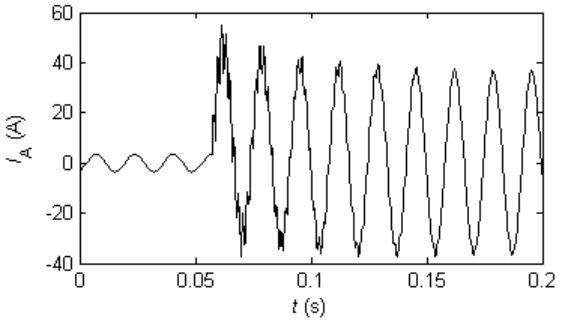

Figure 37 Phase-A current waveform

As shown in Table 6 the results are compared with the conventional full cycle DFT (FCDFT), half cycle DFT (HCDFT) methods, least error square method (LES), simplified algorithm (SIM3) in [31] and hybrid method (HM) in [30]. In Table 6 t_s is the

time (in cycles) when the TVEs are measured. For the high accuracy the algorithm was adjusted to a three-quarter cycle window span. Results show that the accuracy is comparable to those of LES, SIM3 and HM methods while the proposed algorithm requires shorter data window, which results in faster response.

Table 6 Test results for decaying DC offset

Filter	t_s (cycle)	I_A TVE (%)	I_B TVE (%)	I_C TVE (%)
FCDFT	5	0.9487	0.9559	0.9540
HCDFT	12.5	1.0156	1.0144	1.0166
LES	1.0	0.1082	0.1065	0.1062
SIM3	1.0	0.1129	0.1099	0.1118
HM	1.0	0.1202	0.1147	0.1174
RWT	0.75	0.1236	0.1145	0.1162

4.6 Summary

This section proposes a new wavelet function and its recursive wavelet transform. The method allowing real time estimation of power system frequency, magnitude and phase while eliminating the impact of decaying DC component based on RWT is proposed. The algorithm advantages are summarized as follows:

- The algorithm features rapid response and accurate result over a wide range of frequency deviations. It uses only a quarter cycle of input signals for outputting frequency, magnitude and phase results for a signal contaminated with

harmonics . The sampling rate and observed window size can be chosen to meet selected applications requirements.

- Analysis of the algorithm convergence characteristics indicates that the higher the sampling rate, the shorter the computation data window and faster the rate the method outputs phasor, and vice versa.
- The decaying DC component can be completely removed by estimating its parameters using RWT.
- The performance of the proposed algorithm is evaluated under a variety of conditions including static state, dynamic state and transient state. Comparing with other techniques results demonstrate the advantages.
- Computation burden analysis indicates that the computation requirement is moderate. Thus this approach can satisfy the time critical demand of the real time applications in power systems.

5. CHARACTERIZING DYNAMIC BEHAVIOR USING STEP SIGNALS*

5.1 Introduction

As the development of Smart Grid projects, a number of commercial PMUs have been deployed in the eastern and western systems in North America. There are many companies competing in this market. Thus the performance of each individual PMU potentially becomes an essential aspect that could directly affect the performance of the entire system. The issues for current test methodology and tools have been discussed in Section 1.2.2, that talks about the PMU responses to a step signal, which is a typical signal in dynamic conditions, have not been studied in past efforts [33]-[51].

This section presents a test methodology and tools for characterizing dynamic behavior of PMUs when exposed to step signals. A least-square linear-fit based phasor estimation method for achieving high accuracy of reference phasors and a method for interleaving signal steps with timestamps to equivalently increase the reporting rate of output phasors so that they precisely depict PMU step behavior are presented. Three commercial PMUs are selected to perform step tests using the synchrophasor test system,

---

* Part of the material in this section is reprinted from "Characterizing dynamic behavior of PMUs using step signals" by Jinfeng Ren, Mladen Kezunovic and Gerard Stenbakken, *European Transactions on Electrical Power*, DOI: 10.1002/etep, copyright © 2010 by John Wiley & Wiley & Sons, Ltd.

which will be described in this section. A set of programs are developed based on the dynamic test system to automate step test procedures. Four types of tests are performed with balanced and unbalanced three-phase step signals as reference signals to characterize the step responses of PMUs. Four performance indices for step tests are defined to evaluate the dynamic performance.

The rest of this section is organized as follows: this section presents the method for estimating reference phasors. The test implementation framework of the step test programs are described in Section 5.3. The test plan and performance indices for characterizing PMU responses are specified in this section as well. Test results and contributions are summarized in Section 5.4 and Section 5.5 respectively.

5.2 Computing Reference Phasors

5.2.1 Phasor Estimation Method

PMUs provide values for the voltage and current phasors at reporting times synchronized to UTC, which provided by time code. This is done by sampling the respective signals around the UTC time code, selecting a number of the samples (windowing), and analyzing the data with a model. When testing PMUs the test systems do something very similar. They sample the voltage and current signals applied to the PMUs with a sampler synchronized to PPS (a series of pulse chain per second) obtained through GPS receiver and analyze the measurements to determine the reference values

to which the PMU output values are compared. This section describes the model and windowing methods used in the step tests.

To estimate the amplitude, phase angle and dc component of the reference measurement, a three-parameter linear fit model is employed. Consider a sinusoidal signal model expressed as follows:

$$y = A \cdot \cos(2\pi \cdot f_0 \cdot t + \theta) + B \tag{5.1}$$

where A is the amplitude, f_0 is the fundamental frequency, θ is the phase angle, and B is the dc component.

If we rewrite (5.1) we have

$$y = A \cdot \cos\theta \cdot \cos(2\pi \cdot f_0 \cdot t) - A \cdot \sin\theta \cdot \sin(2\pi \cdot f_0 \cdot t) + B. \tag{5.2}$$

If we have a series of samples $y = y_1, y_2, \cdots, y_n$ at times $t = t_1, t_2, \cdots, t_n$ from the measurement system, for example, then these samples can be fit to the matrix model X consisting of the three column vectors as

$$X = [\cos(2\pi \cdot f_0 \cdot t) \quad \sin(2\pi \cdot f_0 \cdot t) \quad 1]. \tag{5.3}$$

The vector of fit coefficients $\overline{\beta}^T = [\beta_0 \quad \beta_1 \quad \beta_2]$, where $\overline{\beta}^T$ is the transpose of $\overline{\beta}$, are determined in the least square error sense by $\overline{y} \cong X \cdot \overline{\beta}$ using the Normal equation. Then we can compute the amplitude, phase angle, and dc component as follows:

$$A = \sqrt{\beta_0^2 + \beta_1^2}, \quad \theta = \arctan(\beta_1 / \beta_0), \quad B = \beta_2. \tag{5.4}$$

The step change in a signal may affect the accuracy of phasor estimation,

particularly when the data window crosses the step point. In order to avoid or minimize this impact, a special routine is applied to achieve accurate values, which act as reference measurements to evaluate the errors of the PMU being tested. There are two cases that need to be discussed: step point at an output timestamp and step point between two output timestamps. Figure 38 gives an example for the first case where a step occurs at the timestamp t_m. P_{m-1} and P_{m+1} are the output phasors at corresponding timestamps t_{m-1} and t_{m+1}. To estimate the phasor at t_m, one can use the data window either before or after t_m. They are P'_m and P''_m as shown in Figure 38, and the phase angle should be calculated at the end and beginning of the data window correspondingly.

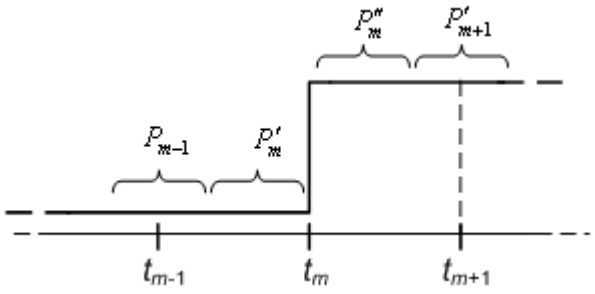

Figure 38 Example of the step point at a time stamp

For the second case, to estimate P_m and P_{m+1} appropriate data windows should be selected to eliminate the impact of the step position, as shown in Figure 39. The step position should be known precisely in advance so that the data windows for the “special”

timestamps contain samples on only one side of the step. In the synchrophasor test system, which is described more fully in section 6, the signal waveforms are typically generated with D/A converters operation at 200 ksps and the data is sampled with A/D converters operating at 50 ksps. At these sampling rates the step transitions show no samples or at most one sample. At generation and sampling rates of 500 ksps, the step transitions generally show 2 to 3 samples.

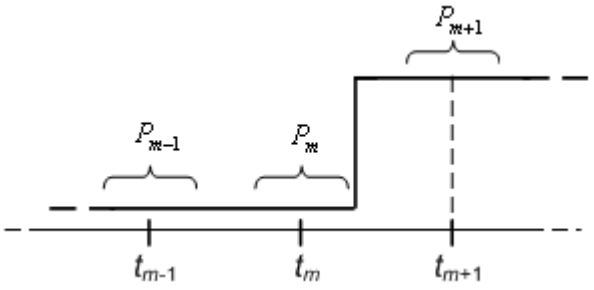

Figure 39 Example of the step point between timestamps

5.2.2 Increasing Phasor Output Rate

A PMU outputs synchrophasors at submultiples of the nominal power system frequency. The IEEE C37.118 standard requires reporting rates from 10 frames per second up to a maximum of 25 frames per second and 30 frames per second for 50 Hz and 60 Hz nominal frequencies respectively. Although many commercial PMUs feature even higher rates of up to 50 frames per second and 60 frames per second for 50 Hz and

60 Hz nominal frequencies respectively, some details of the response of PMU facing a step change of signal could be lost under low output rates. The method described below, which makes use of equivalent time sampling, provides a solution for this problem. A higher resolution measurement of the PMU's step response is made from samples taken on repeated measurements of time shifted step input signals. Because the signal generation is synchronized with UTC, the absolute phase values are the same for times $t = t_1, t_2, \cdots, t_n$ relative to any UTC on second time.

Assume a set of output phasors $\cdots P_{m-1}, P_m, P_{m+1} \cdots$ at timestamps $\cdots t_{m-1}, t_m, t_{m+1} \cdots$ is measured when applying a step signal, so we have the reporting rate $R = 1/(t_m - t_{m-1})$. We repeatedly apply the same step signal N times, however, with a timeshift of $\Delta t = (t_m - t_{m-1}) / N$ among each other relative to the PMU reporting times.

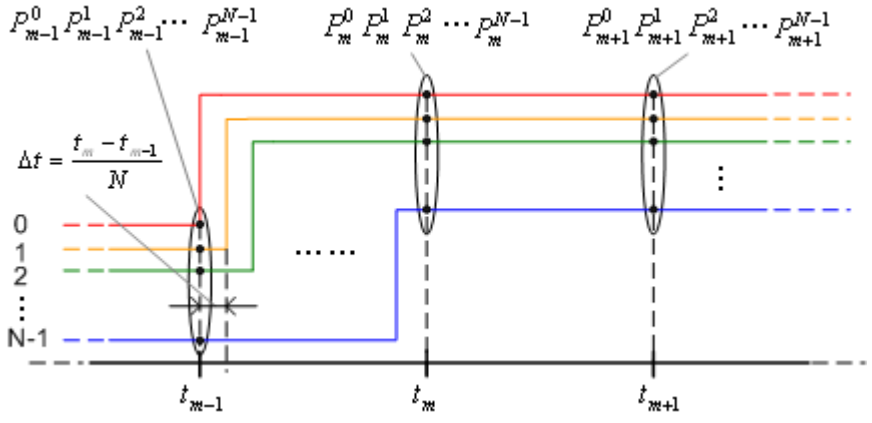

Figure 40 N sets of output phasors obtained by repeated measurements

As shown in Figure 40 we obtain N sets of output phasors: $\cdots P_{m-1}^{0}, P_{m}^{0}, P_{m+1}^{0} \cdots$, $P_{m-1}^{1}, P_{m}^{1}, P_{m+1}^{1} \cdots, \cdots, \cdots P_{m-1}^{N-1}, P_{m}^{N-1}, P_{m+1}^{N-1}$. If one interleaves those phasors in accordance with their timestamps relative to the step time by the way depicted in Figure 41, then one achieves the reporting rate $R' = 1/\Delta t = N/(t_m - t_{m-1})$, which is an N multiple of the original reporting rate R. The effectiveness is presented in Figure 42 and Figure 43, which display output phasors of a PMU before and after interleaving respectively, where N is 10.

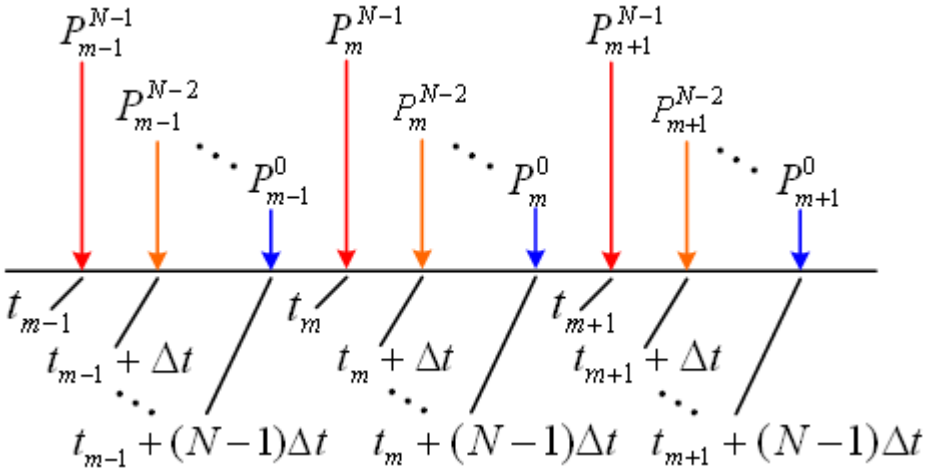

Figure 41 Interleaving of phasors

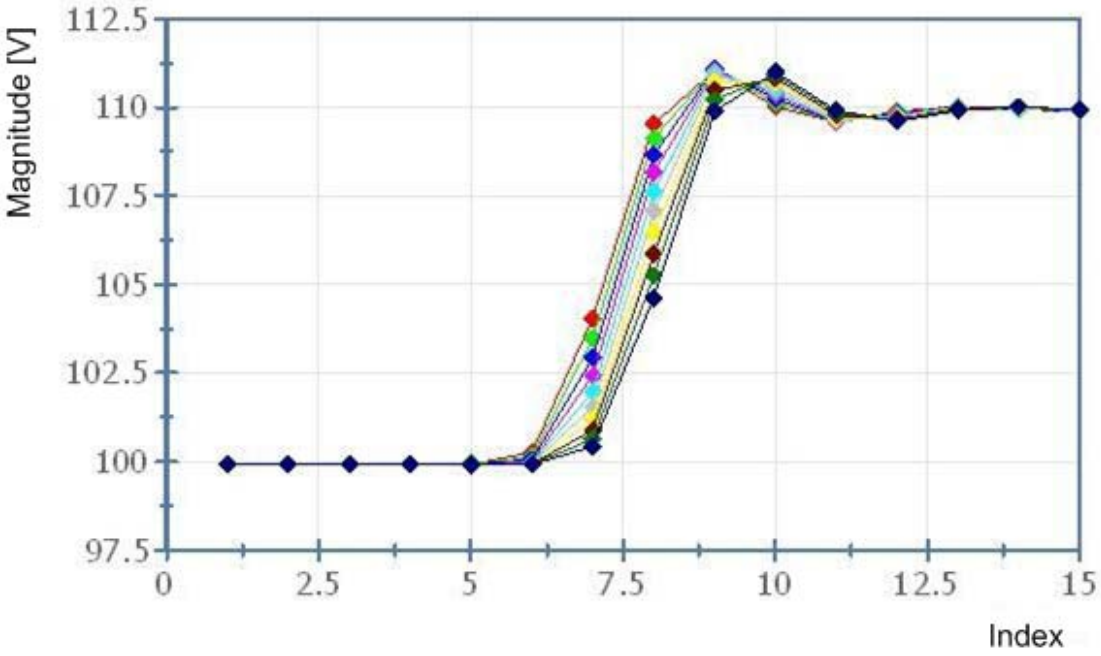

Figure 42 Output phasors of a PMU before interleaving

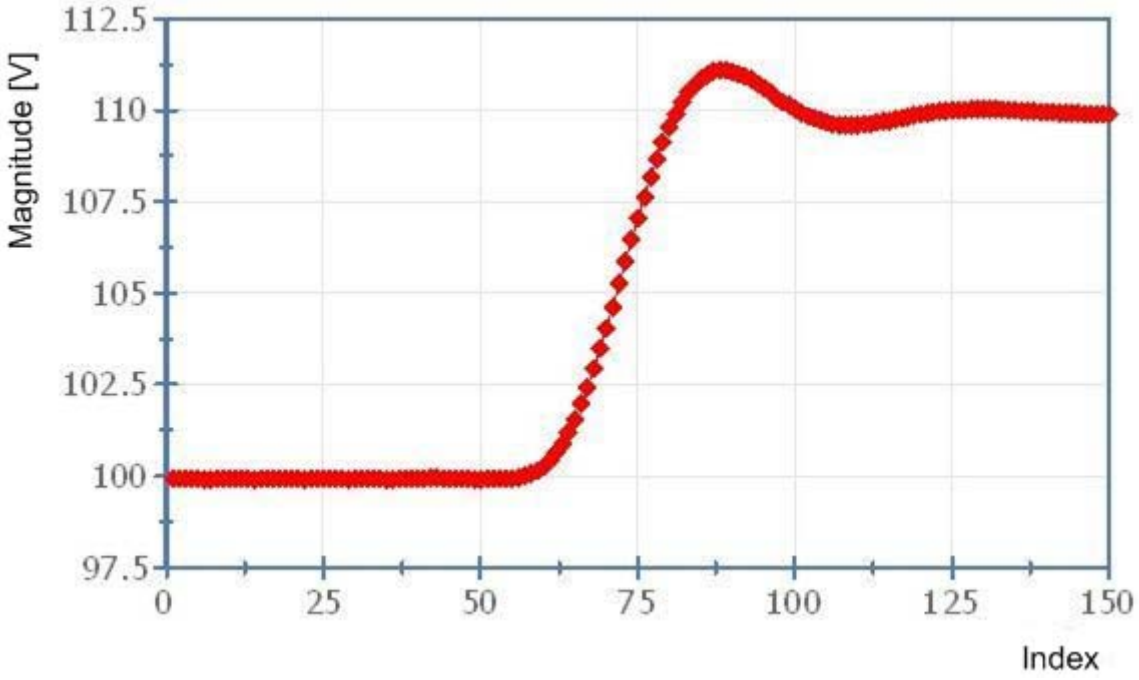

Figure 43 Output phasors of a PMU after interleaving

5.3 Implementation of Step Test

The step tests were performed on the synchrophasor test laboratory setup developed at TAMU. The system will be described in detail in Section 6. This section will focus on what to test and how to perform the test.

5.3.1 Test Plan

Three commercial PMUs were selected to investigate the dynamic behavior using the proposed step test method and tools. These PMUs have various features, such as filter type, output phasor type, reporting rate, communication medium, and so on, which are summarized in Table 7. Three-phase voltages and currents are represented as VA, VB, VC, IA, IB and IC, while three-sequence voltages and current are represented as V1, V2, V0, I1, I2 and I0.

Table 7 Feature summary of PMUs being tested

Feature	PMU A	PMU B	PMU C
Filter Type	Optional	Optional	Optional
Adaptive Tuning	Always on	Always on	Selectable
Output Phasors	VA, VB, VC, V1, IA, IB, IC, I1	VA, VB, VC, V1,V2,V0, IA, IB, IC, I1, I2, I0	VA, VB, VC, V1,V2,V0, IA, IB, IC, I1, I2, I0
Max Reporting Rate (frame /sec)	50 for 50 Hz 60 for 60 Hz	50 for 50 Hz 60 for 60 Hz	50 for 50 Hz 60 for 60 Hz
Communication	Serial Port	Ethernet	Ethernet
GPS Receiver	IRIG-B input	IRIG-B input	Built-in

Table 8 Description of test types and conditions

Test Type	Reference Condition	Description
Magnitude: ±10% step of nominal magnitude	Balanced 3-phase voltage and current signals, magnitude nominal, nominal frequency	From a steady state, apply a balanced magnitude step, followed by a reversed step back to the starting state.
Phase: 10° step of inception angle	Balanced 3-phase voltage and current signals, nominal magnitude, nominal frequency	From a steady state, apply a balanced phase step, followed by a reversed step back to the starting state.
Recovery magnitude: from zero magnitude of one phase to nominal.	Unbalanced, magnitude of non-stepped phases nominal, normal phase angle, nominal frequency	From a steady state, magnitude of one phase steps from zero to nominal, followed by the reversed step back to the starting state.
Recovery phase: from normal phase angle of one phase to 180°	Balanced, magnitude of all phases nominal, normal phase angle on non-stepped phases, nominal frequency	From a steady state, phase angle of one phase steps from normal to 180°, followed by the reversed step back to the starting state.

In terms of a proposed update of Section 5.3 of IEEE C37.118-2005, to accommodate dynamic phasor compliance four types of step tests: magnitude test, phase test, recovery magnitude test and recovery phase test were performed on three selected PMUs described above. Descriptions of test types and test conditions are listed in Table 8.

Four performance indices are measured to characterize the dynamic response of PMUs when exposed to step signals: response time, settling time, overshoot and undershoot, as illustrated in Figure 44. Response time is defined as the time interval from when the step change response leaves the 1% TVE until it re-enters 1% TVE of the

final value. Settling time is defined as the time interval from when the transient signal first enters 1% TVE of the final value until it stays within 1% TVE of the final value. Overshoot and undershoot are defined as the differences between maximum, minimum values of transient signal after first entering 1% TVE of the final value and the final value respectively. Besides, TVE, errors of the magnitude, phase angle, frequency and rate of change of frequency are measured as well to evaluate the accuracy levels of PMUs. Once the magnitude error Δv (in percent of the nominal value) and the phase error $\Delta\theta$ (in degrees) are available, the expression for TVE is given by $\mathrm{TVE} = \sqrt{(\Delta v)^2 + (\Delta\theta / 0.573)^2}$, where 0.573 is the arcsine of 1% in degree.

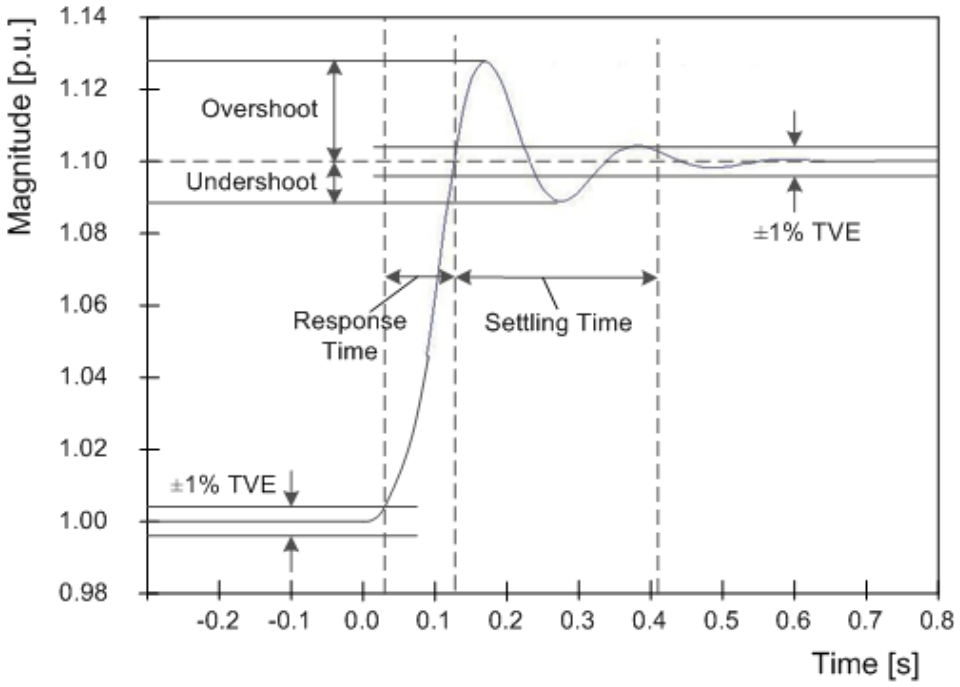

Figure 44 Illustration of performance indices

5.3.2 Test Procedure

One challenge for the step test is how to efficiently perform hundreds of test cases on different PMUs. A set of programs for the step tests are developed based on the dynamic test system to automate the test procedures. The algorithms for estimating the reference phasor are used in these programs. Figure 45 displays the implementation framework of the step test programs. The test procedures are outlined as follows:

a. Initiate test environment, such as generation and sampling rates, signal types and etc., set up calibrator and PMU being tested.
b. Generate test signals and apply to the PMU under test. It should be noted that the calibrator and PMU receive exactly the same test signals.
c. Estimate reference phasors using the method proposed in 5.2, collect and decode phasors measured by PMU.
d. Line up reference and measurement phasors according to the timestamps, and calculate performance indices.
e. Display and store test results through GUI.

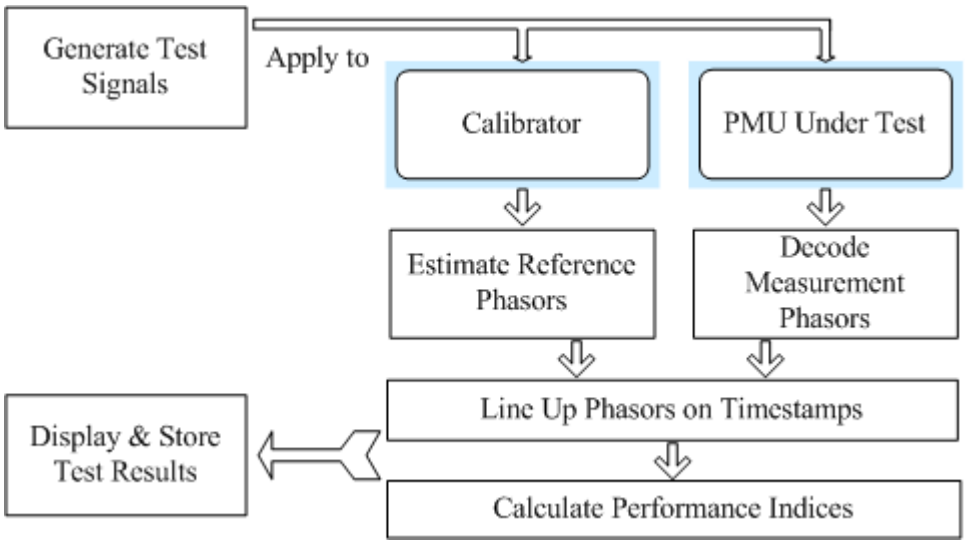

Figure 45 Framework of step test programs

5.4 Test Results

Four types of step tests as described in Table 8 were performed on the three commercial PMUs described in Table 7. The reporting (output) rate for the PMUs was set to 30 frames per second, i.e. the reporting period F_s = 1/30 s. To study the effect of the inception angle on test results, each test runs with the inception angle of voltages and currents from 10º to 340º in 30º steps. The inception angle is the positive sequence phase angle of the applied signals at the time of the step. Various digital filter types for each PMU were studied as well. In sum, over one thousand step cases were performed on each PMU.

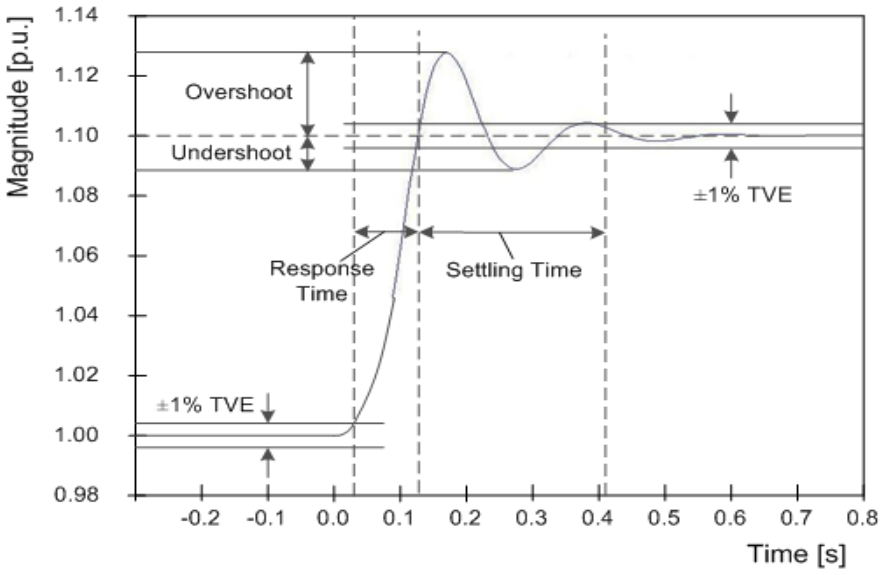

Figure 46 Illustration of performance indices

Test results are presented in Appendix C. Figure 55 - Figure 58 display the magnitude or phase angle and TVE of the positive sequence voltage for the four types of step tests. For PMU A, two steps for each type of step tests were applied at 0.4 s and 0.8 s, respectively. For PMU B and PMU C, two steps for each type of step tests were applied at 0.2 s and 0.4 s, respectively. Each curve consists of the result with different inception angles from 10º to 340º in 30º steps by overlaying them. Some of the performance indices describing the dynamic step transition progresses are given in Table 16 - Table 19, where T_{resp}, T_{set}, O_s and U_s are response time, settling time, overshoot and undershoot, respectively as illustrated in Figure 46. Their values are calculated as maximum values among different inceptions for the first step part. The uncertainty in

these values for the test system is about 0.5 μs for time and 0.05% for magnitude. This data was taken with an interleave factor N of 10. The values of T_{resp}, and T_{set} are measured in units of reporting rate periods, rrp. For these tests the reporting rate was 30 frames per second so rrp = 33.3 ms. The overshoot and undershoot, O_s and U_s , are measured in percent of the step height.

From the test results, we can conclude:

- PMU A exhibits a large post step ripple on all tests. The settling time in all tests exceeds 1.0 rrp and the overshoot is over 10% of the step. That may result from the characteristics of the filter being used.
- PMU B shows very little ripple on all tests and PMU C shows a small symmetric pre step ripple and post step ripple. Their response time and settling time are limited within 1.0 rrp for magnitude and phase tests while 2.0 rrp for recovery magnitude and recovery phase tests.
- The recovery tests present similar transient responses with the normal step tests except that they are measured relative to the higher step values in performance indices.
- The inception angle for both voltage and current has barely any effect on the dynamic performance. Thus, any angle from -180° to +180° can be picked as the reference condition for testing.

5.5 Summary

PMUs as a tool for measuring synchronized phasors has gained wide acceptance in enhancing the monitoring of power grids. However, the performance of each individual PMU manufactured by different companies may vary greatly. Standards for the performance requirements have been made to promote the interoperability of PMUs. These standardization efforts should facilitate their rapid introduction into many power system applications. To promote the common response of PMUs to rapid grid changes, this section proposes an approach to characterize the dynamic performance of PMUs when exposed to step signals, which are summarized as follows:

- The techniques used to achieve high accuracy and high resolution of reference phasors includes the least square linear fit, adaptive data window, and interleaving method.
- Four test types with balanced and unbalanced step signals are described. Step test programs are developed to automate the test procedures.
- Three commercial PMUs are selected to perform step tests using the synchrophasor test system.
- Test results including output phasors and performance indices indicate unique characteristics for some PMUs and good dynamic behavior consistency among most of the tested PMUs.

6. EVALUATING CONFORMANCE PERFORMANCE

6.1 Introduction

In the deployment of the IEDs for substation synchronized measurement applications, the focus at the moment is on two approaches: a) use of PMUs (dedicated high precision recording instruments), and b) use of PMU-enabled IEDs (DFRs, DPRs, DDRs, etc. that have PMU measurement capability). Many utilities will use mixed solutions from multiple vendors due to various equipment purchasing practices and/or phased expansions of system solution over an extended period of time. Using PMUs from different vendors or mixing PMUs and PMU-enabled IEDs may produces interoperability issues in a system solution. To resolve such issues, reference algorithms and test plan need to be developed to verifying the interoperability performance.

As addressed in Section 1.1.2 and Section 1.2.2, the issue how to evaluate the conformance performance of PMUs and PMU-enabled IEDs against the new synchrophasor standard so that the interoperability performance can be improved has not been studied earlier. The dissertation develops a test methodology and tools to fulfill this objective. The rest of this section is organized as follows. The reference signals and scenarios for verifying the conformance test are described in Section 6.2. Section 6.3 specifies the platform for performing the conformance test. This includes descriptions of

a reference PMU and a laboratory setup. Test results and a brief summary for six commercial synchrophasor units are presented in Section 6.4 and 6.5 respectively.

6.2 Conformance Test References

The conformance under specific test conditions is evaluated by comparing the total vector error (TVE), amplitude, phase angle, frequency, and rate of change of frequency (ROCOF) estimates to the corresponding reference values. The test conditions including steady-state and dynamic state are consistent with those defined in C37.118-2005 [5] and C37.118.1 (draft) [52]. The mathematical models used to create test signals for steady and dynamic states are given in Table 9.

Table 9 Test signal models for conformance test

Test Type		Signal Model	Note
Steady state		$x(t) = X_m \cos(2\pi f t + \varphi)$	X_m: amplitude φ: initial angle f: frequency
Dynamic	Modulation	$x(t) = X_m[1 + k_x \cos(2\pi f_m t)] \cdot \cos[2\pi f_0 + k_a \cos(2\pi f_m t - \pi)]$	k_x, k_a : amplitude, phase modulation factor f_m: modulation frequency
	Step change	$x(t) = X_m[1 + k_x u(t)] \cdot \cos[2\pi f_0 t + k_a u(t)]$	$u(t)$: unit step function k_x, k_a : amplitude, phase step factor
	Frequency ramp	$x(t) = X_m \cos(2\pi f_0 t + \pi f_d t^2 + \varphi)$	f_0: nominal frequency f_d: frequency changing rate

The reference scenarios for steady state conditions are described in Table 10. For dynamic scenarios, including the modulations and step changes in amplitude and phase angle, and the ramp changes in frequency are described in Table 11, Table 12 and Table 13, respectively.

Table 10 Test scenarios for steady state condition

Varying Quantity	Reference Condition	Varying Range	
		Class P	Class M
Voltage amplitude	100 % rated, constant phase and nominal frequency	80 – 120%	10 – 120%
Current amplitude		10 – 200%	10 – 200%
Phase angle	Constant angle	± π rad	± π rad
Frequency	Nominal frequency	± 2.0 Hz	$F_s \leq 10$: ± 2.0 Hz; $F_s > 10$: lesser of $\pm F_s/5$ Hz or ±5 Hz

Table 11 Test scenarios for bandwidth condition

Varying Quantity	Reference Condition	Varying Range	
		Class P	Class M
Amplitude and pahase angle modulation: k_x = 0.1 p.u. k_a = 0.1 rad	100 % rated, nominal frequency	Modulation frequency f_m: 0.1 Hz to lesser of $F_s/10$ Hz or 2 Hz	Modulation frequency f_m: 0.1 Hz to lesser of $F_s/5$ Hz or 5 Hz
Phase angle modulation: k_a = 0.1 rad	100 % rated, nominal frequency		

Table 12 Test scenarios for step change condition

Varying Quantity	Reference Condition	Varying Range	
		Class P	Class M
Amplitude	100 % rated, nominal frequency	± 10%	± 10%
Phase angle	100 % rated, nominal frequency	± π/18 rad	± π/18 rad

Table 13 Test scenarios for frequency ramp condition

Varying Quantity	Reference Condition	Varying Range	
		Class P	Class M
Linear frequency ramp: +1.0 Hz/s	100 % rated, nominal frequency	± 2.0 Hz	Lesser of ± Fs/5 Hz or ± 5.0 Hz
Linear frequency ramp: –1.0 Hz/s	100 % rated, nominal frequency		

6.3 Synchrophasor Test System

6.3.1 Laboratory Setup

The conformance tests are performed using a synchrophasor test and calibration system developed at TAMU's lab, as shown in Figure 47. It consists of a GPS receiver used to synchronize the system to UTC, a signal acquisition system used to generate and sample test signals up to 500 kHz, three voltage and current amplifiers connected to PMUs and PMU enabled IEDs providing test signals at typical level, three voltage attenuators and three current shunts. GPS signal, IRIG-B and IEEE 1588 v2 are available for various synchrophasor devices. A series of software models is developed in LabVIEW [102] for implementing steady state and dynamic tests. The software is capable of automating test procedures and analyzing test results.

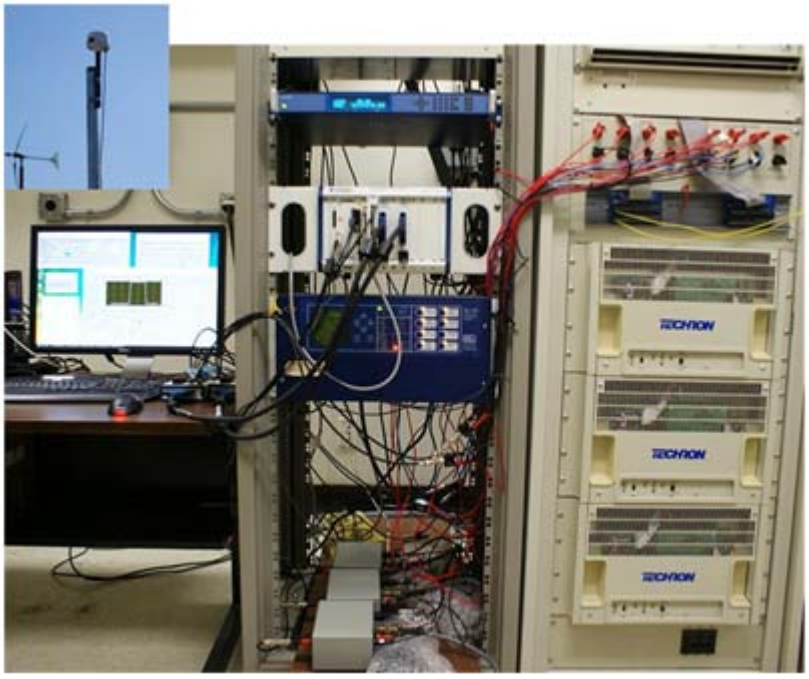

Figure 47 Synchrophasor test and calibration system

The detailed descriptions for the hardware and software of the test system are presented respectively as follows.

a. Hardware

Figure 48 shows the architecture of the synchrophasor test system. Its modules are presented as follows:

- Time synchronization options – provides reference UTC time sources to device under test. The options include direct GPS signal, IRIG-B and IEEE 1588 PTP.
- Data acquisition system – converts digital test signals to analog signals as inputs to amplifiers or synchrophasor units with low-voltage interfaces; samples

voltage and current signals for phasor estimation module.

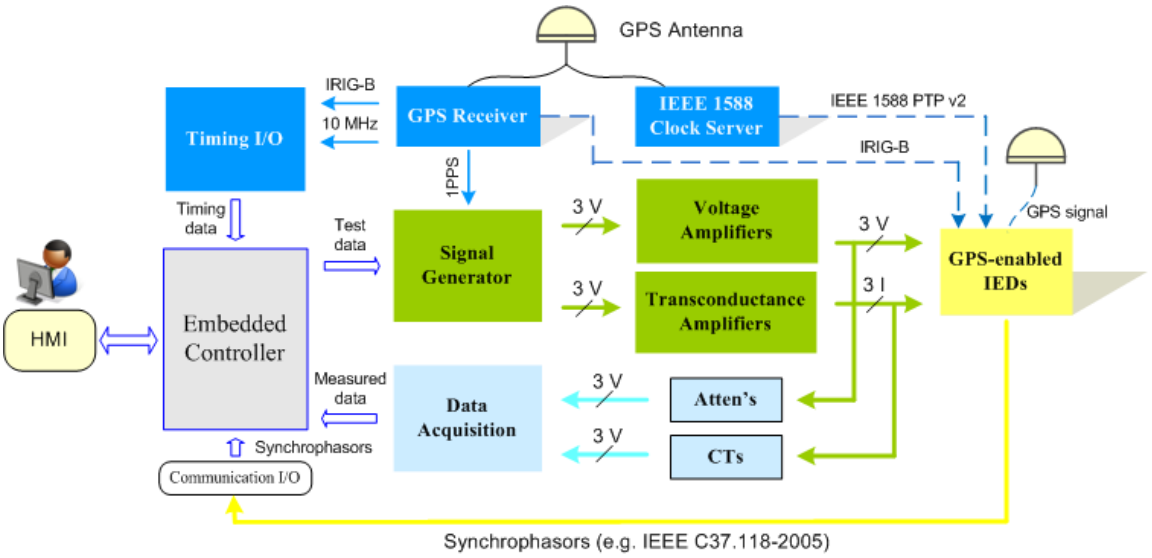

Figure 48 Synchrophasor test system architecture

- Reference signal source and conditioner – provides voltage and current signals in nominal level (voltage: 100 V, current: 5A or 1A); scales high voltage signals down to the low level voltage (≤10 V) for data acquisition system.
- Syncrophasor data interface – provides connection and data transfer for PMUs. The interfaces include serial port and Ethernet connection.
- Reference PMU – provides reference phasors compared to the phasors measured by device under test. The detailed description will be presented in the following section.

- GUI Interface – provides a console for controlling, monitoring and collecting test results.

b. Software

The software for performing the conformance test consists of over 80 routines, five of which operate as main interfaces for user to run steady state and dynamic tests. The step test has individual programs because of the use of special process. One can refer to Section 5 for detail. The main programs and their functions are described as follows:

- Test initialization – initializes test conditions, such as setting the parameters of test signals, signal generation and sampling configurations, PT and CT ratios, output phasors and etc. A screenshot of the front panel is given in Figure 49.
- Data transfer – connects PMUs under test to controller and transfers data between them. This program has two options: one for connection using serial port; another for connection using Ethernet. The control panel of the program for an Ethernet connection is given in Figure 50. The program for serial port uses similar interface but different communication modules.
- Data processing – includes the processes of computing reference phasors, decoding measured phasors from binary data defined in synchrophasor standards, and align the reference phasors and measured phasors according to UTC time. A screenshot of front panel for aligning data again timestamp is given in Figure 51.

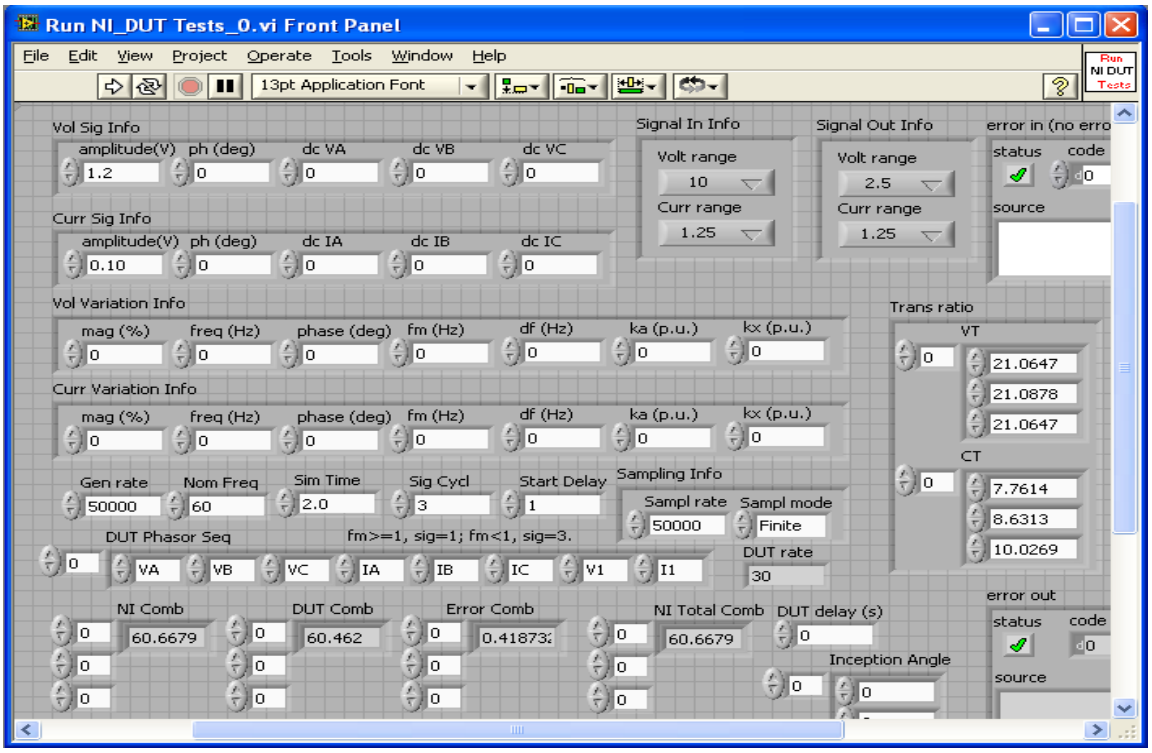

Figure 49 A screenshot of front panel for test initialization

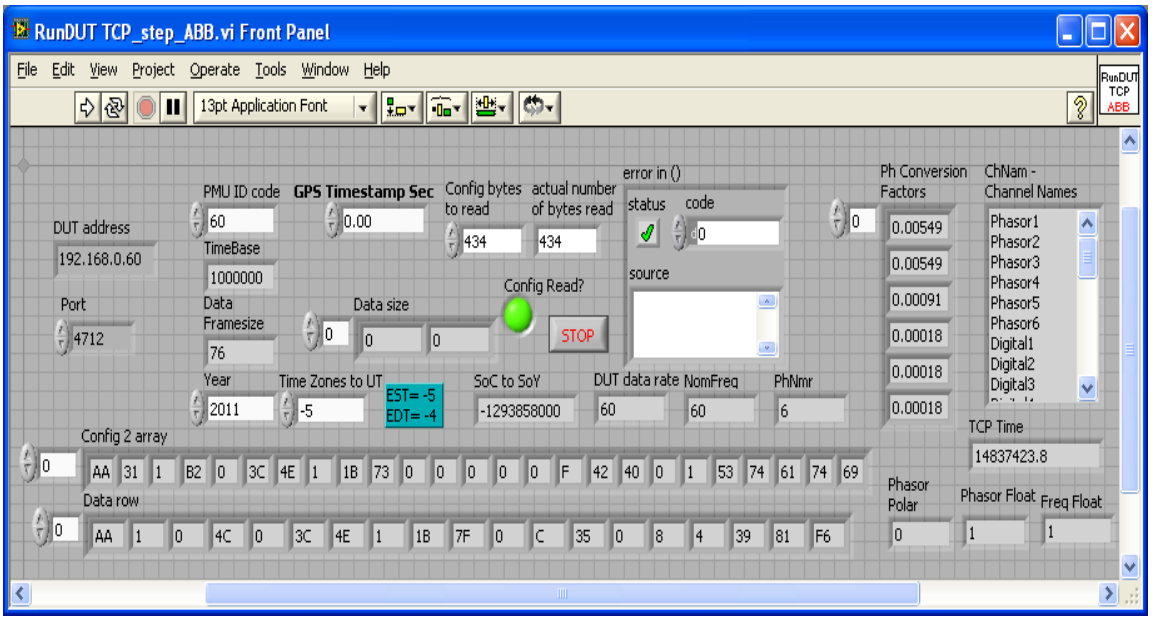

Figure 50 A screenshot of front panel for data transfer

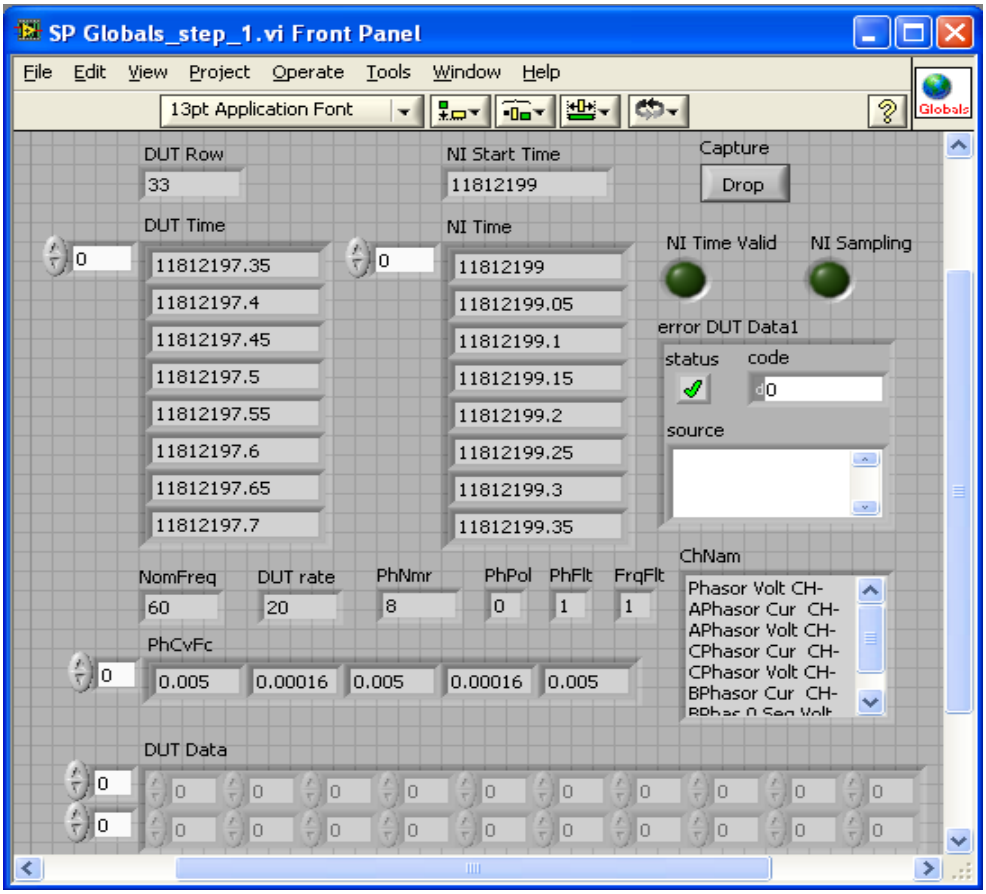

Figure 51 A screenshot of front panel for phasor alignment

- Error analysis – reforms the reference measurements according to the output form of device under test; computes the performance indices (TVE, magnitude error, phase error, frequency error and rate of change of frequency error) and displays the results of interest. A screenshot of front panel for error analysis is given in Figure 52.

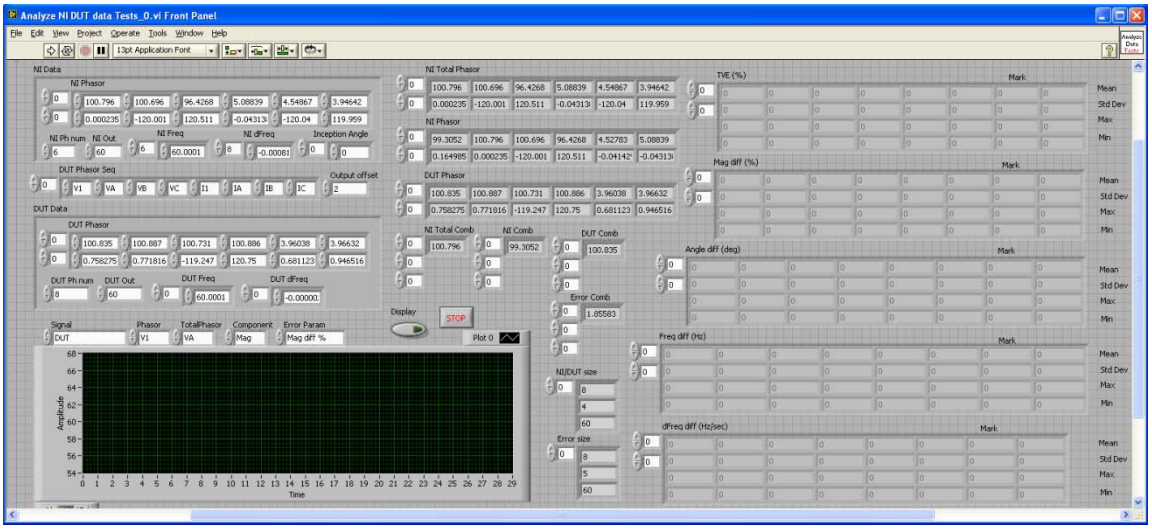

Figure 52 A screenshot of front panel for error analysis

6.3.2 Reference PMU

The reference algorithm for estimating phasors is described in Section 3.4.2. It is derived based on a dynamic signal model and uses a quadratic form to approach the changing parameters. For real-time application, this algorithm can achieve very good accuracy against the requirements specified in the standards. For testing, because the frequency variable of a test signal is known, instead of using the estimated frequency, we use the true value of a test signal's frequency to achieve higher accuracy.

We use constant frequency (f_s = 50 kHz) to sample the input voltage and current signals. The size of data window for estimating phasor is one cycle period of the nominal frequency, i.e. the number of samples within a data window is $50000/60 \approx 833$. Let F_s be the PMU reporting rate (frame per second). For some reporting rate, the output

interval is not an integer, for example, F_s = 30/s, the output interval is 50000/30 = 1666.67. In this case the phase compensation is performed using equation (6.1) as follows:

$$\Delta\varphi = 2\pi f \cdot [1/F_s - \text{round}(f_s/F_s)/f_s] \tag{6.1}$$

where f is the frequency of input signals. Figure 53 illustrates the compensation method. It should be noted that the phase compensation is unnecessary for the measurement at each integer second, i.e. pps.

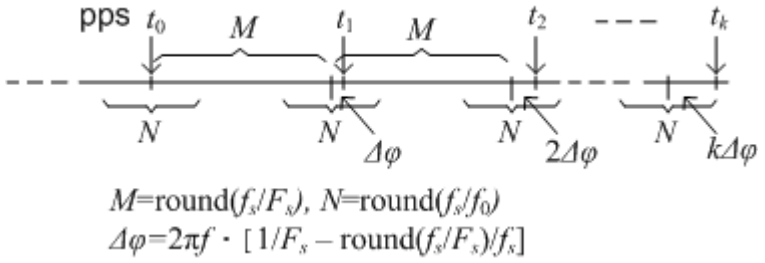

Figure 53 Phase compensation for phasor measurements

Figure 54 shows a diagram for performing conformance test on PMUs and PMU-enabled IEDs using reference PMU. The test system includes a test signal generator, reference time clock with 30 ns RMS (corresponding to 0.0012% TVE), and an error analyzer. The PMU under test and reference PMU see the same voltage and current signals, thus the uncertainty caused by the signal generator can be neglected. The accuracy of the entire test system depends on the accuracy of the phasor estimation

algorithm, time clock and data acquisition system. The data acquisition has an uncertainty of less than 0.0015% TVE [103].

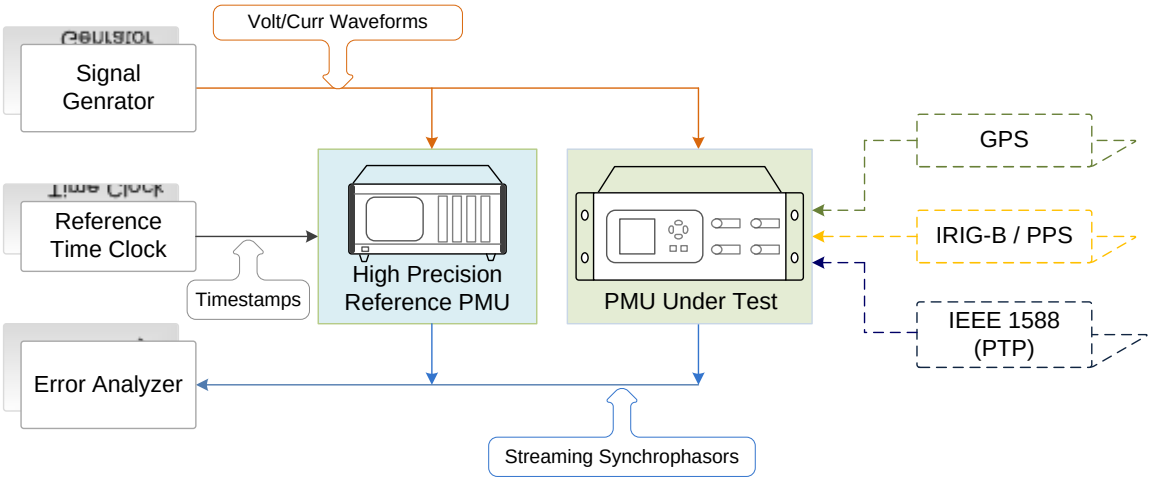

Figure 54 Diagram for performing conformance tests

Table 14 Test signal models for accuracy study

Test Type		Signal Model	Note
Steady state		$x(t) = X_m \cos(2\pi f t + \varphi)$ X_m: 10–200% ; φ: -π–π; f: -5Hz –5Hz	X_m: amplitude φ: initial angle f: frequency
Dynamic	Modulation	$x(t) = X_m[1 + k_x \cos(2\pi f_m t)]$ $\cdot \cos[2\pi f_0 + k_a \cos(2\pi f_m t - \pi)]$ k_x=0.1, k_a=0.1, f_m: 0.1Hz–5Hz	k_x, k_a : amplitude, phase modulation factor f_m: modulation frequency
	Frequency ramp	$x(t) = X_m \cos(2\pi f_0 t + \pi f_d t^2 + \varphi)$ f_d=±1Hz, f: ±5Hz	f_0: nominal frequency f_d: rate of change of frequency

The accuracy study for the reference algorithm has been performed using the signals given in Table 14, which include the signal models representing steady state and dynamic state conditions in power system. The frequency and rate of change of frequency have high accuracy because the real value is used. The maximum TVEs are recorded in Table 15. One can refer to reference [60] for the step test approach. Combining the uncertainties of phase estimation algorithm, time clock and DAQ, the overall testing system has an uncertainty of less than 0.08% TVE.

Table 15 Results of reference algorithm accuracy study

Test Type		Performance	Max TVE (%)
Steady state		Class P	8.3-e12
		Class M	1.2-e11
Dynamic	Modulation	Class P	7.8-e04
		Class M	0.08
	Frequency ramp	Class P	1.3-e07
		Class M	1.6-e05

6.4 Test Results

The configurations for nine commercial PMUs and PMU-enabled IEDs from seven different vendors, denoted as A – F which have been selected for performing conformance tests, are given in Table 20 in Appendix D. For each scenario the magnitude error, phasor error, TVE, frequency error and rate of change of frequency

error are recorded. Due to the limited space, only the summary of the test results is presented in the dissertation, as shown in Table 21 and Table 22 in Appendix D, in which "S" stands for "pass" while "F" stands for "failure". The performance summary for each PMU is given as follows:

- PMU A: The performance of the PMU is unstable. Given by the phase angle results, they vary in a large range (from a half to two degrees (1% to 4% TVE accordingly) for each test. This may be caused by the time synchronization method it uses, which is external IRIG-B time code. Each test case was performed five times and the "best" result was recorded. According to the new standard, test results show that the PMU failed in some cases. From the frequency ramp test we observe that the rate of change of frequency measured by the PMU has a certain number of multiples (100) against the real value. This may be because the PMU "forgot" to multiply with 100 (as required by the standard C37.118) before packing ROCOF measurement into data frame.
- PMU B: This PMU uses a dedicated time receiver which provides time code to PMU for synchronizing outputs while compensating phase errors. Compared to PMU A, this PMU performed consistently. The phase errors are quite small. This PMU has the same issue as PMU A with packing the rate of change of frequency measurement. It also failed on some dynamic conditions.

- PMU C: This unit achieves very good performance. It uses external reference time clock (IRIG-B) as the PMU A does, but performs better. It failed on some conditions as well. This unit passed the Step Test.
- PMU D: This unit has built-in GPS receiver. It has the same issue as PMU A and B with packing the rate of change of frequency measurement. It failed on some dynamic conditions as well.
- PMU E: This unit has built-in GPS receiver. The communication for sending out phasor data through Ethernet connection was unstable. The connection interrupted frequently while performing tests. This PMU failed in class M of frequency variation tests, and some dynamic tests.
- PMU F: This unit uses external IRIG-B input. It has the same issue as PMU A with packing the rate of change of frequency measurement. This PMU has poor accuracy working under off nominal frequency. It failed in some dynamic conditions, but it passed the step test.

6.5 Summary

This section provides a solution for how to evaluate the conformance performance of PMUs and PMU-enabled IEDs against the new synchrophasor standard by developing a test methodology and associated tools to fulfill the test. The reference signals and scenarios for verifying the conformance test are described. The laboratory setup and

reference PMU are specified in detail. The accuracy study indicates that the test system achieves adequate accuracy for testing the commercial devices. Test configurations for the commercial PMUs and PMU-enabled IEDs are provides. Test results for performing the conformance test on these units are presented as well. This demonstrates the efficiency and advantages of the test method. From the results, we can conclude that:

- Most PMUs and PMU-enabled IEDs passed the steady state tests, as specified in standard [5]. Some of them have noticeable errors under off-nominal frequency.
- None of the PMUs and PMU-enabled IEDs passed the entire dynamic tests, as specified in standard PC37.118.1. For measurement bandwidth, most of the units met the class P requirements [52]. For frequency ramp tests, none of the units satisfy the frequency and rate of change of frequency accuracy. Only two units passed the step test.
- Some of the PMUs and PMU-enabled IEDs have the issues of not following the standard for packing the measurement of rate of change of frequency.
- Some PMUs or PMU-enabled IEDs have the issues using external time clock. Extra calibrations may be needed to improve the accuracy for such device.
- For most PMUs and PMU-enabled IEDs, which have been tested in this study, improvement needs to be made to achieve better performance under dynamic conditions.

7. CONCLUSIONS

7.1 Summary of Achievements

The synchronized phasor measurement is able to reflect the state of power grids with a high resolution and wide-area perspective. The use of synchrophsor measurement in power system monitoring, protection and control to enhance the grid situational awareness, and improve the reliability, is gaining increasing attention as the development of Smart Grid technology. Meanwhile the issues that are the unsatisfactory performance of prevailing phasor estimation algorithms when exposed to transients and the inadequate test methods for evaluating the conformance performance of the PMUs and PMU-enabled IEDs exist.

This dissertation aims to resolve the issues, improving the accuracy of synchrophasor measurements, from both the theoretical and methodology perspectives. New algorithms for improving the phasor accuracy under power system transients are proposed after carefully studied by comparing to the existing solutions. This will directly improve the performance of synchrophasor based applications. The methods and tools for evaluating the conformance performance of synchrophasor units from various perspectives are proposed as well. The contributions of this dissertation are summarized as follows:

Section 2 introduces the fundamentals of the synchrophasor measurement and associated technology. The main components, such as PMUs, time clocks and PDCs and their functionalities are described in detail. The techniques for transferring synchrophasor data in wide area and the applications using synchrophasor data in power system are described as well. This led to better understanding of the existing problems and the interoperability requirements of future solutions.

Section 3 develops an adaptive phasor estimation approach for studying the dynamic characteristics and improving the dynamic performance of synchrophasor measurement under transient conditions. Such approach is capable of:

- Identifying and localizing the disturbance while discriminating from various noise within a given data window, thus the effect of electromagnetic transients can be eliminated by using adaptive data window;
- Achieving better accuracy during power oscillations by using the quadratic polynomial model;
- Implementing computational improvements for real-time synchrophasor estimation. And it can also be used as the reference algorithm for testing devices performing synchrophasor measurements;
- Indicating the phasor quality so that the power system applications are able to be aware of whether the phasors they use or the results based on the phasors are

valid or not.

Section 4 proposes a new frequency and phasor estimation algorithm for real-time applications. This algorithm uses a newly constructed recursive wavelet and the formulae for computing the waveform parameters (frequency amplitude and phase angle) are derived based the wavelet transform coefficients. The method features:

- Fast response;
- Better dynamic performance;
- Capability of eliminating decaying DC components;
- Flexible window size;
- Low computation burden.

The performance of each individual phasor unit manufactured by different vendors may vary greatly. An approach to characterizing the dynamic behavior of PMUs and PMU-enabled IEDs when exposed to step signals is proposed in Section 5. The techniques used to achieve high accuracy and high resolution of reference phasors include the least square linear fit, adaptive data window, and interleaving method. Test results indicate unique characteristics for each phasor unit and good dynamic behavior consistency among most of the tested PMUs.

Section 6 developed a methodology for evaluating the conformance performance of PMUs and PMU-enabled IEDs. The method includes:

- A reference PMU using proposed phasor estimation approaches providing reference phasors for PMUs and PMU-enabled IEDs under test;
- Reference signal models and test scenarios;
- A synchrophasor test system on which various tests can be performed.

Nine commercial PMUs and PMU-enabled IEDs were tested using the method. Test results demonstrate the concerns of existing issues in synchrophasor measurement. The new algorithms proposed in the dissertation can be used to resolve the issues.

7.2 Research Contribution

The contributions of this dissertation may benefit both theoretical research and practical applications in improving the synchrophasor measurement of power grids. The existing research efforts barely study the characteristics of voltage and current waveforms under transients. And the testing method is unable to deal with the dynamic behavior of synchrophasor device when exposed to the signals with abrupt change in magnitude. This dissertation studies the signals composition under both electromagnetic and electromechanical conditions, and proposes a method which is able to identify the changing components, thus improving the accuracy by eliminating the impact. New method and tools for evaluating the performance of synchrophasor devices are developed in the dissertation. The performance issues of current phasor device can be found by using this methodology. The proposed algorithm can be used to improve the

performance of the current device. Now the interoperability tests can be performed because the reference methodology has been developed. The benefits for using those methods have been demonstrated clearly in the dissertation.

7.3 Conclusions

- Adaptive method eliminates the transition effect caused by disturbances which effectively improves the quality of phasor measurements;
- New phasor estimation algorithm achieves high accuracy under various conditions of power system;
- Reference algorithms developed for testing have been implemented. Test results demonstrate their effectiveness and advantages;
- Interoperability issues existing in PMUs and PMU-enabled IEDs under test were revealed through performing test using the test plan.

7.4 Suggestions for Future Work

The research and study in this dissertation can be continued in the future. The exploration in new techniques for improving the phasor computation and frequency estimation under transient conditions should be extended using a hybrid approach for frequency and phasor estimation based on Taylor series expansion and Fourier algorithm. The approach can be derived using a dynamic signal model with varying parameters. The changing envelope of a power signal within an observation data window may

approximated with a second order Taylor series. A Fourier algorithm based method can be proposed to compute the parameters of such signal model. Inheriting from the use of Fourier algorithm, this hybrid algorithm would be is immune to power system harmonics. It would achieve excellent performance for signals with dynamic variations. The Prony's method can be used to resolve the dynamic sinusoidal signal models because of its native damping model. Modifications are needed to fit the power system signal models and the results are expected to be efficient.

Besides the evaluation of the conformance performance, the interoperability verifications and application performance tests for system solutions consisting of many diverse types of PMU-capable IEDs, time synchronization methods, PDCs and associated communication networks need to be investigated. The issues need to be concerned are as follows:

- Interchangeability (producing consistent accuracy) among different PMUs, PMU-enabled IEDs, time synchronization options and PDCs.
- Application performance with variations of PMUs and PMU-enabled IEDs, and time synchronization options;
- Application performance with various PDCs and mixed communication protocols in a network.

REFERENCES

[1] P. Bonanomi, “Phase angle measurements with synchronized clocks,” *IEEE Trans. on Power Apparatus and Systems*, vol. PAS-100, no. 12, pp. 5036-5043, December 1981.

[2] A. G. Phadke, “Synchronized phasor measurements in power systems,” *IEEE Computer Applications in Power*, vol. 6, no. 2, pp. 10-15, April 1993.

[3] R. O. Burnett, Jr., M. M. Butts, P. S. Sterlina, “Power system applications for phasor measurement Units,” *IEEE Computer Applications in Power*, vol. 7, no. 1, pp. 8-13, Jan 1994.

[4] G. Andersson, P. Donalek, R. Farmer, N. Hatziargyriou, I. Kamwa, P. Kundur, N. Martines, J. Paserba, P. Pourbeik, J. Sanchez-Gasca, R. Schulz, A. Stankovic, C. Taylor, and V. Vittal, “Causes of the 2003 major grid blackout in North America and Europe, and recommended means to improve system dynamic performance,” *IEEE Trans. on Power Systems*, vol. 20, no. 4, pp. 1922-1928, Nov. 2005.

[5] *IEEE Standard for Synchrophasors for Power Systems*, IEEE Standard C37.118-2005, March 2006.

[6] IEEE PSRC (Power System Relaying Committee) WG (Work Group) D6, “Power swing and out-of-step considerations on transmission lines,” June 2005. [Online] Available: http://www.pes-psrc.org.

[7] North American Electric Reliability Corporation, “Real-time application of synchrophasors for improving reliability,” October, 2010. [Online]. Available: http://www.nerc.com/docs/oc/rapirtf/RAPIR%20final%20101710.pdf.

[8] C. P. Steinmetz, “Complex quantities and their use in electrical engineering,” in *Proc. AIEE Int. Electrical Cong*., Chicago, IL, 1893, pp. 33-74.

[9] A. G. Phadke and J. S. Thorp, *Computer Relaying for Power Systems*. New York: John Wiley and Sons, 1988.

[10] J. A. de la O. Serna, K. E. Martin, “Improving phasor measurements under power system oscillations,” *IEEE Trans. on Power Systems*, vol. 18, no. 1, pp. 160-166, Feb. 2003.

[11] J. A. de la O. Serna, “Dynamic phasor estimates for power system oscillations,” *IEEE Trans. on Instrumentation and Measurement*, vol. 56, no. 5, pp. 1648-1657, Oct. 2007.

[12] W. Premerlani, B. Kasztenny, M. Adamiak, “Development and implementation of a synchrophasor estimator capable of measurements under dynamic conditions,” *IEEE Trans. on Power Delivery*, vol. 23, no. 1, pp. 109-123, Jan. 2008.

[13] R. Mai, Z. He, L. Fu, B. Kirby, Z. Bo, “A dynamic synchrophasor estimation algorithm for online application,” *IEEE Trans. on Power Delivery*, vol. 25, no. 2, pp. 570-578, April 2010.

[14] A. G. Phadke, B. Kasztenny, “Synchronized phasor and frequency measurement under transient conditions,” *IEEE Trans. on Power Delivery*, vol. 21, no. 1, pp. 89-95, Jan. 2009.

[15] T. S. Sidhu, M. S. Sachdev, “An iterative technique for fast and accurate measurement of power system frequency,” *IEEE Trans. on Power Delivery*, vol. 13, no. 1, pp. 109-115, 1998.

[16] G. Benmouyal, “An adaptive sampling interval generator for digital relaying,” *IEEE Trans. on Power Delivery*, vol. 4, no. 3, pp. 1602-1609, 1989.

[17] D. Hart, D. Novosel, Y. Hu, B. Smith, M. Egolf, “A new frequency tracking and phasor estimation algorithm for generator protection,” *IEEE Trans. on Power Delivery*, vol. 12, no. 3, pp. 1064-1073, 1997.

[18] P. J. Moore, J. H. Allmeling, A. T. Johns, “Frequency relaying based on instantaneous frequency measurement,” *IEEE Trans. on Power Delivery*, vol. 11, no. 4, pp. 1737-1742, 1996.

[19] M. D. Kusljevic, “Simultaneous frequency and harmonic magnitude estimation using decoupled modules and multirate sampling,” *IEEE Trans. on Power Instrumentation and Measurement*, vol. 59, no. 4, pp. 954-962, 2010.

[20] A. Lopez, J. C. Montano, M. Castilla, J. Gutierrez, M. D. Borras, J. C. Bravo, “Power system frequency measurement under nonstationary situations,” *IEEE Trans. on Power Delivery*, vol. 23, no. 2, pp. 562-567, 2008.

[21] A. A. Girgis, W. L. Peterson, “Adaptive estimation of power system frequency deviation and its rate of change for calculating sudden power system overloads,” *IEEE Trans. on Power Delivery*, vol. 5, no. 2, pp. 585-594, 1990.

[22] I. Kamwa, R. Grondin, “Fast adaptive schemes for tracking voltage phasor and local frequency in power transmission and distribution systems,” in *Proc.* Power Eng. Soc. Transm. Distrib. Conf, Dallas, TX, 1991, pp. 930-936.

[23] K. M. El-Naggar, H. K. M. Youssef, “A genetic based algorithm for frequency relaying applications,” *Electric Power Systems Research*, vol. 55, no. 3, pp. 173-178, 2000.

[24] L. L. Lai, W. L. Chan, “Real time frequency and harmonic evaluation using artificial networks, *IEEE Trans. on Power Delivery*, vol. 14, no. 1, pp. 52-57, 1999.

[25] G. Benmouyal, “Removal of DC-offset in current waveforms using digital mimic filtering,” *IEEE Trans. on Power Delivery*, vol. 10, no. 2, pp. 621-630, April 1995.

[26] J. C. Gu, S. L. Yu, “Removal of DC offset in current and voltage signals using a novel Fourier filter algorithm,” *IEEE Trans. on Power Delivery*, vol. 15, no. 1, pp. 73-79, Jan. 2000.

[27] J. Z. Yang, C. W. Liu, “Complete elimination of DC offset in current signal for relaying applications,” in *Proc*. 2000 *IEEE Power Eng. Soc. Winter Meeting*, Jan 2000, vol. 3, pp. 1933-1938.

[28] T. S. Sidhu, X. Zhang, F. Albasri, M. S. Sachdev, “Discrete-Fourier-Transform-based technique for removal of decaying DC offset from phasor estimates,” *IEE Proc. Generation, Transmission and Distribution*, vol. 150, no. 6, pp. 745-752, Nov. 2003.

[29] S. H. Kang, D. G. Lee, S. R. Nam, P. A. Crossley, Y. C. Kang, “Fourier Transform-based modified phasor estimation method immune to the effect of the DC offsets,” *IEEE Trans. on Power Delivery*, vol. 24, no. 3, pp. 1104-1111, 2009.

[30] S. R. Nam, J. Y. Park, S. H. Kang, M. Kezunovic, “Phasor estimation in the presence of DC offset and CT saturation,” *IEEE Trans. on Power Delivery*, vol. 24, no. 4, pp. 1842-1849, 2009.

[31] Y. Guo, M. Kezunovic, "Simplified algorithms for removal of the effect of exponentially decaying DC-offset on the Fourier algorithms," *IEEE Trans. on Power Delivery*, vol. 18, no. 3, pp. 711-717, July 2003.

[32] C. S. Yu, "A Discrete Fourier Transform-based adaptive mimic phasor estimator for distance relaying applications," *IEEE Trans. on Power Delivery*, vol. 21, no. 4, pp. 1836-1846, Oct. 2006.

[33] G. Stenbakken, T. Nelson, "NIST support of phasor measurements to increase reliability of the North American electric power grid," in *Proc. IEEE Power Eng. Soc. General Meeting*, 18-22 June 2006.

[34] G. Stenbakken, T. Nelson, "Static calibration and dynamic characterization of PMUs at NIST," in *Proc. IEEE Power Eng. Soc. General Meeting*, 24-28 June 2007.

[35] G. Stenbakken, M. Zhou, "Dynamic phasor measurement unit test system," in *Proc. IEEE Power Eng. Soc. General Meeting*, 24-28 June 2007.

[36] G. Stenbakken, T. Nelson, M. Zhou and V. Ceneno, "Reference values for dynamic calibration of PMUs," in *Proc. the 41st Hawaii International Conference on System Sciences*, Jan, 2008.

[37] J. F. Hauer, “Validation of phasor calculations in the Macrodyne PMU for California-Oregon transmission project tests of March 1993,” *IEEE Trans. on Power Delivery*, vol. 11, no. 3, pp. 1224-1231, 1996.

[38] J. Depablos, V. Centeno, A. G. Phadke, M. Ingram, “Comparative testing of synchronized phasor measurement units,” in *Proc. IEEE Power Eng. Soc. General Meeting*, 6-10 June 2004, pp. 948-954.

[39] K. Martin, T. Faris, J. Hauer, “Standardized testing of phasor measurement units,” in *Proc*. *Fault and Disturbance Analysis Conference*, Atlanta, GA, 2006.

[40] Z. Huang, J. F. Hauer, K. E. Marthin, “Evaluation of PMU dynamic performance in both lab environments and under field operating conditions,” in *Proc. IEEE Power Eng. Soc. General Meeting*, 24-28 June 2007.

[41] K. E. Martin, J. F. Hauer, T. J. Faris, “PMU testing and installation considerations at the Bonneville Power Administration,” in *Proc. IEEE Power Eng. Soc. General Meeting*, 24-28 June 2007.

[42] K. Narendra, Z. Zhang, J. Lane, B. Lackey, E. Khan, “Calibration and testing of TESLA phasor measurement unit (PMU) using Doble F6150 test instrument,” in *Proc. 2007 iREP Symposium*, 19-24 August 2007.

[43] T. Bi, Y. Zhang, X. Xiao, P. Forsyth, R. Wierckx, "Large scale power system simulation and PMU testing using a real time digital simulator," in *Proc. International Power Engineering Conference*, 3-6 Dec. 2007, pp. 383-388.

[44] F. Steinhauser, T. Schossig, "Testing phasor measurement units," in *Proc. IET 9th International Conference on Developments in Power System Protection*, 17-20 March 2008, pp. 606-610.

[45] Z. Huang, B. Kasztenny, V. Madani, K. Martin, S. Meliopoulos, D. Novosel, J. Stenbakken, "Performance evaluation of phasor measurement systems," in *Proc. IEEE Power Eng. Soc. General Meeting*, 20-24 July 2008.

[46] Y. Hu, D. Novosel, "Progresses in PMU testing and calibration," in *Proc. the 3rd International Conference on Deregulation and Restructuring and Power Technologies (DRPT 2008)*, 6-9 April 2008, pp. 150-155.

[47] P. Komarnicki, C. Dzienis, Z. A. Styczynski, J. Blumschein, V. Centeno, " Practical experience with PMU system testing and calibration requirements," in *Proc. IEEE Power Eng. Soc. General Meeting*, 20-24 July 2008.

[48] Q. B. Dam, S. Mohagheghi, R. H. Alaileh, G. K. Stefopoulos, G. J. Cokkinides, S. Meliopoulos, "A laboratory setup for relay and GPS-synchronized equipment transient testing," in *Proc. IEEE Power Eng. Soc. General Meeting*, 20-24 July 2008.

[49] V. Terzija, S. S. Wu, J. Fitch, "Setup of the laboratory for synchronized measurement for PMU's testing," in *Proc. IEEE Power Tech Conference*, Bucharest, Romania, June 28th – July 2nd 2009.

[50] M. Chenine, K. Zhu, L. Nordstrom, "Survey on priorities and communication requirements for PMU-based applications in the Nordic region," in *Proc. IEEE Power Tech Conference*, Bucharest, Romania, June 28th – July 2nd 2009.

[51] B. Vandiver, A. Apostolov, F. Steinhauser, "Testing of phasor measurement units," in *Proc. 63rd Protective Relay Engineers*, 2010.

[52] *IEEE Standard for Synchrophasors for Power Systems*, IEEE Standard PC37.118.1, Draft May 2011.

[53] *IEEE Standard for Synchrophasors Data Transfer for Power System*, IEEE Standard PC37.118.2, Draft May 2011.

[54] PMU System Testing and Calibration Guide. *North American Synchrophasor Initiative (NASPI), Performance and Standards Task Team (PSTT)*, December 2007. [Online] Available: http://www.naspi.org/

[55] J. Ren, M. Kezunovic, "An adaptive phasor estimator for power system waveforms containing transients", *IEEE Trans. on Power Delivery*, under review.

[56] J. Ren, M. Kezunovic, “Real time power system frequency and phasor estimation scheme using recursive wavelet transform”, *IEEE Trans. on Power Delivery*, vol. 26, no. 3, pp. 1392-1402, July 2011.

[57] J. Ren, M. Kezunovic, “A wavelet method for power system frequency and harmonic estimation,” in *Proc. North American Power Symposium*, Arlington, TX, September 2010.

[58] J. Ren, M. Kezunovic, “Use of recursive wavelet transform for estimating power system frequency and phasors,” in *Proc. IEEE Power. Eng. Soc. Transm. Distrib. Conference and Exposition*, New Orleans, Louisiana, April 2010.

[59] J. Ren, M. Kezunovic, “Elimination of DC offset in accurate phasor estimation using recursive wavelet transform,” in *Proc. IEEE Power. Eng. Soc. PowerTech*, Bucharest, Romania, July 2009.

[60] J. Ren, M. Kezunovic, J. Stenbakken, “Characterizing dynamic behavior of PMUs using step signals”, *European Transactions on Electrical Power*, DOI: 10.1002, Oct. 2010.

[61] J. Ren, M. Kezunovic, J. Stenbakken, “Dynamic characterization of PMU using step signals,” in *Proc. IEEE Power. Eng. Soc. General Meeting*, Calgary, Canada, July 2009.

[62] Consortium for Electric Reliability Technology Solutions, “Phasor Real Time Dynamic Monitoring System,” Feb. 2006. [Online] Available: http://www.phasor-rtdms.com/.

[63] North American Synchrophasor Initiative, “IEEE C37.118 Compatible PMU-capable Devices,” June 2010. [Online] Available: http://www.naspi.org/pmu/compatiable_pmu_capable_devices_20100607.pdf

[64] National Research Council (U.S.) Committee on the Future of the Global Positioning System, “The Global Positioning System,” *National Academy of Public Administration*, 1995.

[65] IRIG Standard 200-04 – IRIG Serial Time Code Formats – September 2004, Timing Committee, Telecommunications and Timing Group, Range Commanders Council, U.S. Army White Sands Missile Range, NM.

[66] *IEEE Standard for a Precision Clock Synchronization Protocol for Networked Measurement and Control Systems*, IEEE Standard 1588 – 2002, Nov. 2002.

[67] *IEEE Standard for a Precision Clock Synchronization Protocol for Networked Measurement and Control Systems*, IEEE Standard 1588 – 2008, July 2008.

[68] *IEEE Standard Profile for Use of IEEE 1588 Precision Time Protocol in Power System Applications*, IEEE Standard C37.238, 2011.

[69] Phasor Data Concentrator Functional and Performance Requirements, *North American Synchrophasor Initiative (NASPI), Performance and Standards Task Team (PSTT),* April 2011. [Online] Available: http://www.naspi.org/

[70] Phasor Gateway Technical Specifications for North American SynchroPhasor Initiative Network, *North American Synchrophasor Initiative (NASPI),* May 2009. [Online] Available: http://www.naspi.org/

[71] J. De La Ree, V. Centeno, J. S. Thorp, A. G. Phadke, "Synchronized phasor measurement applications in power systems," *IEEE Trans. on Smart Grid,* vol. 1, no. 1, pp. 20-27, June 2010.

[72] J. S. Thorp, A. G. Phadke, S. H. Horowitz, M. M. Begovic, "Some applications of phasor measurements to adaptive protection," *IEEE Trans. on Power Systems*, vol. 3, no. 2, pp. 791-798, 1988.

[73] H. Zhu, Z. Cai, H. Liu, Y. Ni, "Multi-infeed HVDC/AC power system modeling and analysis with dynamic phasor application," in *Proc. Asia and Pacific Transm. Distrib. Conference and Exhibition*, 2005.

[74] T. L. Baldwin, L. Mili, M. B. Boisen, Jr., R. Adapa, "Power system observability with minimal phasor measurement placement," *IEEE Trans. on Power Systems*, vol. 8, no. 2, pp. 707-715, May 1993.

[75] S. E. Stanton, C. Slivinsky, K. Martin, J. Nordstorm, "Application of phasor measurements and partial energy analysis in stabilizing large disturbances," *IEEE Trans. on Power Systems*, vol. 10, no. 1, pp. 297-306, Feb. 1995.

[76] S. Chakrabarti, E. Kyriakides, "PMU measurement uncertainty considerations in WLS state estimation," *IEEE Trans. on Power Systems*, vol. 24, no. 2, pp. 1062-1071, May 2009.

[77] J. Ma, P. Zhang, H. Fu, B. Bo, Z. Dong, "Application of phasor measurement unit on locating disturbance source for low-frequency oscillation," *IEEE Trans. on Smart Grid*, vol. 1, no. 3, pp. 340-346, 2010.

[78] A. H. Al-Mohammed, M. M. Mansour, M. A. Abido, "Application of phasor measurement units (PMUs) for fault location in SEC-EOA interconnected network," in *Proc. EnergyCon*, 2010 pp. 435-439.

[79] J. F. Hauer, W. A. Mittelstadt, K. E. Martin, J. W. Burns, H. Lee, J. W. Pierre, D. J. Trudnowski, "Use of the WECC WAMS in wide-area probing tests for validation of system performance and modeling," *IEEE Trans. on Power Systems*, vol. 24, no. 1, pp. 250-257, Feb. 2009.

[80] R. Emami, A. Abur, "Robust measurement design by placing synchronized phasor measurements on network branches," *IEEE Trans. on Power Systems*, vol. 25, no. 1, pp. 38-43, Feb. 2010.

[81] J. Jiang, C. Liu, C. Chen, "A novel adaptive PMU-based transmission-line relay-design and EMTP simulation results," *IEEE Trans. on Power Delivery*, vol. 17, no. 4, pp. 930-937, Oct. 2002.

[82] M. G. Adamiak, A. P. Apostolov, M. M. Begovic, C. F. Henville, K. E. Martin, G. L. Michel, A. G. Phadke, J. S. Thorp, "Wide area protection – technology and infrastructures," *IEEE Trans. on Power Delivery*, vol. 21, no. 2, pp. 601-609, April 2006.

[83] R. Diao, K. Sun, V. Vittal, R. J. O'Keefe, M. R. Richardson, N. Bhatt, D. Stradford, S. K. Sarawgi, "Decision tree-based online voltage security assessment using PMU measurements," *IEEE Trans. on Power Systems*, vol. 24, no. 2, pp. 832-839, May 2009.

[84] S. Corsi, G. N. Taranto, "A real-time voltage instability identification algorithm based on local phasor measurements," *IEEE Trans. on Power Systems*, vol. 23, no. 3, pp. 1271-1279, Aug. 2008.

[85] A. Bose, "Smart transmission grid applications and their supporting infrastructure," *IEEE Trans. on Smart Grid*, vol. 1, no. 1, pp. 11-19, June 2010.

[86] S. Mallat, W. L. Hwang, "Singularity detection and processing with wavelets," *IEEE Trans. on Information Theory*, vol. 38, no. 2, pp. 617-643, March 1992.

[87] Y. Yuan, L. Yang, J. Liu, “Characterization of Dirac-structure edges with wavelet transform,” *IEEE Trans. on System, Man and Cybernetics-Part B: Cybernetics*, vol. 30, no. 1, Feb. 2000.

[88] J. Canny, “A computational approach to edge detection,” *IEEE Trans. on Pattern Analysis and Machine Intelligence*, vol. 8, pp. 679-698, 1986.

[89] Stephane Mallat, A Wavelet Tour of Signal Processing, Third Edition, Burlington, MA: Academic Press, 2008.

[90] Power System Relaying Committee, “EMTP reference models for transmission line relay testing report,” draft 10a, Dec. 2004. [Online]. Available: http://www.pes-psrc.org.

[91] A. G. Phadke and J. S. Thorp, *Computer Relaying for Power Systems*. New York: John Wiley and Sons, 1988.

[92] M. V. V. S. Yalla, “A digital multifunction protective relays,” *IEEE Trans. on Power Delivery*, vol. 7, no. 1, pp. 193-201, 1992.

[93] A. G. Phadke, T. Hlibka, M. Ibrahim, “A digital computer system for EHV substation: analysis and field tests,” *IEEE Trans. on Power Apparatus and Systems*, vol. PAS-95, pp. 291-301, Jan. /Feb. 1976.

[94] N. T. Stringer, “The effect of DC offset on current-operated relays,” *IEEE Trans. on Industry Applications*, vol. 34, no. 1, pp. 30-34, Jan/Feb 1998.

[95] O.Chaari, M.Meunier, “A recursive wavelet transform analysis of earth fault currents in Petersen-coil-protected power distribution networks,” in *Proc. 1994 IEEE-SP International Symposium on Time-Frequency and Time-Scale Analysis*, Oct. 1994, pp. 162-165.

[96] O.Chaari, M.Meunier, F.Brouaye, “Wavelets: A New Tool For the Resonant Grounded Power Distribution Systems Relaying,” *IEEE Trans. on Power Delivery*, Vol. 11, No. 3, pp. 1301-1308, July 1996.

[97] Y. Assef, O. Chaari, M. Meunier, “Classification of power distribution system fault currents using vavelets associated to artificial neural networks,” in *Proc. 1996 IEEE-SP International Symposium on Time-Frequency and Time-Scale Analysis*, Oct. 1996, pp. 421-424.

[98] C. Zhang, Y. Huang, X. Ma, W. Lu, G. Wang, “A new approach to detect transformer inrush current by applying wavelet transform,” in *Proc. 1998 POWERCON*, Aug. 1998, vol. 2, pp. 1040-1044.

[99] Xiang-ning Lin, Hai-feng Liu, “A fast recursive wavelet based boundary protection scheme,” in *Proc. 2005 IEEE Power Eng. Soc.y General Meeting*, June 2005, vol. 1, pp. 722-727.

[100] A. Abur, A. G. Exposito, *Power System State Estimation*. New York, NY: CRC Press, 1st edition, March 2004.

[101] A. R. Bergen, V. Vittal, *Power Systems Analysis*, 2nd edition, Prentice Hall, Upper Saddle River, NJ, August 1999.

[102] National Instruments Corporation, 2011. [Online]. Available: http://www.ni.com

[103] National Instruments, DAQ S Series User Manual, May 2009. [Online]. Available: http://www.ni.com/pdf/manuals/370781h.pdf

APPENDIX A

DERIVATION FOR PHASOR PARAMETERS

From equation (3.16) and (3.17) we have,

$$a(t)\cos[\varphi(t)] = q_0 + q_1 t + q_2 t^2 \tag{A.1}$$

$$a(t)\sin[\varphi(t)] = r_0 + r_1 t + r_2 t^2 \tag{A.2}$$

For $t = 0$ they are equivalent to $a(0)\cos[\varphi(0)]=q_0$, $a(0)\sin[\varphi(0)]=r_0$. Then we obtain,

$$A_1 = a(0) = (q_0^2 + r_0^2)^{1/2} \quad , \quad \varphi_1 = \arctan(r_0 / q_0) \tag{A.3}$$

Take first derivative on both sides of equation (A.1) and (A.2), for $t = 0$ we have,

$$a'(0)\cos[\varphi(0)] - a(0)\varphi'(0)\sin[\varphi(0)] = q_1 \tag{A.4}$$

$$a'(0)\sin[\varphi(0)] + a(0)\varphi'(0)\cos[\varphi(0)] = r_1 \tag{A.5}$$

Substitute $a(0)\cos[\varphi(0)]=q_0$, $a(0)\sin[\varphi(0)]=r_0$, and eliminate $a'(0)$ we obtain,

$$\varphi'(0) = \frac{q_0 r_1 - r_0 q_1}{q_0^2 + r_0^2} \tag{A.6}$$

APPENDIX B

DERIVATION FOR PHASOR FORMULEAE

The RWT coefficient of a given signal $x(n)$ is expressed as:

$$W_{x(n)}(a,k) = \frac{\Delta T}{\sqrt{a}} \cdot \sum_{n=0}^{k} x(n) \cdot \psi^*(\frac{n-k}{a}\Delta T),\ k = 0, 1, 2, \cdots$$

$$= \frac{\Delta T}{\sqrt{a}} \cdot \sum_{n=0}^{k} \sum_{m=1}^{M} A_m \cos(2\pi f_m \cdot n\Delta T + \varphi_m) \cdot [\frac{\sigma}{2}(\frac{n-k}{a})\Delta T$$

$$+ \frac{\sigma^2}{2}(\frac{n-k}{a})^2 \cdot \Delta T^2 + \frac{\sigma^3}{3}(\frac{n-k}{a})^3 \cdot \Delta T^3] \cdot e^{(\sigma - j\omega_0)\cdot(\frac{n-k}{a})\Delta T} \qquad \text{(B.1)}$$

Denote $n = l \cdot a + k,\ l \in [-k/a, 0]$, we have,

$$W_{x(n)}(a,k) = \frac{\Delta T}{\sqrt{a}} \cdot \sum_{l=-k/a}^{0} \sum_{m=1}^{M} A_m \cos(2\pi f_m k\Delta T + \varphi_m$$

$$+ 2\pi f_m a \cdot l\Delta T) \cdot [\frac{\sigma}{2}(l\Delta T) + \frac{\sigma^2}{2}(l\Delta T)^2 + \frac{\sigma^3}{3}(l\Delta T)^3] \cdot e^{(\sigma - j\omega_0)\cdot l\Delta T} \qquad \text{(B.2)}$$

Expand the cosine part and rearrange the equation we obtain,

$$W_{x(n)}(a,k) = \sum_{m=1}^{M} u_m^c(a, f_m, k) \cdot x_m^c(k) + \sum_{m=1}^{M} u_m^s(a, f_m, k) \cdot x_m^s(k) \qquad \text{(B.3)}$$

where

$$x_m^c(k) = A_m \cos(2\pi f_m k\Delta T + \varphi_m) \qquad \text{(B.4)}$$

$$x_m^s(k) = A_m \sin(2\pi f_m k\Delta T + \varphi_m) \qquad \text{(B.5)}$$

$$u_m^c(a, f_m, k) = \frac{\Delta T}{\sqrt{a}} \cdot \sum_{l=-k/a}^{0} \cos(2\pi f_m a \cdot l\Delta T) \cdot Q \qquad \text{(B.6)}$$

$$u_m^s(a, f_m, k) = -\frac{\Delta T}{\sqrt{a}} \cdot \sum_{l=-k/a}^{0} \sin(2\pi f_m a \cdot l\Delta T) \cdot Q \qquad \text{(B.7)}$$

$$Q = [\frac{\sigma}{2}(l\Delta T) + \frac{\sigma^2}{2}(l\Delta T)^2 + \frac{\sigma^3}{3}(l\Delta T)^3] \cdot e^{(\sigma - j\omega_0)\cdot l\Delta T}$$

Similarly for signal $y(n)$ we have the expression for RWT coefficient:

$$W_{y(n)}(a,k) = \frac{\Delta T}{\sqrt{a}} \cdot \sum_{n=0}^{k} y(n) \cdot \psi^*(\frac{n-k}{a}\Delta T), k = 0, 1, 2, \cdots$$

$$= W_{x(n)}(a,k) + \frac{\Delta T}{\sqrt{a}} \cdot \sum_{n=0}^{k} A_\tau \cdot e^{-n\Delta T\tau}[\frac{\sigma}{2}(\frac{n-k}{a})\Delta T$$

$$+ \frac{\sigma^2}{2}(\frac{n-k}{a})^2 \cdot \Delta T^2 + \frac{\sigma^3}{3}(\frac{n-k}{a})^3 \cdot \Delta T^3] \cdot e^{(\sigma - j\omega_0)\cdot(\frac{n-k}{a})\Delta T} \quad \text{(B.8)}$$

Denote $n = l \cdot a + k, l \in [-k/a, 0]$, we have,

$$W_{y(n)}(a,k) = W_{x(n)}(a,k) + u_\tau(a,\tau,k) \cdot x_\tau(k) \quad \text{(B.9)}$$

where

$$x_\tau(k) = A_\tau \cdot e^{-k\Delta T\cdot\tau} \quad \text{(B.10)}$$

$$u_\tau(a,\tau,k) = \frac{\Delta T}{\sqrt{a}} \cdot \sum_{l=-k/a}^{0} e^{-al\Delta T\cdot\tau} \cdot Q \quad \text{(B.11)}$$

The true value of frequency, amplitude and phase angle at output sample *k* for the modulated signal model can be computed as:

$$f(k) = f_0 - k_a f_a \sin(2\pi \cdot f_a \cdot k\Delta T - \pi) \quad \text{(B.12)}$$

$$X_m(k) = A \cdot (1 + k_x \cos(2\pi \cdot f_a \cdot k\Delta T) \quad \text{(B.13)}$$

$$\varphi(k) = k_a \cos(2\pi \cdot f_a \cdot k\Delta T - \pi) \quad \text{(B.14)}$$

APPENDIX C

TEST RESULTS FOR PERFORMING STEP TESTS

The magnitude or phase angle and TVE of the positive sequence voltage for the four types of step tests described in Section 5 are presented as follows.

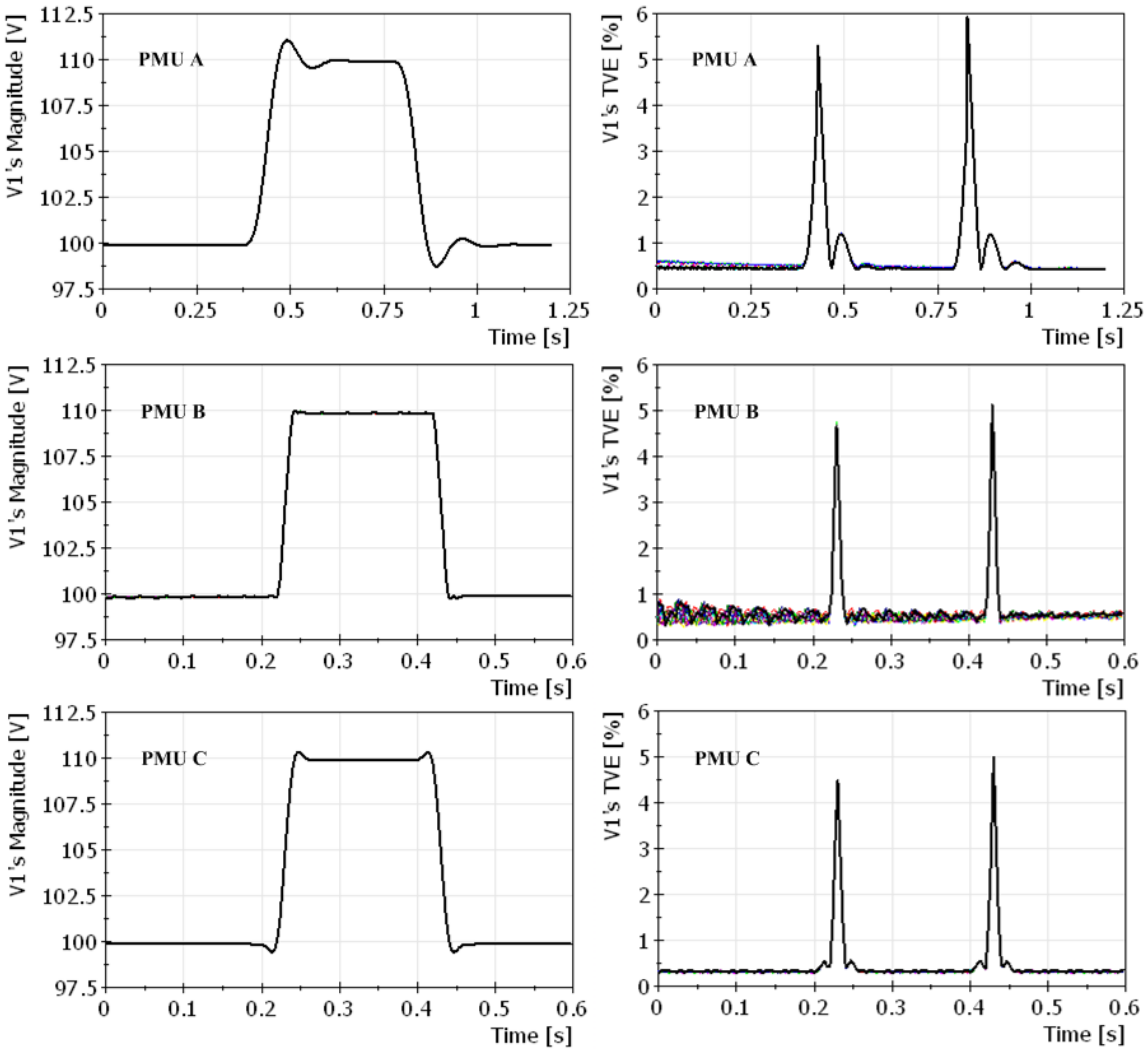

Figure 55 Results of magnitude test

Table 16 Performance indices of magnitude tests

DUT	T_{resp} (/F_s)	T_{set} (/F_s)	O_s (% of step)	U_s (% of step)
PMU A	1.62	1.45	11.87	-3.21
PMU B	0.43	0.00	2.43	-0.56
PMU C	0.48	0.00	4.56	-0.09

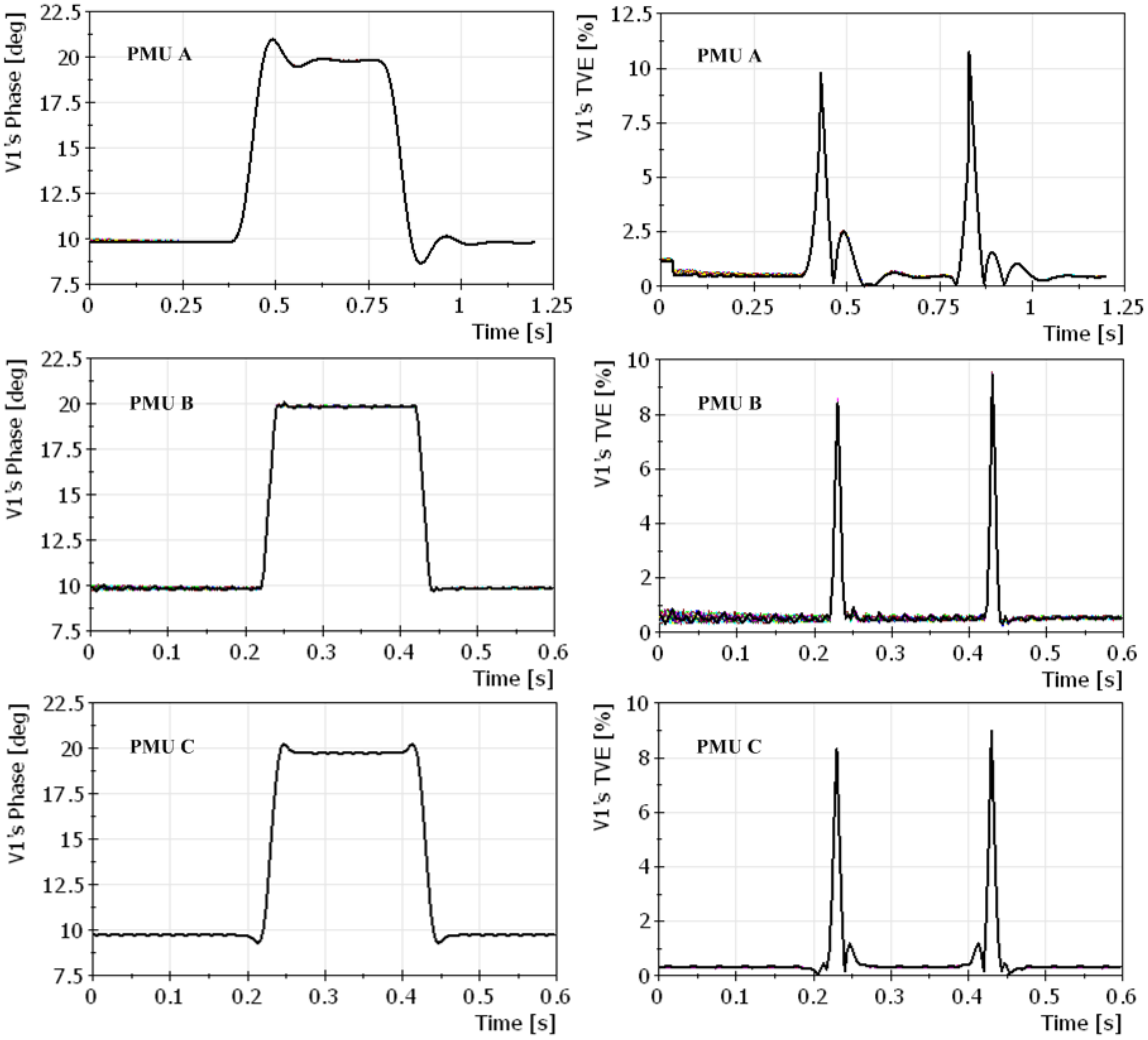

Figure 56 Results of phase test

Table 17　Performance indices of phase tests

DUT	T_{resp} (/F_s)	T_{set} (/F_s)	O_s (% of step)	U_s (% of step)
PMU A	1.91	1.91	12.78	-3.32
PMU B	0.51	0.00	2.54	-0.94
PMU C	0.55	0.34	4.83	-0.22

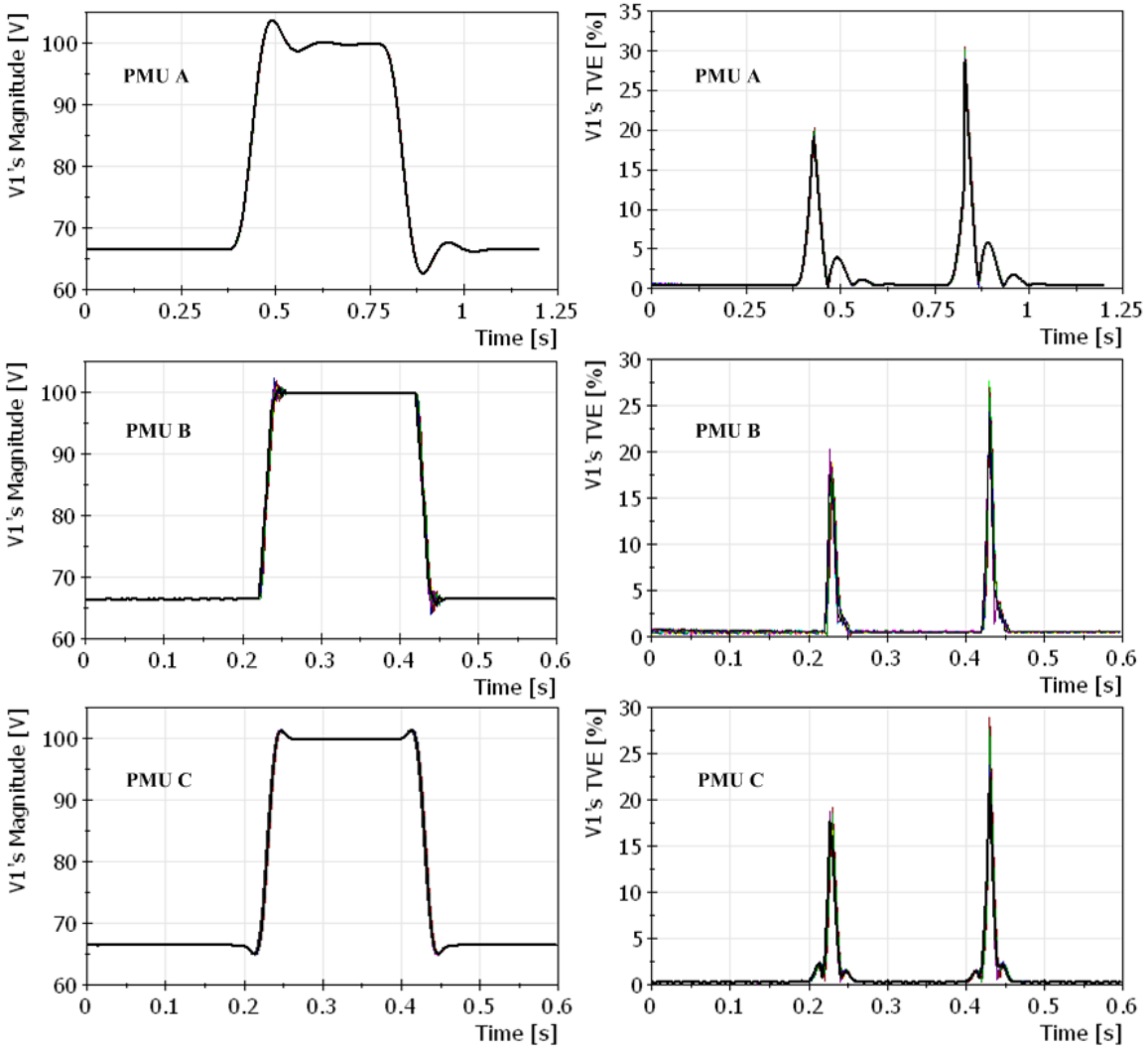

Figure 57　Results of recovery magnitude test

Table 18　Performance indices of recovery magnitude tests

DUT	T_{resp} (/F_s)	T_{set} (/F_s)	O_s (% of step)	U_s (% of step)
PMU A	2.18	3.24	12.07	-3.18
PMU B	0.83	0.00	7.63	-4.07
PMU C	1.11	0.33	5.04	-0.07

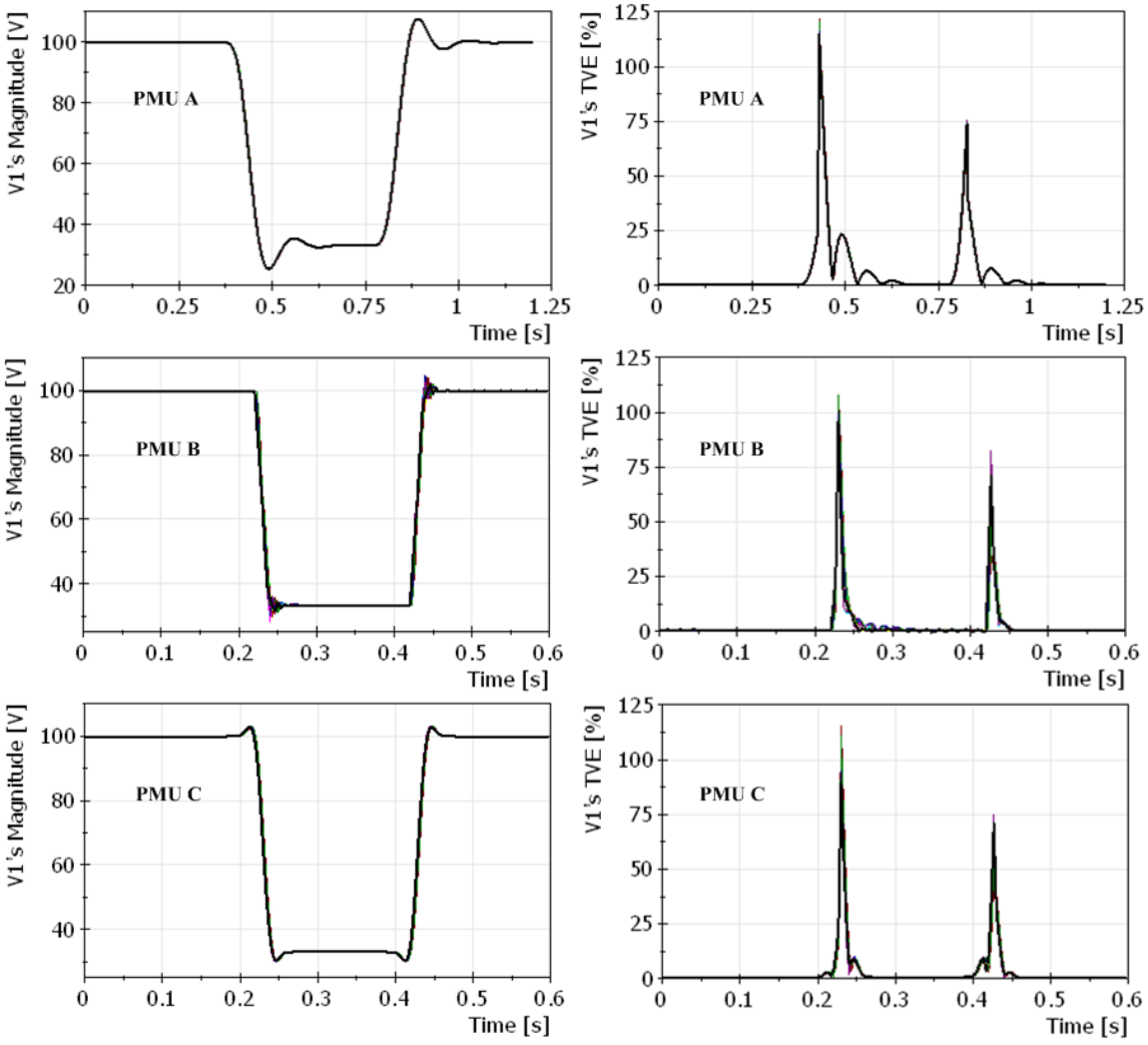

Figure 58　Results of recovery phase test

Table 19 Performance indices of recovery phase tests

DUT	T_{resp} (/F_s)	T_{set} (/F_s)	O_s (% of step)	U_s (% of step)
PMU A	4.26	3.70	-12.07	3.20
PMU B	1.29	1.72	-7.55	4.48
PMU C	0.45	1.51	-4.90	0.08

APPENDIX D

TEST CONFIGURATIONS AND RESULTS FOR CONFORMANCE TESTS

The configurations for performing conformance tests on selected six commercial PMUs and PMU-enabled IEDs is given in Table 20. The settings include synchronization method, type of communication interface, phasor format and vendors' proprietary parameters. Test results are summarized in Table 21, in which "S" stands for pass while "F" stands for failure.

Table 20 Configurations for PMUs and PMU-enabled IEDs

#	Device	Synchro. Method	Comm. Type	Phasors	Proprietary
1	A	IRIG-B/PPS Reference clock	Serial Port	Format: C37.118; Rate: 30 /s; Phasor: Float, Polar; Freq: Float.	Filter: Fast Response
2	B	IRIG-B/PPS Dedicated clock	TCP/IP	Format: C37.118; Rate: 30 /s; Phasor: Float, Rectangular; Freq: Float.	N/A
3	C	IRIG-B/PPS Reference clock	TCP/IP	Format: C37.118; Rate: 30 /s; Phasor: Float, Rectangular; Freq: Integer.	Filter: Symm 3-point
4	D	Direct GPS signal	TCP/IP	Format: C37.118; Rate: 60 /s; Phasor: Float, Rectangular Freq: Float.	Time tagging: Center
5	E	Direct GPS signal	TCP/IP	Format: C37.118; Rate: 30 /s; Phasor: Float, Rectangular Freq: Float	N/A
6	F	IRIG-B/PPS Reference clock	TCP/IP	Format: C37.118; Rate: 30 /s; Phasor: Float, Rectangular Freq: Float	N/A

Table 21 Conformance test result: steady state test

Device under Test	Test Class	Steady State Test								
		Magnitude Variation			Phase Angle Variation			Frequency Variation		
		TVE	FE	RFE	TVE	FE	RFE	TVE	FE	RFE
A	P	S	S	S	S	S	S	S	S	S
	M	S	S	S	S	S	S	F	S	S
B	P	S	S	S	S	S	S	S	S	S
	M	S	S	S	S	S	S	S	S	S
C	P	S	S	S	S	S	S	S	S	S
	M	S	S	S	S	S	S	S	S	S
D	P	S	S	S	S	S	S	S	S	S
	M	S	S	S	S	S	S	S	S	S
E	P	S	S	S	S	S	S	S	S	S
	M	S	S	S	S	S	S	F	S	F
F	P	S	S	S	S	S	S	F	S	S
	M	S	S	S	S	S	S	F	S	S

Table 22 Conformance test result: dynamic state test

Device under Test	Test Class	Dynamic State Test								
		Measurement Bandwidth			Frequency Ramp			Step Change		
		TVE	FE	RFE	TVE	FE	RFE	RT	DT	MO
A	P	S	F	S	S	F	F	F	F	F
	M	S	F	S	F	F	F	S	F	F
B	P	S	F	S	S	F	F	S	F	S
	M	F	F	S	F	F	F	S	F	S
C	P	S	F	S	S	F	F	S	S	S
	M	S	S	S	F	F	F	S	S	S
D	P	S	F	S	S	F	F	F	F	F
	M	F	F	S	F	F	F	S	F	F
E	P	S	F	S	S	F	F	F	S	F
	M	F	F	S	S	F	F	S	S	F
F	P	S	F	S	F	F	F	S	S	S
	M	F	F	S	F	F	F	S	S	S

TVE: total vector error; FE: frequency error; RFE: rate of change of frequency error;

RT: response time; DT: delay time; MO: maximum over/under shoot.

VITA

Jinfeng Ren received his B.S. degree from Xi'an Jiaotong University, Xi'an, China, in electrical engineering in 2004, and continued research on electric power systems until 2006. He received his Ph.D degree from Texas A&M University, College Station, TX, USA, in electrical engineering in 2011. He was a student researcher at National Institute of Standards and Technology (NIST), Gaithersburg, MD from March 2008 to August 2008. His research interests are new algorithms and test methodologies for synchrophasor measurements and their applications in power system monitoring, protection and control, new digital signal processing techniques for power system measurement and instrumentation, automated simulation methods for multifunctional IEDs testing, protective relaying testing and applications.

Jinfeng Ren may be reached at 3128 Department of Electrical and Computer Engineering, College Station, TX 77843-3128. His email is renjinf@gmail.com.